THE EFFECTS OF RADIAL SUPPORT CHARACTERISTICS ON SUBMARINE HULL INSTABILITY PRESSURES

by
Andre Delano Smith

B.S. Mechanical Engineering
Northwestern University (1992)

Submitted to the Department of
Mechanical Engineering
In Partial Fulfillment of the Requirements
for the Degree of

MASTER OF SCIENCE IN MECHANICAL ENGINEERING

at the

MASSACHUSETTS INSTITUTE OF TECHNOLOGY

MAY 1994

Signature of Author_____
Department of Mechanical Engineering

Approved by_____
James Gorman
Technical Supervisor

Certified by_____
Professor David Parks
Thesis Supervisor

Accepted by_____
Professor Ain A. Sonin
Chairman, Department Graduate Committee

THE EFFECTS OF RADIAL SUPPORT CHARACTERISTICS ON SUBMARINE HULL INSTABILITY PRESSURES

by
Andre Delano Smith

Submitted to the Department of Mechanical Engineering
in partial fulfillment of the requirements for the
degree of Master of Science in Mechanical Engineering

ABSTRACT

In practice, the submarine's major internal equipment is mounted to welded plating foundations, but submarine designers have been looking at the recent French innovation whereby the major internal equipment is mounted to a large truss/cradle structure through point supports. The focus of this research investigates the effects of radial point supports on the stability behavior of cylindrical shells under hydrostatic loading conditions . To investigate the stability phenomena of a point supported circular shells, the critical loads of point supported circular rings and cylinders were estimated numerically using an eigenvalue extraction routine. Next, shape imperfections were introduced to the geometry of the point supported cylinder, and this modified structure's buckling behavior was also estimated by eigenvalue extraction. To test the validity of using a linear numerical scheme, a nonlinear numerical scheme (RIKS Method) was used to predict the critical loads of the radially stiffened cylindrical shells, and the results were compared to the eigenvalue solutions. Furthermore, other important design parameters such as stresses, shell thickness, and shell weight were parameterized in evaluating the effectiveness of the point supports. Finally, an internal truss was attached to the submarine hull, and the effects of a this geometry on the buckling load were evaluated. The key findings of this research are the following: increasing the number of radial stiffeners dramatically improves the critical load of circular rings and cylinders, eigenvalue extraction was sufficient for predicting the buckling load in cylindrical shells, radial stiffener effectiveness drops as shell thickness increases for a constant radial stiffness value, and truss stiffness only plays a role in the stability behavior for low stiffness values of the radial supports.

Technical Supervisor: James Gorman

Thesis Supervisor : Dr. David Parks
Professor, Mechanical Engineering

ACKNOWLEDGMENTS

I would like to thank Richard Sapienza for time he spent looking over my thesis, and for the helpful information he has given me on the design of submarines. Also, I would like to thank Kevin Dyer for the endless help with computer hardware problems and program glitches.

Special thanks to my thesis advisor James Gorman and professor David Parks for providing guidance and support for my efforts.

My gratitude goes to The Charles Stark Draper Laboratory, and the GEM Fellowship Program for providing generous financial support for my education.

Finally, a special thanks to my mother and friends for providing endless support and encouragement for this educational endeavor.

This thesis was supported by The Charles Stark Draper Laboratory, Inc. (DFY '94 IR&D Project # 502). Publication of this thesis does not constitute approval by The Charles Stark Draper Laboratory, Inc., of the findings or conclusions contained herein. It is published for the exchange and stimulation of ideas

TABLE OF CONTENTS

LIST OF FIGURES

LIST OF TABLES

CHAPTER ONE

Introduction

1.0 Summary

This thesis investigates the effects of point radial supports on the buckling performance of externally pressurized cylindrical shells. Such a problem is shown to be an issue of growing importance in the design of submarine pressure hulls. Here an attempt is made to provide some useful insight into the problem. To accomplish the particular task, the research performed involves:

- Combined analytical/numerical analysis
- Phased Approach
    - Unstiffened Ring (Analytical)
    - Radially Supported Ring (Finite Element)
    - Ring on an Elastic Foundation (Analytical)
    - Unstiffened Cylinders (Analytical)
    - Point Supported Cylinders (Finite Element)
    - Truss Supports and Point Stress Analysis (Finite Element)
- Comparison of Methods
    - Eigenvalue Analysis
    - Linear Load Step Analysis
    - Nonlinear Load-Deflection Analysis
- Key Results
    - Eigenvalue Analysis (cheap) gives good results
    - Can get significant improvement in buckling for small weight increase

1.1 **Background**

Since World War II, the world's navies have demonstrated incredible advances in the design and the operational capability of submarines. The primary technology responsible for these advances was the development of nuclear power. Nuclear power allowed the vessel to be a true submarine, remaining totally submerged while traveling at high speeds for long periods of time. This development allowed the navies to break away from the combustion process that required oxygen from the atmosphere. It should be remembered that the submarines of the two World Wars were really surface ships with the ability to submerge for short periods. The nuclear submarine, except while approaching docks, is always submerged, which provided tactical and strategic advantages. Concurrent with the development of nuclear power, new low-drag hydrodynamic forms were developed allowing very high underwater speeds. Furthermore, extremely sensitive sonar systems were developed to allow reliable detection of submarines at large distances and effective weapon launching. These improvements required that further developments in materials and fabrication methods associated with building submarines be implemented. Since submarines needed to go deeper, faster, and be quieter, the performance parameters of the submarine hull design had to be optimized. **Table 1.1.1** illustrates the typical performance gains for submarines between WW II and the present (References 1&2).

Type	Top Speed Submerged (kts)	Submerged Endurance (hrs)	Maximum Depth (m)
WW II			
U.S. Fleet Boat	10	5	~100
German Type VIIC	7	1	150
German Type XXI	16	72	200
Current			
U.S. SSN688	>30	3 months	~300
Soviet Alfa SSN	45	1 month	~1000
Kockums Gotland*	20	>150	~150

Table 1.1.1: **Submarine Performance Comparison**

* **Note:** Swedish diesel-electric comparable to many current non-nuclear submarines

1.2 Motivation

Recent focus of U.S. submarine designers has been on a French innovation whereby the major internal equipment is mounted to a large truss cradle structure. This cradle is in turn installed within the hull envelope, and attached to the envelope via several point attachments. As compared to the conventional approach of mounting machinery to welded plating foundations, the truss/cradle concept offers improvements in acoustic performance, fabrication, and opportunities for parameter optimization (Reference 3). **Figure 1.2.1** illustrates the differences between the traditional welded plating foundation and the French truss/cradle concept. Current U.S. practice (Top) is to stiffen the hull plating with ring frames of tee-section and to support machinery on rafts isolated from welded plating foundations. The proposed adaptation of the French cradle concept (Bottom) incorporates the truss framework and point isolator attachments.

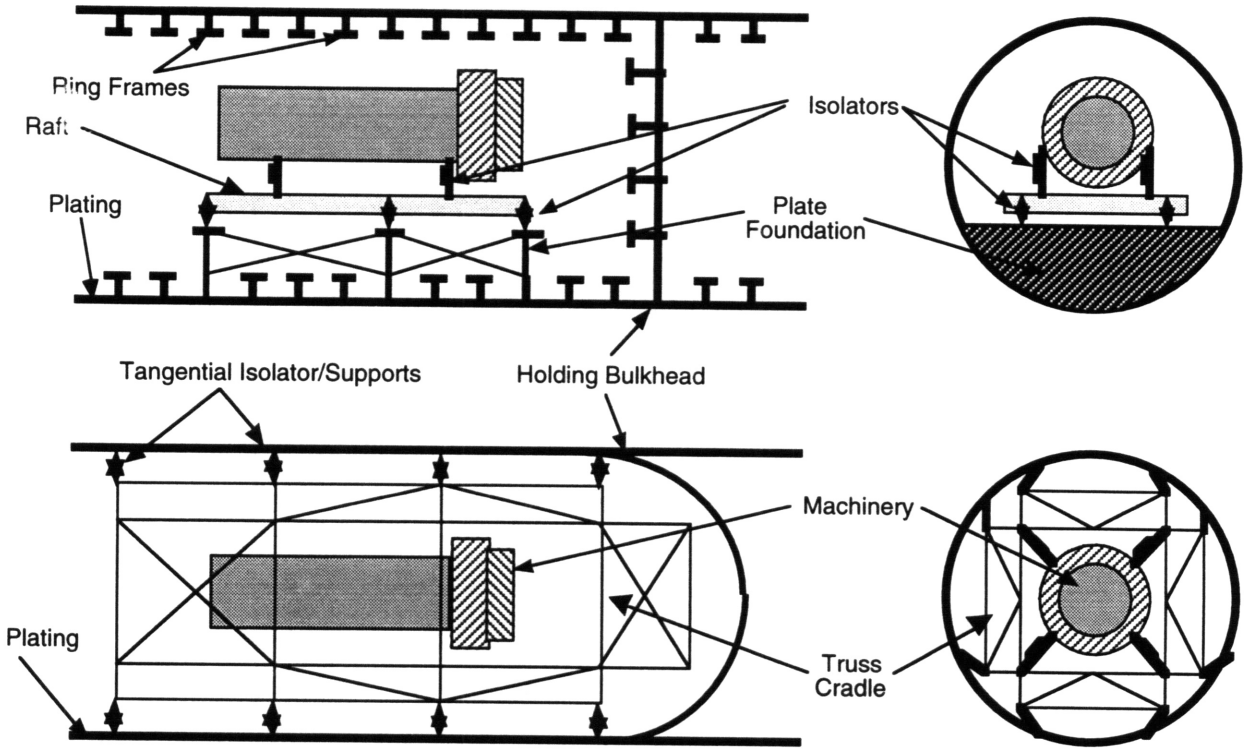

Figure 1.2.1: **Welded Foundations (Top) Compared to Isolator Attachments (Bottom)**

Since this design methodology provides enhanced opportunities for parametric optimization, an efficient way to evaluate the effects of particular performance parameters on other design variables is needed. To solve this problem, integrated design tools can be developed to evaluate these effects. The research described in this thesis will contribute to the structural integrity modules of such integrated hull design tools.

1.2.1 Integrated Submarine Design Tools

Submarine hull design has been at the forefront of naval research because of its complex relationships among many performance parameters. These parameters include structural acoustics, shock & vibration, hydrodynamic shape, flow noise, controllability, equipment packaging, and static structural integrity. Historical design procedures tend to evaluate each parameter separately to meet individual performance requirements, which

in the U.S. has led to incremental development of a single basic type. An integrated multi-discipline design tool evaluating these parameters simultaneously would make the design process more effective. Since the former USSR and France have broken new grounds on submarine hull design, an improved design process will help the U.S. to remain competitive. Draper Laboratory and others within the Naval Sea Systems Command (NAVSEA) and ARPA/ ONR arenas are currently developing integrated hull design tools which address the multi-disciplinary nature of a complex system(hull) design.

A pressure hull design tool will be comprised of several distinct elements, including:

1. Weight & Balance (Ensure Buoyancy and Stability)
2. Static Structural Integrity (Hydrostatic Loads)
3. Structural Dynamics (Sound / Vibration Transmission in Hull)
4. Structural Acoustics (Radiation of noise to water)

Weight, Balance, & Configuration - During this portion of the design process we must keep track of pressure hull weight and center of gravity for comparison to displacement and center of buoyancy. The weight to displacement ratio is used as a measure of the efficiency of the hull structure. It is useful to keep in mind that the sum of submarine component weights must equal the hull's displacement, so that the vessel may float. Weights added to one subsystem must therefore be subtracted from others for a given hull size. This is best described by the expression

$$\sum_{i=1}^{n} \frac{W_i}{D} = 1 \qquad (1.1)$$

where

W_i- individual weight components
D- total displacement

Table 1.2.1 illustrates the typical weight breakdown for a U.S manned submarine. Note that 1/2 of the total displacement is occupied by the structure, which implies that significant benefits are possible with an integrated and optimized design. Finally, the other important parameters are the static moment from the center of gravity (C.G.) and the center of buoyancy (C.B). The center of gravity is the point on the vessel where the resultant of all the weights acts downward, and the buoyant forces acting on the vessel in still water acts on the vessel at the center of buoyancy. Thus, to maintain ship balance the moments due to these forces must be balanced (see fig. 1.2.2).

Component	Displacement
Hull	50%
Propulsion	26%
Electrical	1.50%
Communications	3%
Auxiliary Systems	11.50%
Outfit	4%
Armament	4%
TOTAL	100%

Table 1.2.1: **Displacement Distribution Breakdown**

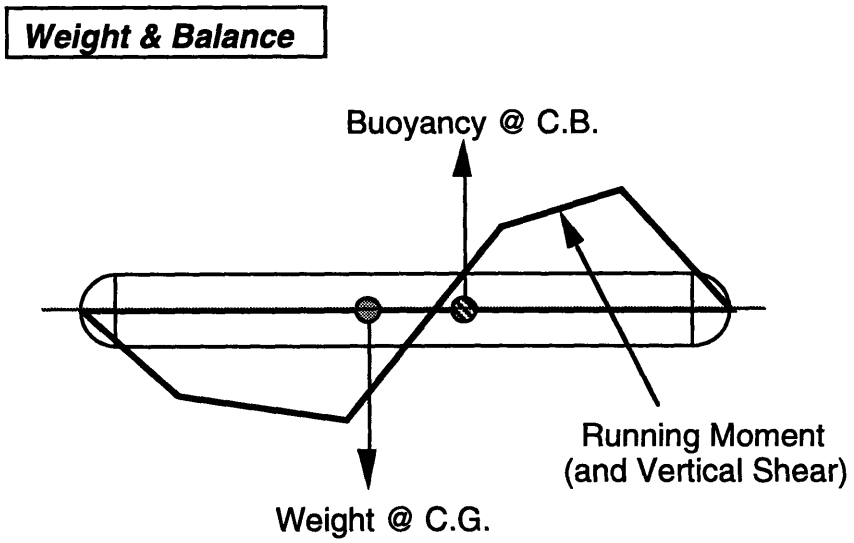

Figure 1.2.2: **Moment Balance Diagram**

Static Structural Integrity - The design tool will be used to help ensure that the pressure hull design concept at hand can provide adequate structural integrity for a sustained hydrostatic pressure load at the design depth. A typical U.S. ring-stiffened hull concept is shown in Figure 1.2.3. To decrease the probability of failure, a safety factor is applied to the design depth for each of several failure modes. These failure modes include plate yielding, local instability (between stiffeners), general instability, and frame crippling. To design against these failure modes, numerous variables (plate material and thickness, frame spacing, bulkhead spacing, frame type (rectangular, tee, hat) and material, frame cross sectional area and moment of inertia, and frame proportions) must be specified in a coordinated fashion. These variables will be modified to optimize the hull design, and the tradeoffs of these modifications must be evaluated.

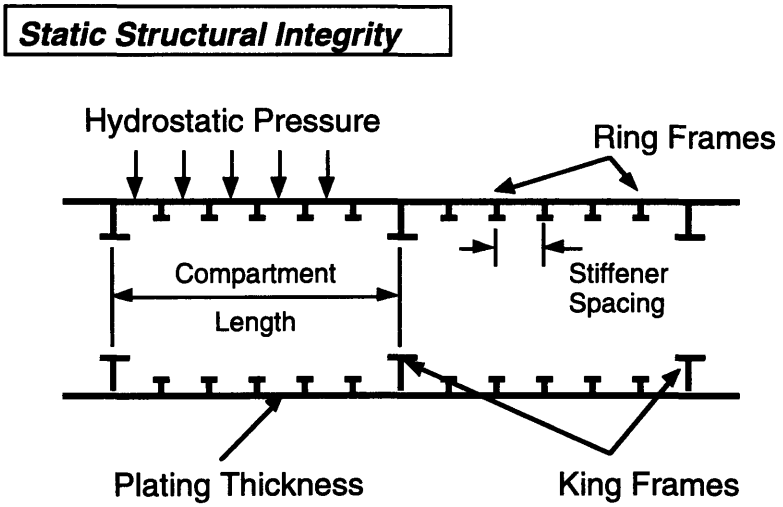

Figure 1.2.3: **Ring Stiffened Hull Schematic**

Structural Dynamics - The design tool must also help calculate and minimize the vibrations associated with the internal machinery and its foundations. The vibrating machinery in the hull transmits energy to the water through several paths between the machine and the hull. The variables affecting the behavior of this coupled system include foundation geometry and member properties, and isolation characteristics of attachment points, the bending stiffness of the hull envelope, and the characteristics of the machinery excitation.

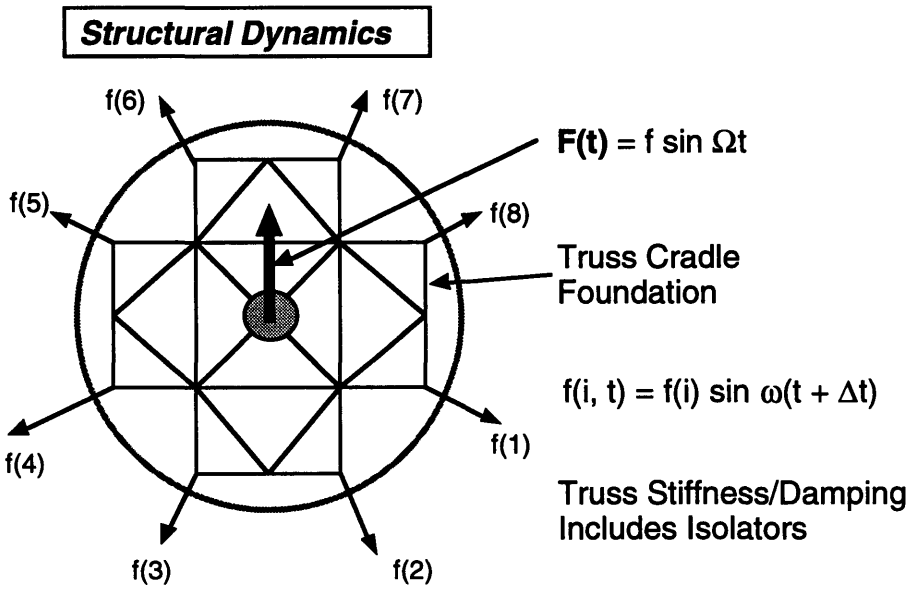

Figure 1.2.4: **Truss-Hull Interaction Dynamics**

Structural Acoustics - Quiet operation is an important requirement in submarine design. A submarine that can suppress noise better than its adversary maintains tactical and strategic advantages. The main objective here is to detect other enemy vehicles before they can detect you. Design measures must be introduced to reduce the radiated noise from the machinery and the submarine's functional systems. When these machines and systems are in operation, the hull vibrates and transmits radiated noise. The random (or harmonic) vibration of these mechanisms that is not absorbed by the special mountings on the hull is transmitted to the water and detectable at large distances as noise. The action of propeller motion and water flowing over the hull both have noise associated with these actions. The structural acoustics tool deals with calculating and minimizing the sound pressure level at some radius remote from the hull. This is affected by the point attachments between the truss and the hull, the hull stiffness characteristics, and any surface treatments that may be applied. The important design variables are the following: excitation frequency, hull areal density, hull envelope meridonal and circumferential bending stiffness, the number of excitation points, and attachment (isolator) properties. Therefore, an optimized design should manipulate a number of interlocked parameters to suppress the noise created by these mechanisms.

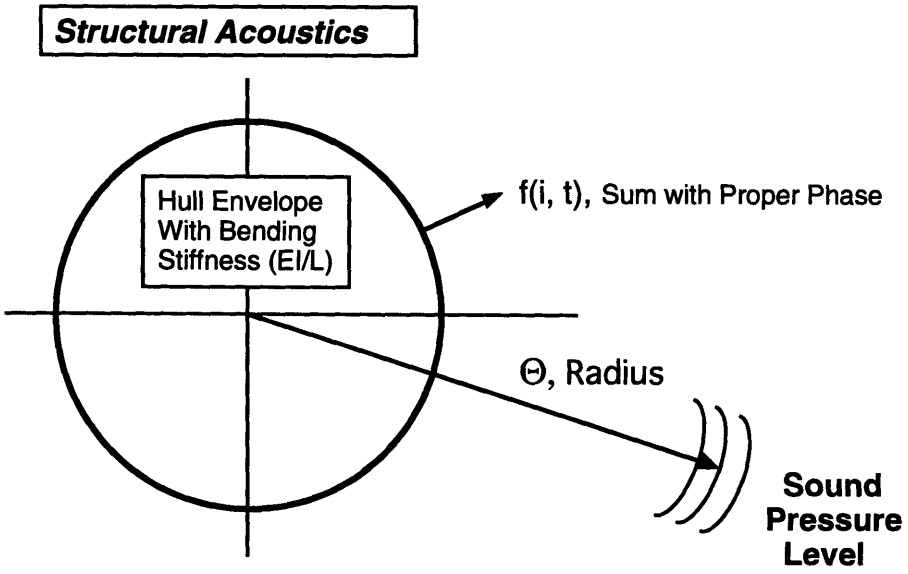

Figure 1.2.5: **Point Excitation Driven Hull Acoustics**

Finally, a significant global tradeoff afforded by the cradle approach is that between the acoustic performance of the system (relatively low radial stiffness at attachments) and the potential benefit of the internal structure stiffness to the hull buckling integrity. Therefore, the relative buckling performance of rings and shells having concentrated radial supports is of major interest. Parametric evaluation of this buckling performance as a function of the number, placement, and stiffness of the radial supports will provide the data necessary to evaluate this global design tradeoff.

1.3 **Approach**

The objective of this thesis is to provide a preliminary parametric evaluation of the effectiveness of the truss/cradle in augmenting hull buckling integrity. The approach taken in this research combines analytical studies of ring and cylinder buckling behavior with finite element calculations for a variety of radially supported ring and cylinder configurations. This incremental approach provides confidence at each step through comparison with the prior steps. The specific path taken in this effort can be separated into four parts. First, the analytical studies to provide a foundation includes the investigation of the instability of a circular ring under hydrostatic loading and the effect of radial supports on its instability pressure. The stiffness of the supports, the bending stiffness (EI) of the ring, and the number of radial supports will be parameterized. Next, the general instability problem of a circular cylindrical shell with point supports under hydrostatic loading will be solved numerically using the ABAQUS finite element code. The buckling of a cylindrical shell with an internal truss attached to the hull with radial supports will be examined. Finally,the effects of these point supports on state of stress in the hull in the vicinity of the support-hull contact point will be determined.

1.4 **Chapter Topics**

Brief summary of the content in the subsequent chapters

Chapter 2: Submarine Design

Discussion the basic concepts behind submarine design such as hull shape, hull configuration, material effects, submarine structure. Explanation of the failure mechanisms along with other design considerations .

Chapter 3: Stability Theory

Derivation of the stability equations for a circular ring and a circular cylindrical shell using the methods stated in Brush & Almroth (Ref. 7), and the methods stated in Timoshenko (Ref. 8).

Chapter 4: Analysis and Results

Overview of the creation of finite element models and the results obtained from these analyses (eigenvalue buckling extraction, nonlinear analysis, stress analysis). Model verification is explained along with some design parameter comparative studies.

Chapter 5: Conclusion

Summary of the work done to date, and the related work that can be performed in the future to increase the structural performance of submarine hulls.

CHAPTER TWO

Submarine Design

2.1 Introduction

Throughout the years of science, there has always been a fascination with the unknown. To satisfy this curiosity, men have dared to go where no one has gone before, and one of their many successful journeys was to the depths of the ocean. To make a successful trip, a structure needed to be designed to hold a crew and their equipment; however, it should also be able to protect them from the high pressure environment with a means of life support. In response to this problem, researchers began looking into the behavior of structures under external hydrostatic pressure. The hydrostatic pressure on a submarine structure is given by the simple relation:

$$P=\rho gH \tag{2.1.1}$$

where

P=Pressure

ρ= density

g= acceleration of gravity

H =depth of submergence

For **P** in psi and depth in feet, the result is P=0.445 psi per foot of submergence

2.2 Hull Shape

Through countless experiments, it can be shown that thin walled shells are effective structures that can withstand external hydrostatic pressure, but the shape of the shell affects its performance. Since a shell structure can withstand pressure loading in a membrane manner more efficiently than through bending, a structural shape must be chosen to exploit this behavior. Using linear membrane shell theory, shape efficiency

factors can be determined for various geometries. Shape efficiency factors are a measure of particular shape's efficiency in resisting applied internal and/or external pressure loads, and the shape efficiency factors for some geometries are shown in **figure 2.2.1**.

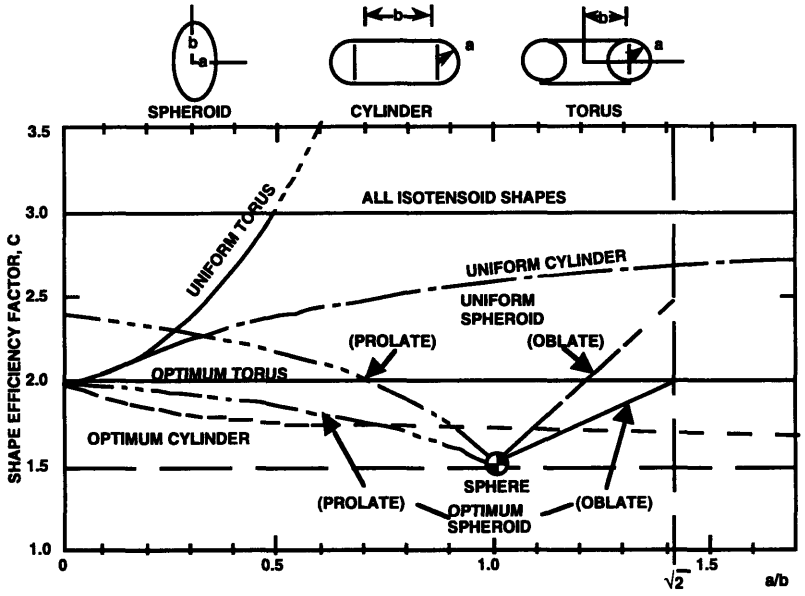

Figure 2.2.1: **Shape Efficiency Factor Comparison**

It should be noted that the lowest achievable value of C represents the most efficient structural shape. With that knowledge, the figure illustrates that the most efficient shape is the sphere, but there are other shapes that have decent efficiencies. Although spheres are the most efficient structure from the structural stand point, closed thin-walled structures such as prolate axisymmetric forms are good candidates for submarine hulls. We can see why spheres are the most efficient shapes in the discussion of the weight-to-displacement ratio (**W/D**).

Also, the shape efficiency factor (**C**) plays a large role in determining the structural efficiency of membrane shells. Researchers Gerard, Bert, and Hoffman have shown that from linear theory that the structural efficiency of membrane shells can be measured by its weight-to-displacement ratio. This ratio can be expressed as

$$\frac{W}{D} = C \cdot \left(\frac{\sigma_a}{\rho} \right)^{-1} \cdot 12H \qquad (2.2.1)$$

where

C is the membrane shape efficiency factor

ρ is the shell weight density (lb/in^3)

σ_a is the shell material uniaxial strength (lb/in^2)

H is the pressure hull design depth (ft)

The W/D ratio is the significant figure of merit used in the design of submersible structures. Ideally, we would like submersible structures to be light weight with a large volume (water displacement). In considering the structural and shape efficiency of the hull, designers have migrated toward particular hull configurations. In general, nonaxisymmetric shells have a lesser efficiency than that of shells with an axisymmetric cross-section. Several German designs as well as a small U.S. submersible have used non-axisymmetric (figure eight or elliptical) sections to solve some peculiar packaging problems.

2.3 **Hull Configuration**

Designers have many different hull configurations available to them, but only a small fraction satisfy the need for shape and structural efficiency. Furthermore, these hull configurations must pass other criteria for selection, and the hull configuration selection depends on the following criteria:

1. Structural efficiency
2. Internal and external arrangements
3. Hydrodynamic form
4. Complexity and cost of fabrication
5. Ease and reliability of structural analysis

Satisfying these selection criteria, designers have settled on three commonly used hull configurations, and they are the following: single sphere, the connected spheres, and the ring stiffened cylinder with hemispherical or ellipsoidal end closures.

From **figure 2.2.1**, we can see that the sphere exhibits the lowest shape efficiency factor; thus, it is the most efficient shape. Since the structural efficiency is dependent upon the shape efficiency, the sphere is also the most structurally efficient. Also, it has been known that the W/D ratio for spheres can be 70% of the W/D for a ring stiffened cylinder, but it depends on depth, material, and other factors. Since thin walled spheres are efficient structures for withstanding external pressure loading, they are used for small manned submersibles. To improve the structural integrity of shell structures, a stiffening scheme is often utilized. Due to the fact that stiffened spheres are hard to fabricate, they are not often used for submersibles.

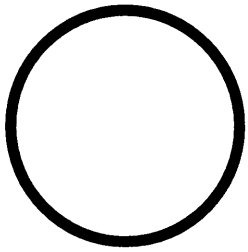

Figure 2.3.1: **Sphere**

On the other hand, unstiffened spheres are frequently used due to their symmetry and good strength -weight ratios. Furthermore, they can be fabricated without inducing stress-concentrations that can lead to failure, but spheres are very sensitive to initial manufacturing imperfections and residual stresses. These sensitivity problems decrease the strength of the spherical hull. Although the sphere is the most efficient structure, we can see that it has some disadvantages, such as :

1. Spheres have poor hydrodynamic form and maneuverability
2. Spheres are hard to manufacture
3. Spheres inefficiently house their personnel
4. Spheres would be hard to dock

To help these disadvantaged areas, another shape must be utilized, and the connected- sphere hull configuration provides needed improvement. Connected spheres utilize the sphere's attractive features, and they improve upon the less attractive features.

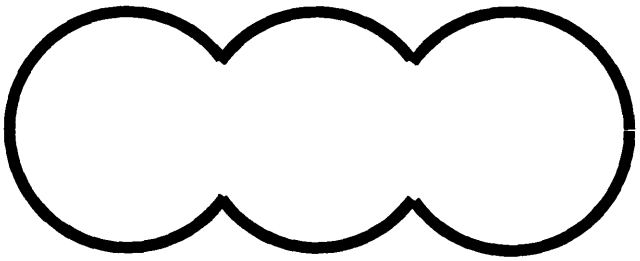

Figure 2.3.2: **Connected Spheres**

To achieve a lower W/D ratio, the fewest possible number of spheres should be used. Although connected-spheres are an improvement, other improvements can still be made, and the cylinder is an effective shape to provide the needed balance between packaging efficiency and structural performance.

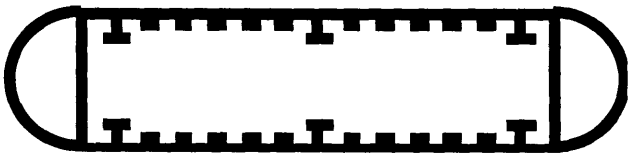

Figure 2.3.3: **Ring-Stiffened Cylinder with End-Closures**

While membrane spheres are more efficient than membrane cylinders, stiffening mechanisms necessary to combat buckling failure are much easier to implement in cylinders than in spheres. Also, it is much easier to fabricate cylinders to a high standard of geometric precision. Ring-Stiffened cyliners have found extensive use in shallow diving submersibles, taking advantage of these several benefits (as compared to spheres) can yield

1. Superior internal arrangement possibilities
2. Superior hydrodynamic form
3. Lower fabrication cost

2.4 **Shell Material Effects**

Once a hull configuration has been decided upon, the designer must select a material. Because material selection plays a large role in determining the efficiency and safety of the structure, the choice of material is a very important part of the design process. To compare materials we must examine their properties.

Criteria for hull material selection

1. Optimize strength-weight ratio and toughness
2. Resistance to stress-corrosion cracking and low cycle fatigue
3. Reduce residual stresses in the fabrication of the hull
4. High Young's Modulus, especially weight-specific modulus
5. Fabricability of material into desired shape
6. Producibility of the material to established specifications in requested shape and size
7. Cost of structure fabrication and in-service maintenance
8. Material flaws and defects in the fabricated structure

For preliminary design purposes, the key parameters are weight-specific strength and stiffness, as will be outlined later. Some reasonable level of toughness is also essential, especially for manned submersibles. In fact, the extraordinary level of toughness found in the HY-80 series steels is the primary reason for their 30 year usage in the U.S. SSN's and SSBN's. Toughness is a measure of the ability of a material to absorb energy up to the point of fracture and depends to some degree on the manner in which the load is applied. With a high toughness materials, the structure can undergo large plastic deformation in the region of stress concentrations (cracks and discontinuities). Thus, in order to obtain good resistance to rapid crack growth and low cycle fatigue, we need to utilize tough and corrosion resistant materials into our design. Also, improving the strength-to-weight ratio allows a lighter and stronger submersible to be built, and this allows more equipment and personnel to be stored on the vessel. Although high strength-to-weight characteristics would improve structural performance, the increase in strength-to-weight ratios usually implies decreased toughness. To choose a material

effectively, the designer must have a good working knowledge of the mechanical behavior of materials and the state of stress due to the applied load, and the designer must use this knowledge to find a material that balances performance, fabrication attributes, and cost.

Although metallic materials gives us a good strength-to-weight ratio, some nonmetallic materials provide substantial improvements. Simple unstiffened shell stress and buckling formulas can be used to illustrate the performance benefits of different hull materials. The weight-to-displacement ratios for yield and buckling failure modes are shown below for both cylinders and spheres. The weight-to-displacement ratio is the key pressure hull paramter and compares structural weight to the weight of water displaced by the hull envelope.

Cylindrical Shells

$$\left(\frac{W}{D}\right)_{Yield} = 24 \times S.F. \times \left(\frac{\sigma_a}{\rho_H}\right)^{-1} \times H(ft) \qquad (2.4.1)$$

$$\left(\frac{W}{D}\right)_{Buckle} = 7.043 \times S.F. \times \left[H \times \left(\frac{E}{\rho_H}\right)^{-1} \times \left(\frac{\rho_H}{\rho_{SW}}\right)^{2}\right]^{1/3} \qquad (2..4.2)$$

Spherical Shells

$$\left(\frac{W}{D}\right)_{Yield} = 18 \times S.F. \times \left(\frac{\sigma_a}{\rho_H}\right)^{-1} \times H(ft) \qquad (2.4.3)$$

$$\left(\frac{W}{D}\right)_{Buckle} = 3.856 \times S.F. \times \sqrt{6 \times H(ft) \times \left(\frac{E}{\rho_H}\right)^{-1} \times \left(\frac{\rho_H}{\rho_{sw}}\right)} \qquad (2.4.4)$$

where

ρ= density
E=elastic modulus
σ=Strength
subscripts *sw*=seawater
H=depth(ft)
S.F.= safety factor
subscripts *H*=hull material

Since the W/D ratio due to buckling is directly proportional to a fractional power of hull material specific gravity, a material with a lower density will be lighter than one with a higher density even though they have identical specific strength and stiffnesses. For design purposes we compare the required W/D ratios for yield and buckling, and choose the larger as the controlling factor. **Table 2.4.1** shows the properties of several interesting pressure hull materials. **Figures 2.4.1** and **2.4.2** illustrate plots of W/D versus depth for several important materials. Note that for spherical shells, there is a depth at which the critical failure made switches from buckling(shallow) to yielding (deep). Unstiffened cylinders are buckling dominated at any practical depth.

MATERIAL	DENSITY	ALLOWABLE STRENGTH (KSI)	ELASTIC MODULUS (MSI)	$\frac{\sigma}{\rho}$ (10^3 in.)	$\frac{E}{\rho}$ (10^6 in.)
HY-80 STEEL	0.284	80	30	282	106
4340 STEEL	0.283	275	30	972	106
H-11 STEEL	0.281	300	30	1067	107
7075 AL (T73)	0.101	55	10.4	545	103
7075 AL (T6)	0.101	75	10.4	743	103
6AL-4V TITANIUM	0.160	150	16.5	938	103
INCONEL 700 SERIES	0.296	150	30	507	101
KEVLAR 149/EPOXY [1.]	0.050	203	15.4	4060	308
KEVLAR 49/EPOXY [1.]	0.050	167	10.5	3340	210
E GLASS/EPOXY [2.]	0.071	154	5.6	2169	78
S GLASS/EPOXY [2.]	0.069	200	6.6	2900	96
GRAPHITE, T300/EP. [3.]	0.056	218	20	3890	357
GRAPHITE, T40/EP. [3.]	0.056	335	25.2	5980	450
GRAPHITE, P100/EP. [3.]	0.065	144	66	2215	1015

1. UNIDIRECTIONAL COMPOSITE, 58% FIBER VOLUME
2. UNIDIRECTIONAL COMPOSITE, 53% FIBER VOLUME
3. UNIDIRECTIONAL COMPOSITE, 60% FIBER VOLUME

Table 2.4.1: **Pressure Vessel Material Comparison**

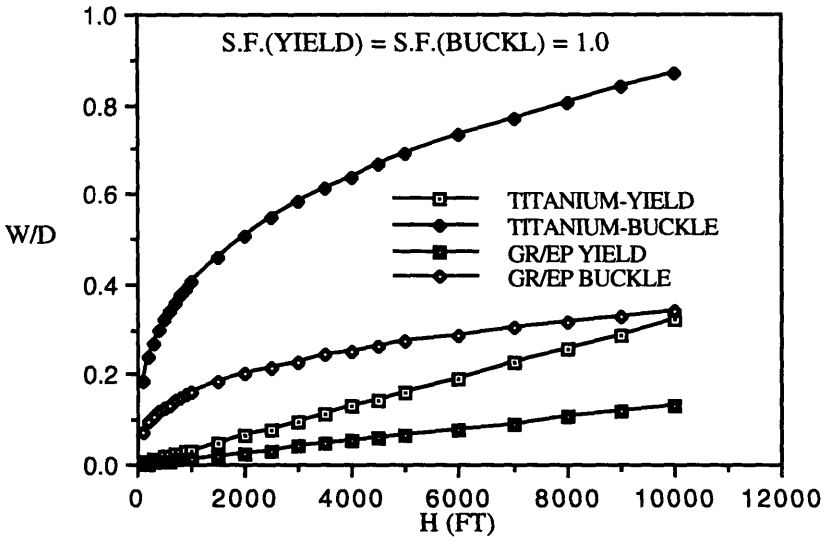

Figure 2.4.1: **Unstiffened Cylinder W/D Trades**

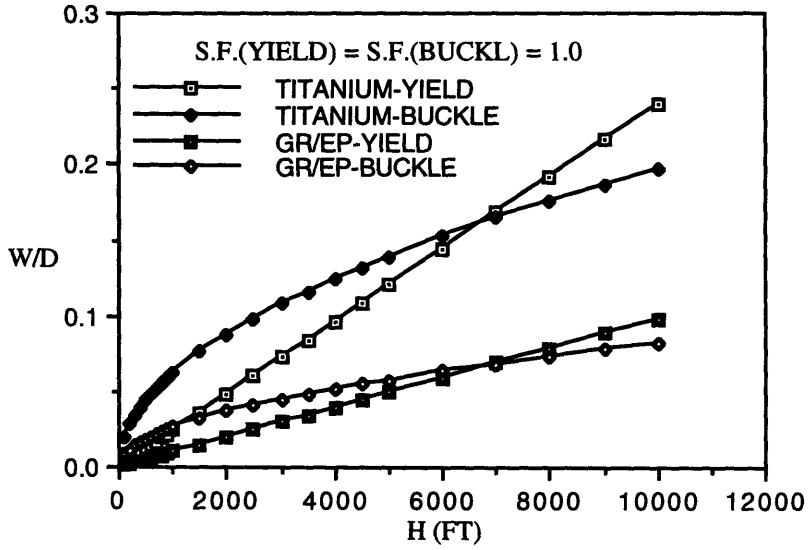

Figure 2.4.2: **Unstiffened Sphere W/D Trades**

2.5 **Submarine Structure**

Submarines are vessels that can travel beneath the surface of the ocean for long periods of time with (perhaps) a sizable crew. Since these vessels are used mostly for military purposes, the vessels' maneuverability, stealthiness, speed, and structural integrity are major concerns. From the shape and structural efficiencies described earlier, hull structure choices normally tend towards stiffened circular cylindrical shells with hemi-spherical end-closures. The major structural components that determine the necessary structural integrity are

1: Shell Plating
2. Shell stiffeners
3. Bulkheads

2.5.1 **Shell Plating**

The shell plating makes up the outer epidermis of the pressure hull, and its major purpose is to resist external hydrostatic loads. Since these loads depends on the desired design depths, the shell thickness becomes a key design factor. The shell thickness is related to other design parameters through the simple relationship

$$t = K\frac{PR}{\sigma_a} \tag{2.5.1}$$

where

P- design pressure R- hull radius

σ_a- allowable stress K- parameter related to degree of stiffning (≤ 1)

Some major influences over the shell thickness are the following:

1. Hull diameter
2. Frame spacing
3. Operating pressure
4. Strength of the material

2.5.2 Stiffeners

Stiffeners are circular rings (and sometimes longitudinal stringers) welded to the skin(plating) to provide increased bending rigidity to suppress buckling. Since cylinder buckling is dominated by the bending of shells, stiffeners provide a needed advantage over unstiffened cylindrical shells in the design against failure, and these appendages can be internal or external. There are several types of internal stiffeners used to stiffen the shell plating, and they are listed as

1. Transverse ring frame
2. Wing bulkhead
3. Internal bulkhead
4. Deep Frame

Circular rings are frequently used hull frames for cylindrical shells. Since stiffness is a function of **EI**, the area moment of inertia determines the effectiveness of the stiffener, and this moment of inertia (**I**) is determined from the shape. The effective shapes commonly used are circular rings having a **T** or **H** cross-section. As mentioned before, these frame stiffeners can be placed internally or externally, but it is used internally for single hull designs. Double Hull configurations are extensively used by Russian submarine designers, with the plating split into two skins with circumferential ring framing sandwiched in between them.

Internal bulkheads are partitions that divide the pressure hull into separate compartments. These internal bulk heads can be separated into three groups, and these groups are subdivision bulkheads, holding bulkheads, and pressure bulkheads. First, the subdivision bulkheads help make each compartment within the submarine water tight, but cannot sustain full depth pressure. Holding bulkheads, as the name implies, are designed to hold against full depth pressure and provide survival/ rescue options for certain types of casualties. U.S. submarines typically have one or two holding bulkheads. Soviet submarines typically have more, while some European diesel-electric submarines have

none. Finally, pressure bulkheads provide boundaries between high pressure (i.e. ballast tanks) and low pressure areas. They must be able to resist the submergence pressure. These 3 different types of bulkheads provide significant radial support to the skin, and the axial distance between the boundaries of dramatically affects the critical buckling load of the hull.

Due to weight and packaging considerations within machinery compartments, deep frames are typically used in this situation. To be effective, deep frames are internal ring frames that must be larger and typically an order of magnitude stiffer than a normal ring frames.

Figure 2.5.1 illustrates the pressure hull structure of a U.S. Navy Sturgeon-Class (SSN637), indicating the various components.

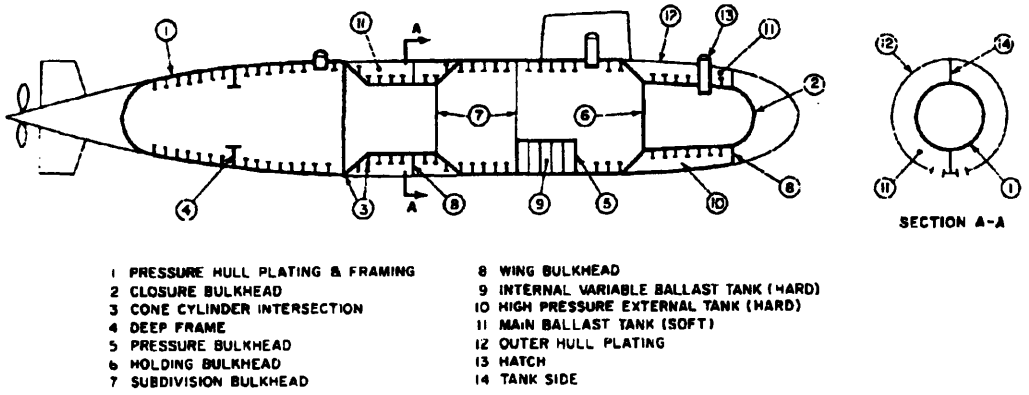

Figure 2.5.1: **SSN637 Submarine Schematic**

The final pieces that are needed for the pressure envelope are the end-closure bulkheads. The end-closure bulkheads used can take on two forms. These two forms are flat-plate bulkheads, and dished bulkheads. Dished bulkheads can take the form of an ellipsoid or hemisphere. Furthermore, they both have their own advantages, for different situations. For instance, flat-plate bulkheads are a good choice for shallow diving depths

where overall length may be limited, while dished bulkheads are much more efficient, albeit more difficult to fabricate.

2.6 **Failure**

Although a design may satisfy many of the specifications that were set, the design could have an unforeseen flaw, and that flaw could lead to failure of the structure. Designer must provide robustness against potentially fatal defects along with other design criteria to increase the life of the structure. In the design of submarines, the failure of stiffened cylindrical shells is the major point of concern. There are three primary failure modes of stiffened cylindrical shells under applied hydrostatic loads, and they are noted as

1. Yielding of the shell at or between ring stiffeners
2. Buckling of the shell between ring stiffeners
3. General Instability or overall collapse

A good starting point for designs is to first size the shell plating to avoid yielding at the operational pressure (depth). Shell yielding occurs between the ring stiffeners, and in this region, the shell plastically deforms. As a result of this deformation, a circumferential pleat is formed **(see figure 2.6.2)**. This step should at least crudely account the effects of ring frames in reducing the shell membrane stresses (if only by the area ratios). Next, the stiffener spacing can be chosen to preclude interstiffener buckling using the previously calculated plating thickness (see equation 2.7). In the event of failure, the structure will undergo localized buckling in this region, and this localized buckling of the shell between the ring stiffener is characterized by dimples forming around the perimeter of the shell between the stiffeners **(see figure 2.6.1)**. Finally the stiffener cross-sections are chosen to provide sufficient bending rigidity (EI per unit length along generator) to prevent failure due to general instability. In general instability

failure, the cylindrical shell and stiffeners deflects as a unit, and this deflection results in lobe formation (**see figure 2.6.3**).

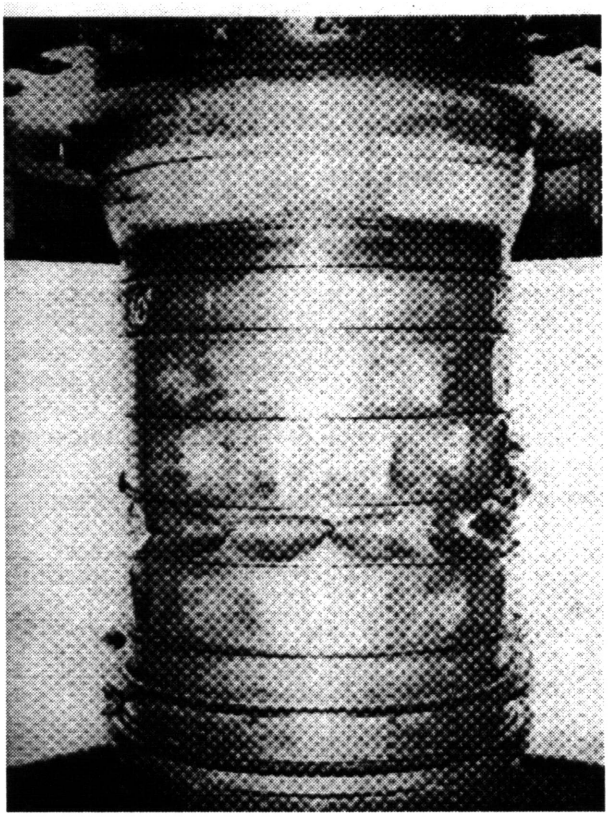

Figure 2.6.1: **Cylinder Interstiffener Buckling** (Ref. 6)

Since most cylindrical hulls will be stiffened in some fashion, we can see that the mixture of the yielding and buckling failure modes become very important. General instability is sensitive to both stiffener and compartment spacing, and these stiffeners include ring bulkheads, wing bulk heads, internal bulkheads, and deep frames. If this axial spacing is too long between their boundaries, general instability may occur. The designer must make the ring frames rigid enough for the desired compartment length to prevent general instability failure of the shell. Also, the structure will fail due to general instability if the ring stiffeners aren't strong enough to resist moments which may be due to noncircularities. In actual structures, the structure may have slight eccentricities, and these eccentricities may lead to progressive frame yielding and then general instability.

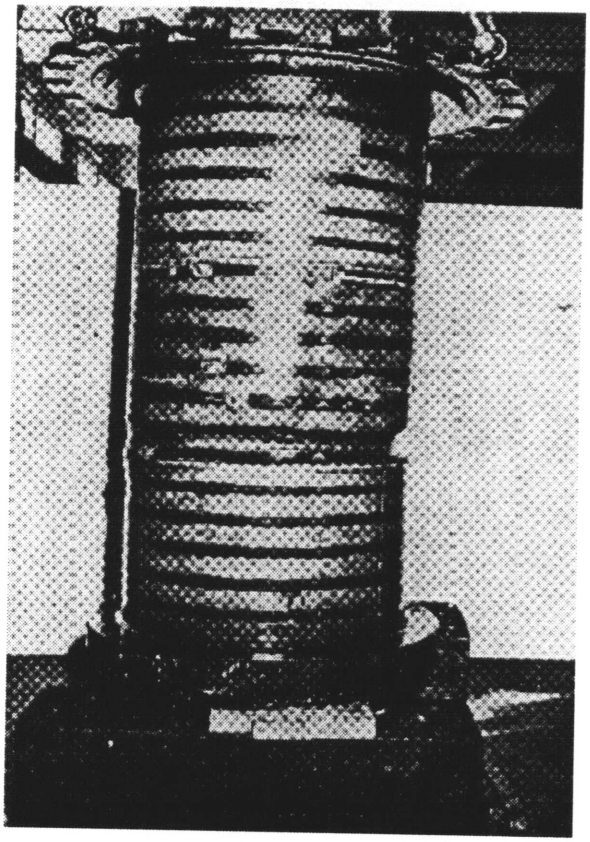

Figure 2.6.2: **Cylindrical Shell Yielding Between Stiffeners** (Ref.6)

Since real manufactured pressure hulls have some small geometric imperfections, the critical buckling load is often lower than estimated. With this information in mind, the structure should be designed robust to inhibit buckling. With the buckling failure mode deleted, the structure would fail due to yielding. An optimum design would have minimal weight, and the shell would fail due to yielding rather than buckling. Also, the theory for yielding provides better predictions for this design situation. Finally, this yield failure mode is commonly found in heavy cylindrical shells with closely spaced stiffeners/frames.

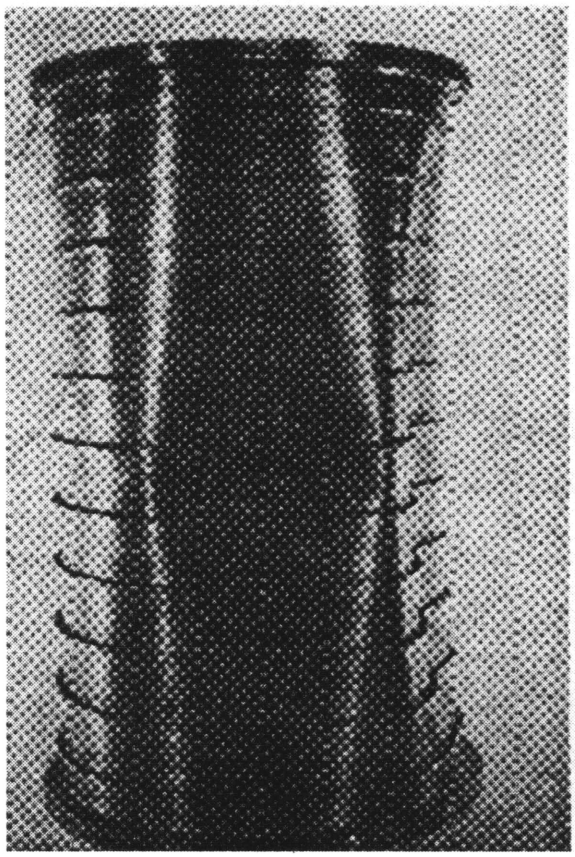

Figure 2.6.3: **General Instability of Cylindrical Shell** (Ref. 6)

2.7 **Other Design Considerations**

Although the major design parameter described previously are very important , their are other parameters to consider. These parameters include cost, time, reserve or excess buoyancy, noise, and safety.

In designing the total system, there is always need to improve performance through advanced technology, but the system must be developed at a reasonable cost and time. Also, cost and time can be reduced by keeping the design simple, and a simplified design has the advantage of minimizing the problems of load and stress analysis, fabrication, and inspection.

2.7.1 **Buoyancy**

A vehicle that is built to operate both at the surface and submerged can be defined as a submersible. To operate alternately in both these modes usually requires that a submersible have a ballasting system for adjusting the volume of displacement. To submerge, the displacement volume must be reduced to realize equilibrium between the vehicle weight and the buoyancy, which is the upward force exerted on an immersed volume. Displacement volume alone determines buoyancy, and the upward force exerted on an immersed body can exceed, be equal to, or be less than the weight of the body. If it exceeds the weight, the body will float; if it is equal, the body will submerse and remain in equilibrium; if it is less, the body will sink.

Furthermore, the placement of these ballast tanks influence the design of the pressure hull. There are three main hull designs used to accommodate these ballast tanks and they are the following: Single hull, Double hull, and Saddle hull.

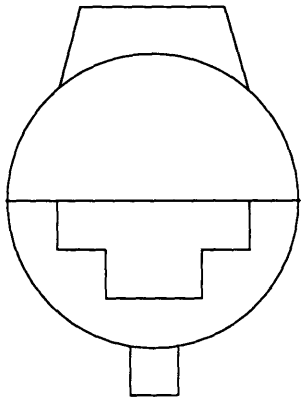

Figure 2.7.1: **Singe Hull**

The main ballast in a single hull submarine are located at the ends of the pressure hull,or sometimes in the middle as in the SSN 637 **(figure 2.5.1)**

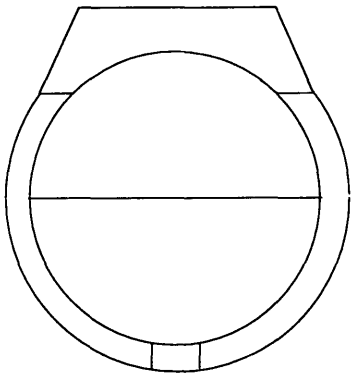

Figure 2.7.2: **Double Hull**

Double hull submarines have an outer hull encompassing the pressure hull. The space between the two hulls is used for the main ballast tanks and other equipment with a fixed ballast keel located within the bottom.

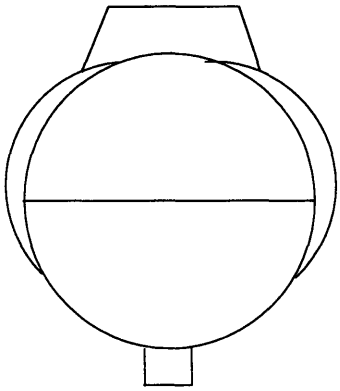

Figure 2.7.3: **Saddle Hull**

Finally, the saddle tank submarines locate their main ballast tanks along the sides of the pressure hull as streamlined appendages. Therefore, we can see that there are various important aspects of submarine design that influence the design of the hull of the submarine.

U.S. and British submarines tend to be single-hulled as this configuration maximizes payload for a given displacement (by minimizing structure weight). One the other hand,

Russian submarines tend to be double-hulled, since they value the improved survivability and robustness more than extreme efficiency.

2.7.2 **Noise**

Silence is an important requirement in submarine design. A submarine that can suppress noise can provide tactical and strategic advantages. The main objective of this feature is to detect other surface or submarine vehicles before they can detect you. Design measures must be taken to reduce the radiated noise from the machinery and the submarine's functional systems. When these machines and systems are in operation, the hull vibrates and transmits radiated noise. The random or harmonic vibration of these mechanisms that are not absorbed by the special mountings on the hull is transmitted to the water and is detectable at large distances as noise. Propeller motion and water flowing over the hull also have noise associated with both sinusoidal and random excitation.

2.7.3 **Safety**

Designers use safety factors to guard against failure at operational depths, and they are used to account for limitations of material and structural analysis. Since buckling is the dominant failure mode for most manned submersibles, engineers primarily use safety factors for the prevention of buckling failure, but they should also consider others such as cracks. Since there is always some element of the unknown, safety factors are used to take care of this unknown element.

Although all the analysis may have seemed to go well, there is still a possibility of failure. To reduce the probability of failure, proof tests are performed. Proof tests are

used to make sure that the pressure vessel can withstand the load at the nominal or slightly greater value of the design depth. While the concept of proof testing is effective, in specific situations there may be significant drawbacks such as

1. the test itself may induce a flaw
2. difficult to simulate the dynamic loads seen in service
3. difficult to simulate cyclic fatigue
4. expensive at full scale

Scaled model tests are often used to overcome these difficulties, but raise their own issues of fidelity. Finally, the penalty for over-conservatism in a design will be loss of payload and/or mission effectiveness. We must always remember that submarine design is a zero-sum game, the weight is fixed by size (displacements).

CHAPTER THREE

Stability Theory

3.1 Introduction

In the design of submersibles, the most critical aspect is designing against failure. We have seen in chapter two that there are different modes of failure which must be considered in realistic designs. In most areas of design, the key is to design against yielding. Although it is an important aspect to look into, submersibles tend to be stability dominated under the applied hydrostatic pressure load, and this load is normally much lower than the load required to yield the structure (at least down to moderate depths, a few thousand feet).

Instability may occur in many different structures, but it depends on the state of the system and often results due to a transition from predominately membrane (direct compression) behavior to bending. M. Farshad describes the state of a system as

> *The state of a system is a collection of values of the system parameters at any instant of time The state of the system depends on system parameters and environmental conditions.*[16]

In structural problems, the system parameters are the geometry of the structure and the material from which it was made. The environmental conditions are the applied loads and other factors such as temperature, which modify the situation. With this understanding of the system state, stability and instability can be defined as

1. Stability -The state of a system is called stable if a small perturbation in a system parameter and/or an environmental condition would have negligible changes in the present state of the system.
2. Instability- The state of a system is called unstable if a small perturbation in a system parameter and/or an environmental condition would have drastic changes in the present state of the system.

The state of equilibrium in a system can be either stable, unstable, or neutral.

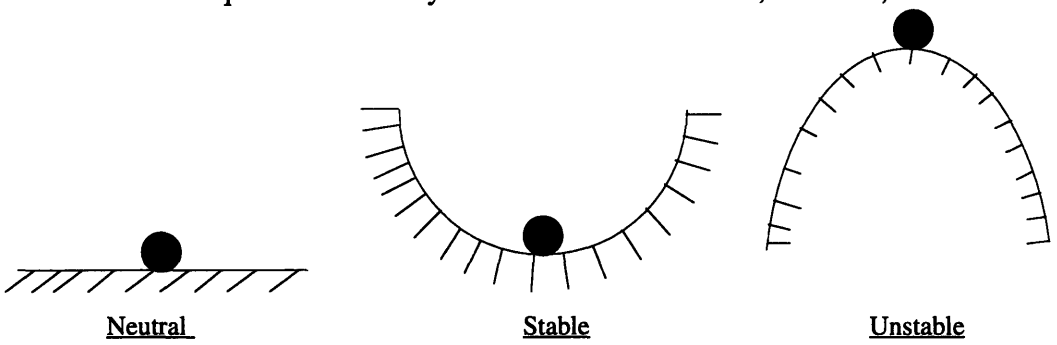

Figure 3.1.1: **Equilibrium States**

Since we know that submersibles may become unstable due to hydrostatic loading, we will concentrate on this aspect. A special case of instability is buckling, and this occurs in structures subjected to compressive loads. In many structural problems, as a load is applied to a structure in equilibrium, the structure could approach another equilibrium state with small variation of the initial equilibrium state. It is the goal of this chapter to explain the theory behind the instability of circular rings and circular cylinders.

3.2 Ring Deformation Theory

The circular ring is an ideal structure that undergoes uniform radial displacement under an external hydrostatic pressure load, but when the critical pressure is reached, the ring becomes unstable and collapses. In design, it is very important to predict the point of failure (collapse) so that the designed structure will not fail under normal operating conditions. The model used in the prediction of the critical buckling load can be developed in at least two ways. One such way is the rigorous approach by Don Brush and Bo Almroth (**Reference 7**). Brush and Almroth used detailed displacement relations of a infinitesimal slice of the ring to formulate to an equation that relates the stiffness of the ring and its radius to the critical buckling load of the structure. On the other hand, Timosheko (**Reference 8**) provided a more intuitive approach to the problem which

examined the bending of a curved bar to derive the prediction equation. First, we will examine the Brush and Almroth approach.

For the Brush & Almroth derivation we will assume that the ring is thin, isotropic, linear elastic, and symmetric about its normal axis. Furthermore, to simplify the equations, only bending in the plane of the ring will be allowed.

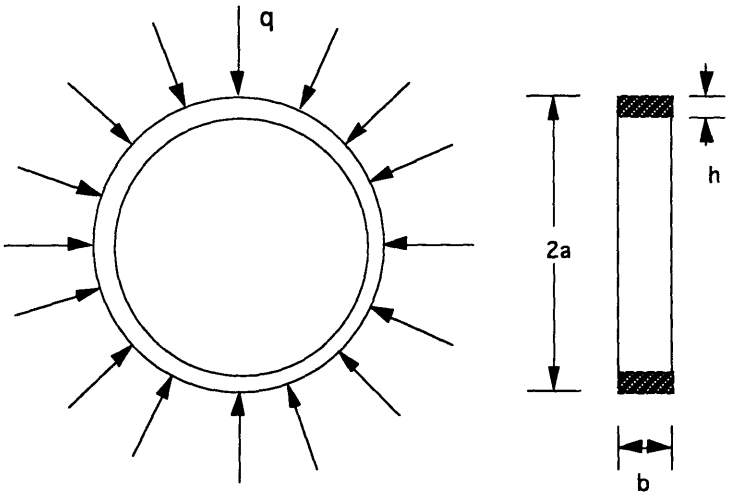

Figure 3.2.1: **Ring Under Hydrostatic Pressure**

In figure 3.2.1, a represents the radius of the ring in the undeformed configuration, h is the thickness of the ring, and b is the width of the ring. Since p represents a uniform pressure load in the form of load per unit area, the uniform load per unit circumferential length is represented by the variable q, which is obtained from the relation $q=pb$ Also, one other assumption taken into account is the fact that **h<<a**.

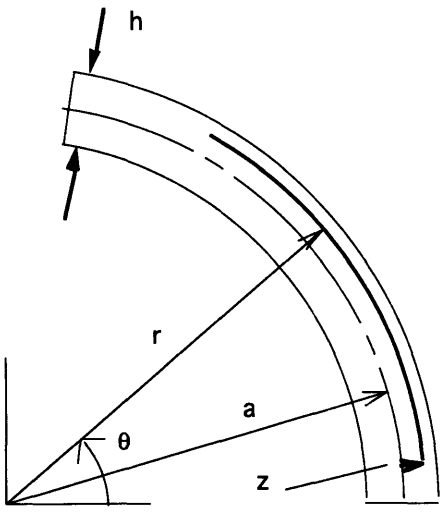

Figure 3.2.2: **Ring Coordinate System**

For convenience, the cylindrical polar coordinate system is adopted. In the new coordinate system (see figure 3.2.2), the variables r and θ describe the positions on the ring. The additional variable z is defined as z=r-a , and it is measured in the positive outward normal direction of the mid-surface of the ring.

In the derivation of the relationship between the undeformed ring and the deformed ring , only a small slice (arc) will be considered. The variables $\overline{v}$ and $\overline{w}$ represent the components of displacement in the θ and z directions respectively. From the kinematic relations for a thin ring, an expression for the extensional strain ($\overline{\varepsilon}$) of the arc at the mid-surface of the ring can be derived, as described in the following paragraphs.

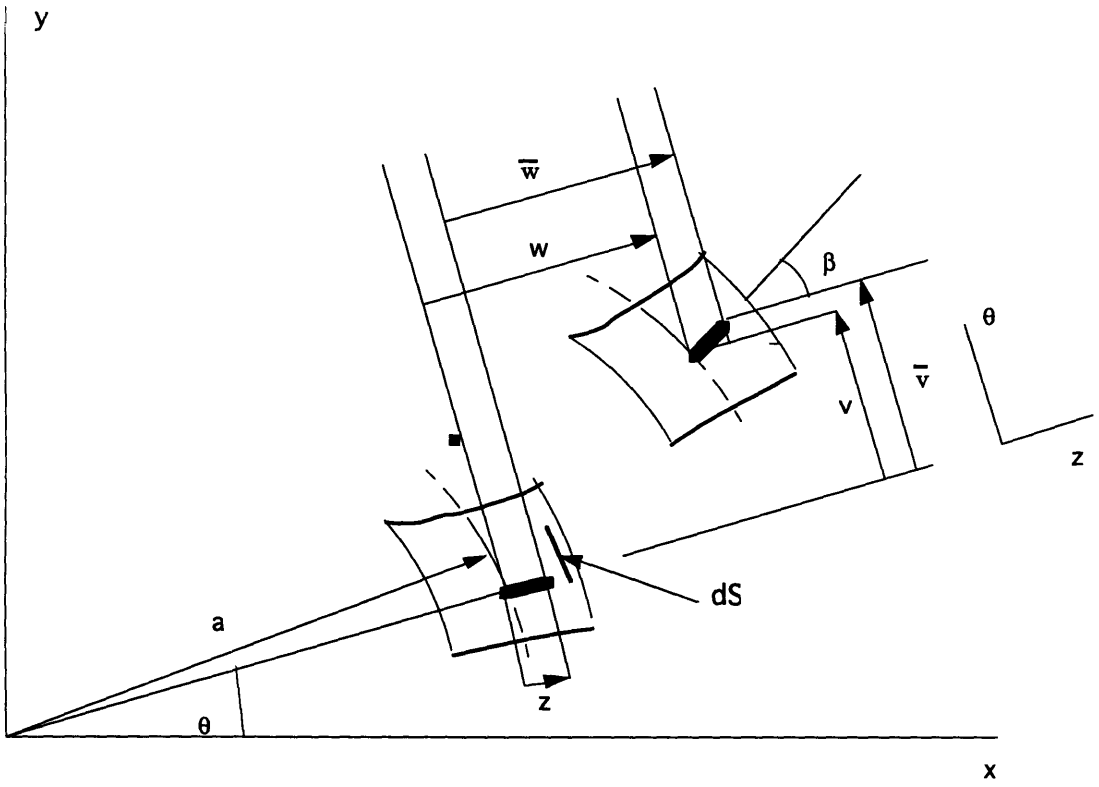

Figure 3.2.3: **Arc Segment Deformation**

The approximations made in **figure 3.2.3** are that the normal to the centroidal surface of the undeformed and deformed arc segments of the ring remain normal during deformation. Also, during the deformation process the length of the normal, measured by the variable z, remains unchanged. The components of displacement($\bar{v}$, $\bar{w}$) can be related to the displacement components of points on the centroidal surface(v,w) through the relations

$$\bar{v} = v + z\beta \tag{3.2.1}$$

$$\bar{w} = w \tag{3.2.2}$$

where β represents the rotation angle of the normal to the centroidal surface during deformation, and this angle is represented as

$$\beta = \frac{v - w'}{a} \tag{3.2.3}$$

In this expression, the " ' " prime denotes differentiation with respect to "θ". Equations 3.2.1-3 are used along with some detailed displacement relationships in **reference 7** to obtain an expression for the extensional strain in the circumferential

direction of the arc segment. The resulting extensional strain in terms of the displacement variables gives

$$\bar{\varepsilon} = \frac{v' + w}{a} + \frac{1}{2}\beta^2 + z\frac{\beta'}{a} \tag{3.2.4}$$

Finally, the change in curvature κ of the arc segment is equal to the rate of change of the angle β, and the extensional strain (ε) of a point on the (non- centroidal) circumferential line can be determine at the position z=0. Thus, the new expression for extensional strain of the line element dS can be represented as the following:

$$\bar{\varepsilon} = \varepsilon + z\kappa \tag{3.2.5}$$

where

$$\varepsilon = \frac{v' + w}{a} + \frac{1}{2}\beta^2 \tag{3.2.6}$$

and

$$\kappa = \frac{\beta'}{a} \tag{3.2.7}$$

3.2.1 **Linear Stability**

The circular ring is said to be in a state of equilibrium until it is perturbed from this position. Thus, the stability of a structural system can be determined from the minimum potential energy criterion. This criterion states

> *A structure is in a configuration of stable equilibrium if and only if the change in total potential energy corresponding to any sufficiently small, kinematically admissible (satisfies particular boundary conditons and continuity equations) displacement is positive.* [17]

The total potential energy is the sum of the bending (U_b) and membrane (U_m) strain energy of the ring and the potential energy of the applied pressure load (Ω). The total potential energy relation is represented in the following expression

$$V = U_m + U_b + \Omega \tag{3.2.8}$$

In looking at the strain energy components of the total potential energy, the total strain energy can be expressed as

$$U = \frac{Ea}{2}\iint (\varepsilon + z\kappa)^2 \, dA d\theta$$

where ε and κ are both unique functions of θ.

Thus, an integration with respect to θ gives a new expression for the strain energy separated into its membrane and bending components.

$$U = \frac{EAa}{2}\int \varepsilon^2 d\theta + \frac{EIa}{2}\int \kappa^2 d\theta \qquad (3.2.9)$$

where

the cross-sectional moment of inertia $I = \int z^2 \, dA$

A= the cross-sectional area

After substituting the full expressions for ε and κ into the previous equation results in

$$U_m = \frac{EAa}{2}\int_0^{2\pi}\left[\frac{v'+w}{a} + \frac{1}{2}\left(\frac{v-w'}{a}\right)^2\right]^2 d\theta \qquad (3.2.10)$$

$$U_b = \frac{EIA}{2}\int_0^{2\pi}\left(\frac{v'-w''}{a^2}\right)^2 d\theta \qquad (3.2.11)$$

For this system, the potential energy of the applied pressure load is equal to the negative of the work during the deformation process. Assuming a hydrostatic pressure loading, the load stays normal to the surface of the ring during deformation, and the ring thickness changes very slightly during this process. Therefore, the change in area enclosed by the centroidal surface and that of the outer surface is approximately the same. With this information, the potential energy of the applied pressure load can be expressed as

$$\Omega = -q(\pi a^2 - A^*) \qquad (3.2.12)$$

where A* is the enclosed area after deformation

To see how the potential energy changes during deformation, equation 3.2.12 can be shown as a function of the displacement terms (v &w) such that it takes the form of the following:

$$\Omega = qa\int_0^{2\pi}\left[w + \frac{1}{2a}\left(v^2 - vw' + v'w + w^2\right)\right] d\theta \qquad (3.2.13)$$

To observe the potential energy for a deformed state, a displacement function is introduced to minimum potential energy criterion.

$$\begin{aligned} v &\rightarrow v_0 + v_1 \\ w &\rightarrow w_0 + w_1 \end{aligned} \tag{3.2.14}$$

where v_0 and w_0 corresponds to the circular equilibrium configuration, and v_1 and w_1 are small variations.

For the circular equilibrium configuration, v_0 , w_0' and their derivatives are equal to zero. Since this circular configurations equilibrium is independent of q, the first variation of the minimum potential energy criterion (δV) is equal to zero. Therefore, the second variation of the criterion needs to be computed, and a collection of all the squared terms of v_1 and w_1 results in

$$\delta^2 V = \delta^2 U_m + \delta^2 U_b + \delta^2 \Omega \tag{3.2.15}$$

where the components give

$$\delta^2 U_m = \frac{EA}{a} \int_0^{2\pi} \left[\left(v_1' + w_1 \right)^2 + \frac{w_0}{a} \left(v_1 - w_1' \right)^2 \right] d\theta \tag{3.2.16}$$

$$\delta^2 U_b = \frac{EI}{a^3} \int_0^{2\pi} \left[\left(v_1' - w_1'' \right)^2 \right] d\theta \tag{3.2.17}$$

$$\delta^2 \Omega = q \int_0^{2\pi} \left({v_1}^2 - v_1 w_1' + v_1' w_1 + {w_1}^2 \right) d\theta \tag{3.2.18}$$

For axisymmetric deformation

$$\frac{w_0}{a} = -\frac{aq}{EA}$$

and the new expression for the second variation of potential energy yields

$$\delta^2 V = \frac{1}{a^3} \int_0^{2\pi} \left[EAa^2 \left(v_1' + w_1 \right)^2 + EI \left(v_1' - w_1'' \right)^2 + qa^3 \left(v_1 w_1' + v_1' w_1 + {w_1}^2 - {w_1'}^2 \right) \right] d\theta$$

To get the equations that describe the loss of stability, the Euler equations must be implemented into the problem, and these equations are

$$\frac{\partial F}{\partial v_1} - \frac{d}{d\theta}\frac{\partial F}{\partial v_1'} = 0$$
$$\frac{\partial F}{\partial w_1} - \frac{d}{d\theta}\frac{\partial F}{\partial w_1'} + \frac{d^2}{d\theta^2}\frac{\partial F}{\partial w_1''} = 0$$

where F is

$$F=\left[EAa^2\left(v_1'+w_1\right)^2+EI\left(v_1'-w_1''\right)^2+qa^3\left(v_1w_1'+v_1'w_1+w_1{}^2-w_1'^2\right)\right] \tag{3.2.19}$$

When these operations are carried out with the function F, the result yields the stability equations, and they are the following:

$$EAa^2\left(v_1'+w_1\right)'+EI(v_1-w_1')''=0 \tag{3.2.20}$$

$$EAa^2(v_1'+w_1)-EI(v_1-w_1')'''+qa^3(w_1''+w_1)=0 \tag{3.2.21}$$

3.3 Calculating the Critical Load

To solve for the critical buckliing load of the ring, the stability equations must be solved for specified boundary conditions. Since the stability equations are homogeneous differential equations, the general solution can easily be found. For the problem at hand, the boundary condition require that v_1, w_1 and their derivatives are periodic in θ. Thus,

$$v_1=\sum_n B_n \sin(n\theta) \qquad n=1,2,3,4.....$$
$$w_1=\sum_n C_n \cos(n\theta) \tag{3.3.1}$$

where B_n & C_n are constants, and the variable n is a positve integer value. Next, these qualified functions can be substituted into the the stability equations, giving

$$\left[n(nB+C)+n^2\frac{I}{Aa^2}(B+nC) \right] \sin(n\theta)=0 \qquad (3.3.2)$$

$$\left[(nB+C)+n^3\frac{I}{Aa^2}(B+nC)-(n^2-1)\frac{qa}{EA}C \right] \cos(n\theta)=0 \qquad (3.3.3)$$

The above equations are valid for all values of θ, and the trigonometric terms (cosine and sine) are generally nonzero. The stability criterion is therefore that the determinant of the coefficients must be zero. The resulting expression takes the following form

$$q=\frac{(n^2-1)EI}{\left(1+\frac{I}{Aa^2}\right)a^3} \quad n=2,3,4,.....$$

In the present case, I/Aa^2 is small compared to unity because of the thin ring assumption stated earlier, and the expression simplifies to:

$$q=\frac{(n^2-1)EI}{a^3} \quad n=2,3,4,.... \qquad (3.3.4)$$

Since n=1 produces rigid body movement, the first mode of interest is n=2. Thus, when n is equal to 2, the critical buckling load is achieved

$$q_{cr}=3\frac{EI}{a^3} \qquad (3.3.5)$$

This result is considered to be the load at which the ring collapses.

3.4 Timoshenko's Bending Theory of Curved Bars

In contrast to Brush and Almroth, Timoshenko's approach to getting the kinematic relations needed for stability analysis involved the bending theory of curved bars. To illustrate this theory further, consider a thin bar (**AB**) that has an initial curvature with radius $\mathbf{r_0}$. When this bar is bent in the same plane of its initial curvature, the resulting radius of curvature of the center line of the bar is represented as **r**, and any point on the center line of the deformed bar can be found in terms of the polar coordinates **r** and θ. These relationships can represented pictorially in **figure 3.4.1**

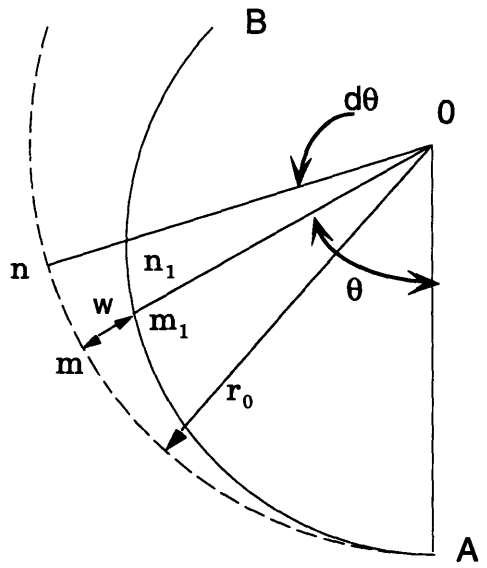

Figure 3.4.1: **Deformed Curved Bar**

To relate the change in curvature of the thin bar to the load which produced this deformation, we must derive the necessary kinematic relation. From basic kinematics, the relationship between the curvature and the applied moment is known as

$$\kappa = \frac{M}{EI}$$

And the new relationship for a change in curvature can be represented as

$$EI\left(\frac{1}{r} - \frac{1}{r_0}\right) = -M \qquad (3.4.1)$$

where (**EI**) is the bending stiffness of the bar.

This bending stiffness can be found from the slope of linear portion of the moment-curvature curve for this configuration. Also, the minus sign on the moment term is due to the fact that the moment that produces an increase in curvature is defined as a negative moment.

Now, the change in curvature will be taken down to an incremental level so that a relationship between radial deflection (**w**) and curvature (κ) can be derived. First, take a small element (**mn**) of the initially curved bar (represented as dashed lines) and define its length as

$$ds = r_0 d\theta \tag{3.4.2}$$

so that $$\frac{d\theta}{ds} = \frac{1}{r_0}$$

In considering only small deformations, the radial displacement (**w**) from a point **m** or **n** is considered positive in the direction toward the center point (**0**). This radial displacement is just one component of the total displacement vector, and the other component is a tangential displacement. Although there exists a tangential component, it will be neglected, and we will assume that the curvature of the segment **mn** will be the same as the deformed segment $\mathbf{m_1 n_1}$.

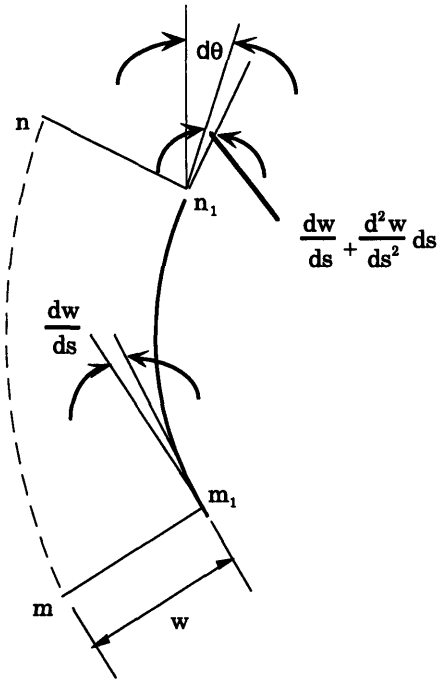

Figure 3.4.2: **Angle Relationship of Segment $\mathbf{m_1 n_1}$**

To get an expression for the deformed curvature as a function of the radial displacement values (v,w), the deformed curvature of the bar is taken as the initial curvature plus a small incremental curvature, and figure 3.4.2 illustrates this fundamental idea. The resulting expression for the deformed curvature is stated as

$$\frac{1}{r} = \frac{d\theta + \frac{d^2w}{ds^2}ds}{ds\left(1 - \frac{w}{r_0}\right)}. \tag{3.4.3}$$

Neglecting higher order terms and substituting equations 3.4.1-2, a differential equation for the curvature can be represented as

$$\frac{d^2w}{d\theta^2} + w = -\frac{Mr_0^2}{EI} \tag{3.4.4}$$

Therefore, the radial displacement can be found at any position θ given the initial radius, the applied moment, the material, and the shape, but the results are dependent upon the applied boundary conditions.

3.5 **Timoshenko's Buckling Theory of Circular Rings**

A perfectly circular ring will remain in equilibrium under uniform lateral pressure, but the magnitude of the load must be lower than that of a critical load at which instability (collapse) occurs. Therefore, a ring with a slight deflection from the circular configuration under uniform lateral pressure can remain in equilibrium, if a small change in the applied load doesn't cause a major change in its existing state. Once the pressure reach a point where small changes in the applied load produces large changes in the existing state, the critical state of the system has been reached. The load required to keep the ring in this deformed shape is the critical load of the structure.

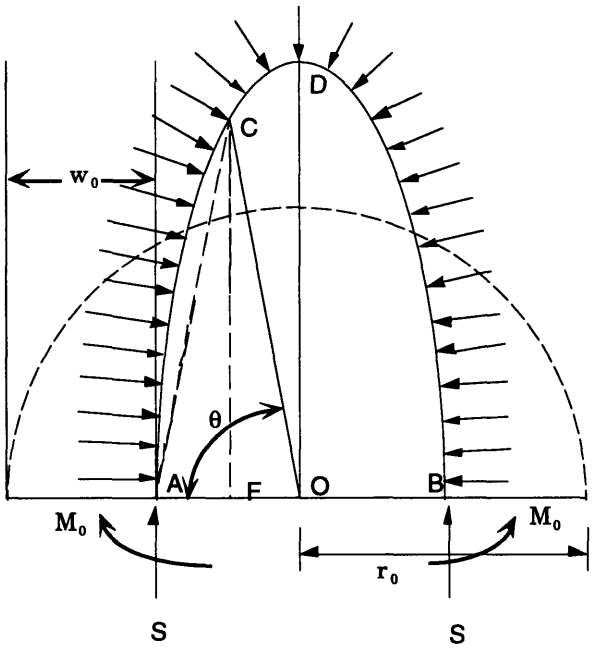

Figure 3.5.1 : **Ring Free Body Diagram**

Since a ring has many planes of symmetry, we will make use of that geometric information, and only use half of the ring in the analysis of this problem. With half the ring being used in the analysis, the reaction forces of the other half must be represented, and they are present in the form of moments ($\mathbf{M_0}$) and normal loads (**S**). This can be shown best in *Figure* **3.5.1**. In this figure, the small deformation is represented (exaggerated) by the solid line with the uniform lateral load , and the dotted lined is the original circular shape with radius $\mathbf{r_0}$. The radial displacements at points **A** and **B** are represented as $\mathbf{w_0}$, and the normal compressive load (**S**) at these points is shown to be

$$S=q(r_0 - w_0) \tag{3.5.1}$$

where **q** is the load per unit circumferential length.

The total moment at any point on the deformed ring is given as

$$M = M_0 - qr_0(w_0 - w) \tag{3.5.2}$$

where

$$w = r_0 - \overline{OC}$$

After substituting this equation into the differential *equation* 3.4.4, we obtain

$$\frac{d^2w}{d\theta^2}+w\left(1+\frac{qr_0^3}{EI}\right)=\frac{-M_0r_0^2+qr_0^3w_0}{EI}. \tag{3.5.3}$$

Solving the differential equation 3.5.4 yields the general solution and particular solution for the radial displacement (**w**), and it is given as

$$w=A\sin(k\theta)+B\cos(k\theta)+\frac{-M_0r_0^2+qr_0^3w_0}{EI+qr_0^3} \tag{3.5.4}$$

where

$$k=\sqrt{1+\frac{qr_0^3}{EI}} \tag{3.5.5}$$

Next, to solve for the constants **A** and **B**, the boundary conditions (**B.C.'s**) of symmetry are applied in the form of

$$\left(\frac{dw}{d\theta}\right)_{\theta=0}=0 \qquad \text{and} \qquad \left(\frac{dw}{d\theta}\right)_{\theta=\frac{\pi}{2}}=0$$

As a result of applying the first B.C., the constant **A**=0. Also,it can be shown that either **B**=0 or $\sin\frac{k\pi}{2}=0$ to satisfy the second B.C., but we notice that the smallest root other than zero is $\frac{k\pi}{2}=\pi$ with k=2. Therefore, the critical pressure can be solved for by substituting this **k** value into *equation* **(3.5.5)** to yield

$$q_{cr}=\frac{3EI}{r_0^3} \tag{3.5.6}$$

This is the same result as found by Brush and Almroth. It should be noted that the same solution can be achieved by using rigorous energy methods and by using intuitive deformation of curved bars.

3.6 **Stability of a Ring on an Elastic Foundation**

A limiting case of a point-supported ring would be a ring on an elastic foundation, and the foundation consist of an infinite set of elastic radial springs. The configuration of this setup is shown in **figure 3.6.1.** In the previous cases for a uniform ring, we have seen how a uniform ring buckles due to a radially applied external pressure load. In this case, the elastic foundation acts as stiffening agent and effectively increases the critical buckling load of the ring. The pressure load q_f for this elastic foundation problem is given as

$$q_f = -k_f w \tag{3.6.1}$$

where

q_f - is in pounds per inch between the ring and foundation

k_f - is a constant foundation modulus(lbs / in^2)

w- is the radial deflection

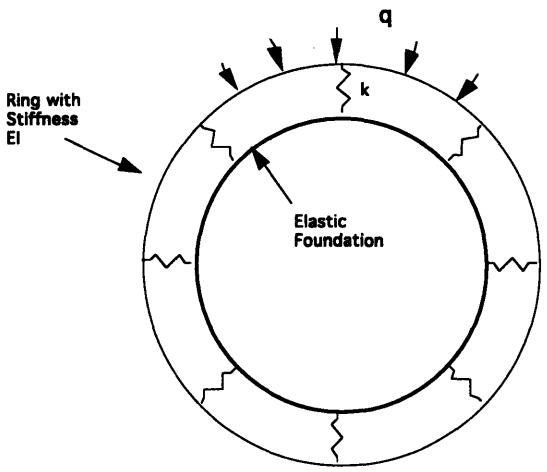

Figure 3.6.1: **Ring On An Elastic Foundation**

In solving this new problem, we will begin with the strain energy of the foundation which can be represented as

$$U_f = -\frac{a}{2}\int_0^{2\pi} q_f w \, d\theta$$

We can substitute **equation (3.6.1)** into the expression above to yield

$$U_f = \frac{ak_f}{2}\int_0^{2\pi} w^2 \, d\theta \tag{3.6.2}$$

With this expression for strain energy, the modified form of the stability equations can be obtain by taking the second variation of this expression and adding it to **eq.3.2.15,** and the second variation of U_f is shown as

$$\delta^2 U_f = ak_f \int_0^{2\pi} w_1^{\,2}\, d\theta$$

After this term is incorporated into the integrand F (**see section 3.2**), the Euler equations are solved, and the stability equations results in

$$EAa^2(v_1' + w_1)' + EI(v_1 - w_1')'' = 0 \qquad (3.6.3)$$

$$EAa^2(v_1' + w_1) - EI(v_1 - w_1')''' + qa^3(w_1'' + w_1) - k_f a^4 w_1 = 0 \qquad (3.6.4)$$

Finally, equations 3.3.1 are introduced to the stability equations above. This action leads to a pair of homogeneous equations. As we all know, these equations can be solved for a nontrivial solution by taking the determinant of the coefficients and setting the expression equal to zero. These coefficients in determinant form gives

$$\begin{vmatrix} n^2\left(1+\dfrac{I}{Aa^2}\right) & n\left(1+n^2\dfrac{I}{Aa^2}\right) \\ n\left(1+n^2\dfrac{I}{Aa^2}\right) & \left(1+n^4\dfrac{I}{Aa^2}+\dfrac{k_f a^2}{EA}\right)-(n^2-1)\dfrac{qa}{EA} \end{vmatrix} = 0 \qquad (3.6.4)$$

Neglecting small terms, the solution can be shown as

$$q = (n^2-1)\frac{EI}{a^3} + \frac{1}{n^2-1}k_f a \qquad n=2,3,4.... \qquad (3.6.5)$$

The critical load of the system can be determined by varying n to find the lowest eigenvalue; thus, this eigenvalue is the critical load. We see that this buckling pressure of a ring on an elastic foundation is equal to that of a thin ring plus a term related to foundation stiffness. Interestingly, this additonal term is inversely proportional to (n^2-1); however, the unstiffened ring result is directly proportional. This means that the critical mode will not necessarily be n=2, but will depend upon the relative stiffness of the ring and foundation.

3.7 L.H. Donnell's Cylindrical Shell Instability Theory

Cylinders are simple geometric shapes that have a variety of structural applications such as bridges, building supports, tanks, pipelines, submarine pressure hulls, and many more. Because of the large usage of cylinders, researchers have been investigating the structural behavior of these configurations. More specifically, stability problems have been researched for many years, and there are some common solutions for specific cylindrical shell stability problems. L.H. Donnell solved the stability problem in the 1930's using his simplified equations. Due to the model's ease of use, they were used widely in the scientific community before computer methods came along. To understand the basis for what the computers solve, we look at Donnell's solution for cylindrical shell buckling.

3.7.1 Cylindrical Shell Kinematic Equations

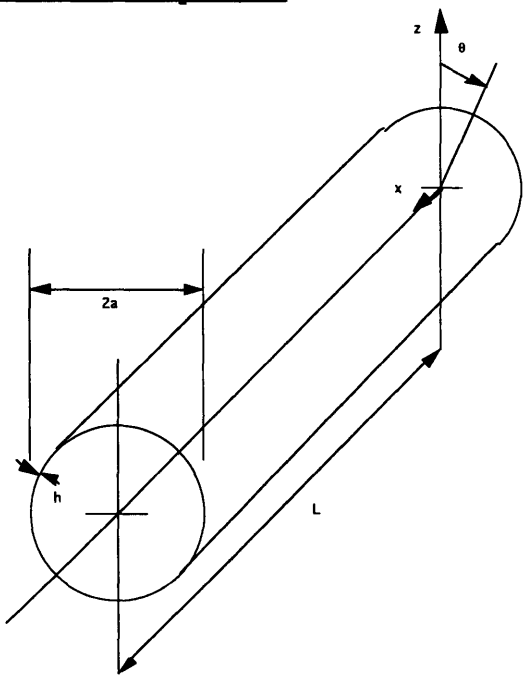

Figure 3.7.1: **Cylinder Parameters**

Assume the cylinder in figure 3.7.1 is a thin-walled cylindrical shell with a length of **L**. Also, we will denote the shell thickness as **h**, and the radius of the undeformed centroidal surface as **a**. To satisfy this thin-walled assumption, we will enforce **h** to be much less than the radius **a**. Furthermore, we need a useful and easy coordinate system to measure the magnitude of these variable, and the obvious choice is to use a cylindrical coordinate system (x,θ,z). From the figure, we can see that x is axial, θ is circumferential, and z is measured radially outward from the centroidal surface.

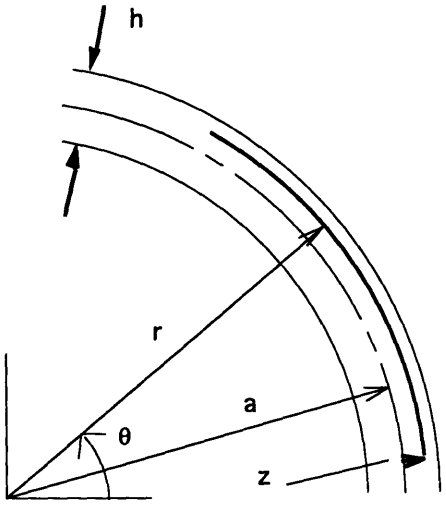

Figure 3.7.2: **Cylinder Coordinate System**

Now, let's consider a cylinder loaded with an external lateral load and an edge load. This loading will induce internal stresses within the shell structure, and we can use this information to find the magnitude of the forces and moments at any section of the shell. For example, take a small piece of the loaded shell with area dx(a dθ), and create a free-body diagrams shown as

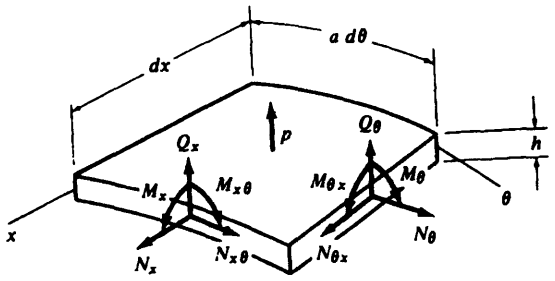

Figure 3.7.3: **Cylindrical Shell Element**

The magnitude of these elemental forces is related to the internal shell stress by the following expressions

In-plane normal and shearing forces(lb/in)

$$N_x = \int_{-h/2}^{h/2} \bar{\sigma}_x \left(1+\frac{z}{a}\right) dz \qquad N_{x\theta} = \int_{-h/2}^{h/2} \bar{\tau}_{x\theta} \left(1+\frac{z}{a}\right) dz$$

$$N_\theta = \int_{-h/2}^{h/2} \bar{\sigma}_\theta dz \qquad N_{\theta x} = \int_{-h/2}^{h/2} \bar{\tau}_{\theta x} dz$$

Bending moments(lb-in/in)

$$M_\theta = a\int_{-h/2}^{h/2} \bar{\sigma}_\theta z \, dz \qquad M_x = a\int_{-h/2}^{h/2} \bar{\sigma}_x \left(1+\frac{z}{a}\right) z \, dz \qquad (3.7.1)$$

Twisting moments(lb-in/in)

$$M_{x\theta} = a\int_{-h/2}^{h/2} \bar{\tau}_{x\theta} \left(1+\frac{z}{a}\right) z \, dz \qquad M_{\theta x} = a\int_{-h/2}^{h/2} \bar{\tau}_{\theta x} z \, dz$$

Transverse shearing forces(lb/in)

$$Q_x = \int_{-h/2}^{h/2} \bar{\tau}_{xz} \left(1+\frac{z}{a}\right) dz \qquad Q_\theta = \int_{-h/2}^{h/2} \bar{\tau}_{\theta z} dz$$

where $\bar{\sigma}_x, \bar{\tau}_{\theta x}$, etc , represents the components of stress through the shell thickness.

For equilibrium of the small patch, the summation of the moments must be equal to zero, and the summation of the forces must be equal to zero. Although this patch should be in equilibrium undeformed, it should also be in equilibrium slightly deformed before

the shell structure buckles. Thus, we will determine the nonlinear equilibrium equations for this condition.

First, let's look at the small slice in the deformed configuration with its acting forces. This deformed structure shown in figure 3.7.4 rotates slightly during deformation through angles β_x and β_θ, but we assume that this rotation is small. As we know for small angles β,

$$\sin\beta \approx \beta$$
$$\cos\beta \approx 1.$$

Also, the interactions of the transverse shear forces with the rotations are assumed small; thus, they will be neglected.

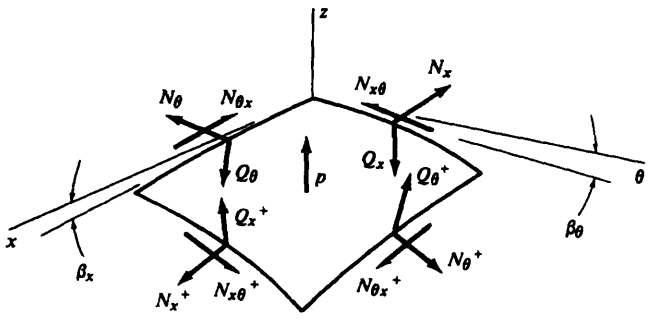

Figure 3.7.4: **Deformed Shell Element**

The equilibrium equations are derived by summing the forces in the coordinate system directions in figure 3.7.4 and by summing the moments in figure 3.7.5. The resulting equations of equilibrium are shown as

$$\begin{aligned} aN_{x,x} + N_{\theta x,\theta} &= 0 \\ aN_{x\theta,x} + N_{\theta,\theta} &= 0 \\ a^2M_{x,xx} + aM_{x\theta,x\theta} + aM_{\theta x,x\theta} + aM_{\theta,\theta\theta} - aN_\theta - a^2N_x\beta_{x,x} & \\ -a^2N_{x\theta}\beta_{\theta,x} - aN_{\theta x}\beta_{x,\theta} - aN_\theta\beta_{\theta,\theta} &= -pa^2 \end{aligned} \qquad (3.7.2)$$

where a subscripted comma refers to differentiation with respect to the variable following the comma. For example, $N_{x,x} = \dfrac{\partial N_x}{\partial x}$.

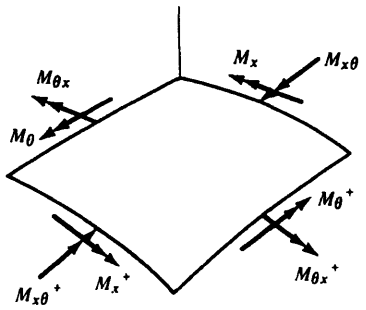

Figure 3.7.5: **Deformed Shell Element**

Finally, Donnell based his equations on the the following kinematic relations:

middle -surface kinematics relations (Eq. 3.7.3)

1. Strains

$$\varepsilon_x = u_{,x} + \frac{1}{2}\beta_x{}^2 \qquad \gamma_{x\theta} = \left(\frac{u_{,\theta}}{a} + v_{,x}\right) + \beta_x\beta_\theta$$

$$\varepsilon_\theta = \frac{v_{,\theta} + w}{a} + \frac{1}{2}\beta_\theta{}^2$$

2. Curvature

$$\kappa_x = \beta_{x,x} \qquad \kappa_{x\theta} = \frac{1}{2}\left(\frac{\beta_{x,\theta}}{a} + \beta_{\theta,x}\right)$$

$$\kappa_\theta = \frac{\beta_{\theta,\theta}}{a}$$

3. Rotations

$$\beta_x = -w_{,x} \qquad \beta_\theta = -\frac{w_{,\theta}}{a}$$

constitutive equations (Eq. 3.7.4)

$$N_x = C(\varepsilon_x + \nu\varepsilon_\theta) \qquad M_x = D(\kappa_x + \nu\kappa_\theta)$$

$$N_\theta = C(\varepsilon_\theta + \nu\varepsilon_x) \qquad M_\theta = D(\kappa_\theta + \nu\kappa_x)$$

$$N_{x\theta} = C\frac{1-\nu}{2}\gamma_{x\theta} \qquad M_{x\theta} = D(1-\nu)\kappa_{x\theta}$$

where

$$C = \frac{Eh}{1-\nu^2}$$

$$D = \frac{Eh^3}{12(1-\nu^2)}$$

3.7.2 **Equilibrium Equations**

In determining the equilibrium equations, we will substitute the constitutive and kinematic relations into the equilibrium equations (3.7.2). Neglecting higher order terms in u,v,w, the resulting action yields the linear equilibrium equations

$$\begin{aligned} aN_{x,x} + N_{x\theta,\theta} &= 0 \\ aN_{x\theta,x} + N_{\theta,\theta} &= 0 \\ D\nabla^4 w + \frac{1}{a}N_\theta &= p \end{aligned} \qquad (3.7.5)$$

3.7.3 **Stability Equations**

In determining the stability equations, we will use the theory of minimum potential energy. This is the same method used to determine the circular ring's stability equations. To get an expression for the total potential energy of the circular cylindrical shell structure in a slightly perturbed state, displacement relations are introduced to the total potential enegy equation (equation 3.2.8).

The displacement relations are

$$\begin{aligned} u &\rightarrow u_0 + u_1 \\ v &\rightarrow v_0 + v_1 \\ w &\rightarrow w_0 + w_1, \end{aligned}$$

where

u_0, v_0, w_0 - prebuckling deformation

u_1, v_1, w_1 - buckled deformation.

Through the use of variational calculus on the resulting expression , the second variation (δ^2) of the total potential energy (V) is taken. Due to the linearity of the potential energy of the applied lateral pressure load, we find that $\delta^2\Omega = 0$. Thus, the resulting equation only has strain energy variations involved. After algerbraic manipulation, this equation is expressed as

$$\frac{1}{2}\delta^2 V = a\frac{C}{2}\iint\left(\varepsilon_{x1}{}^2+\varepsilon_{\theta 1}{}^2+2\nu\varepsilon_{x1}\varepsilon_{\theta 1}+\frac{1-\nu}{2}\gamma_{x\theta 1}{}^2\right)dxd\theta \qquad (3.7.6)$$

$$+\frac{a}{2}\iint\left(N_{x0}w_{1,x}{}^2+N_{\theta 0}\frac{w_{1,\theta}{}^2}{a^2}+2N_{x\theta 0}w_{1,x}\frac{w_{1,\theta}}{a}\right)dxd\theta$$

$$+a\frac{D}{2}\iint\left(w_{1,xx}{}^2+\frac{w_{1,\theta\theta}{}^2}{a^4}+2\nu w_{1,xx}\frac{w_{1,\theta\theta}}{a^2}+2(1-\nu)\frac{w_{1,x\theta}{}^2}{a^2}\right)dxd\theta$$

where

$$N_{x0}=C(\varepsilon_{x0}+\nu\varepsilon_{\theta 0}) \qquad \varepsilon_{x0}=u_{0,x}+\frac{1}{2}w_{0,x}{}^2$$

$$N_{\theta 0}=C(\varepsilon_{\theta 0}+\nu\varepsilon_{x0}) \qquad \varepsilon_{\theta 0}=\frac{v_{0,\theta}+w_0}{a}+\frac{1}{2}\frac{w_{0,\theta}{}^2}{a^2}$$

$$N_{x\theta 0}=C\frac{1-\nu}{2}\gamma_{x\theta 0} \qquad \gamma_{x\theta 0}=(v_{0,x}+\frac{u_{0,\theta}}{a})+\frac{w_{0,x}w_{0,\theta}}{a}$$

$$\varepsilon_{x1}=u_{1,x}+w_{0,x}w_{1,x} \qquad \varepsilon_{\theta 1}=\frac{v_{1,\theta}+w_1}{a}+\frac{w_{0,\theta}w_{1,\theta}}{a^2}$$

$$\gamma_{x\theta 1}=\left(v_{1,x}+\frac{u_{1,\theta}}{a}\right)+\frac{w_{0,x}w_{1,\theta}}{a}+\frac{w_{0,\theta}w_{1,x}}{a}$$

$$N_{x1}=C(\varepsilon_{x1}+\nu\varepsilon_{\theta 1})$$

$$N_{\theta 1}=C(\varepsilon_{\theta 1}+\nu\varepsilon_{x1})$$

$$N_{x\theta 1}=C\frac{1-\nu}{2}\gamma_{x\theta 1}$$

$w_{0,x}$ and $w_{0,\theta}$ are prebuckling rotation terms that are negligibly small in most cases. Therefore, the contribution of these rotations will be deleted. Finally, the integrand (F) of the form shown in equation (3.2.19) can be substituted into the Euler equations.

Euler Equations

$$\frac{\partial F}{\partial u}-\frac{\partial}{\partial x}\frac{\partial F}{\partial u_{,x}}-\frac{\partial}{\partial\theta}\frac{\partial F}{\partial u_{,\theta}}=0$$

$$\frac{\partial F}{\partial v}-\frac{\partial}{\partial x}\frac{\partial F}{\partial v_{,x}}-\frac{\partial}{\partial\theta}\frac{\partial F}{\partial v_{,\theta}}=0$$

$$\frac{\partial F}{\partial w}-\frac{\partial}{\partial x}\frac{\partial F}{\partial w_{,x}}-\frac{\partial}{\partial\theta}\frac{\partial F}{\partial w_{,\theta}}+\frac{\partial^2}{\partial x^2}\frac{\partial F}{\partial w_{,xx}}+\frac{\partial^2}{\partial x\partial\theta}\frac{\partial F}{\partial w_{,x\theta}}+\frac{\partial^2}{\partial\theta^2}\frac{\partial F}{\partial w_{,\theta\theta}}=0$$

Solving these Euler equations and substituting the kinematic and constitutive equations, we obtain the uncoupled the stability equations as

Uncoupled

$$\nabla^4 u_1 = -\frac{\nu}{a} w_{1,xxx} + \frac{1}{a^3} w_{1,x\theta\theta}$$

$$\nabla^4 v_1 = -\frac{2+\nu}{a^2} w_{1,xx\theta} - \frac{1}{a^4} w_{1,\theta\theta\theta} \tag{3.7.7}$$

$$D\nabla^8 w_1 + \frac{1-\nu^2}{a^2} C w_{1,xxxx} - \nabla^4\left(N_{x0} w_{1,xx} + \frac{2}{a} N_{x\theta 0} w_{1,x\theta} + \frac{1}{a^2} N_{\theta 0} w_{1,\theta\theta} \right) = 0$$

3.7.4 Cylinder Buckling Under Uniform Lateral Pressure

Consider a circular cylindrical shell and subject it to a uniform lateral pressure $\mathbf{P_e}$ **(Figure 3.7.6)**. Then constrain the ends of the cylinder to be simply supported. Under these conditions, the prebuckling deformation will be axisymmetric, and when this axisymmetric deformed structure loses stability, the critical pressure ($\mathbf{P_{cr}}$) has been reached.

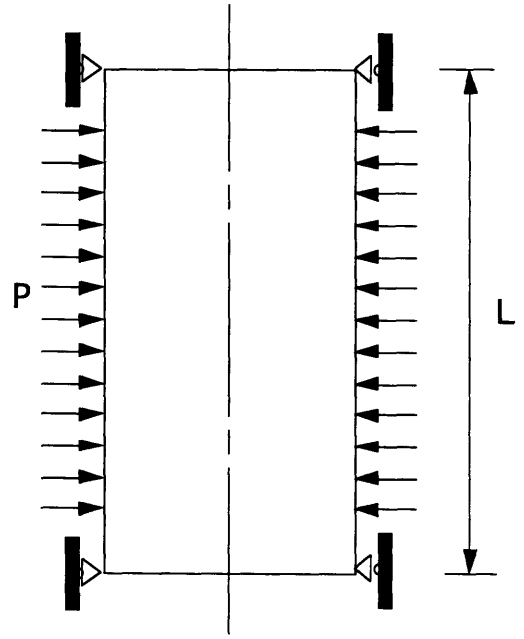

Figure 3.7.6 : **Cylinder Held Circular at the Ends**

Under uniform loading the cylinder will want to extend length wise, and if this motion is not constrained, N_{x0} =0. Since, there is no torsional loading, we neglect the effects of that term, $N_{x\theta 0} = 0$; thus, one of the stability equations can be simplified as

$$D\nabla^8 w + \frac{1-\nu^2}{a^2} C w_{,xxxx} - \frac{1}{a^2}\nabla^4 (N_{\theta 0} w_{,\theta\theta}) = 0 \tag{3.7.8}$$

Since prebuckling deformation involves some bending of the shell, the bending equations(**Eq 3.7.5**) can be specialized for axial symmetry, and this specialization yields

$$N'_x = 0 \tag{3.7.9}$$

$$Dw^{iv} + \frac{1}{a} N_\theta = -p_e \tag{3.7.10}$$

where

$$C = \frac{Eh}{1-\nu^2}$$

$$N_\theta = Eh\frac{w}{a}$$

With the boundary conditions given, there tends to be localized bending near the ends of the cylinder. To simplify the equations, this effect will be neglected, and the cylinder is assumed to be circular down its length. Since bending effects are neglected, the equations are membrane dominated. Membrane equations are equilibrium equations that govern deformation, and they can be derived from the linear equilibrium equation by setting the bending stiffness variable D=0. The resulting equations are

$$\begin{aligned} aN_{x,x} + N_{x\theta,\theta} &= 0 \\ aN_{x\theta,x} + N_{\theta,\theta} &= 0 \\ N_\theta &= pa \end{aligned} \tag{3.7.11}$$

For our proposed problem here, the **last equation** will be modified to reflect the new load orientation (p is negative inward). Therefore,the membrane equation gives us

$$N_{\theta 0} = -p_e a \tag{3.7.12}$$

Now, substitute this into the specialized stability equation (**Eq 3.7.8.**), and the new expression is

$$D\nabla^8 w + \frac{1-\nu^2}{a^2} C w_{,xxxx} + \frac{1}{a} p_e \nabla^4 w_{,\theta\theta} = 0 \qquad (3.7.13)$$

To solve this differential equation, we need to enforce boundary conditions, and as stated previously, the ends are simply supported. "Simply supported" means that the end will not be allowed to moved radially, but rotations are free.

Particular solutions to the differential equation have the form

$$w = C_1 \sin \bar{m}x \sin n\theta \qquad (3.7.14)$$

where

C_1 – constant

$$\bar{m} \equiv \frac{m\pi a}{L}$$

n &m=1,2,3,4,.....

Substituting this solution into **eq 3.7.13.** yields

$$p_e a = \frac{(\bar{m}^2 + n^2)}{n^2} \frac{D}{a^2} + \frac{\bar{m}^4}{n^2(\bar{m}^2 + n^2)^2} (1-\nu^2) C \qquad (3.7.15)$$

where

$$C = \frac{Eh}{1-\nu^2}$$

$$D = \frac{Eh^3}{12(1-\nu^2)}$$

Finally, this equation can be use to solve for the critical buckling load P_{cr} by setting m=1. For all values of m and n, the lowest eigenvalue is achieved when m=1. Implementing this result into equation 3.7.15 yields the final equation

$$\frac{p_e a}{Eh} = \frac{\left[(\pi a/L)^2 + n^2\right]^2}{n^2} \frac{(h/a)^2}{12(1-\nu^2)} + \frac{(\pi a/L)^4}{n^2\left[(\pi a/L)^2 + n^2\right]^2}. \qquad (3.7.16)$$

For a given circular cylindrical shell, equation 3.7.16 can be used to solve for the critcal load (p_e) of the structure.

3.7.5 **Timoshenko Cylinder Buckling Theory**

Timoshenko's derivation of the stability equations includes the nonlinear rotation-shear force interaction that were neglected by Brush and Almroth. Furthermore, Timoshenko assumes that N_θ is large compared to the other resultant forces; thus, the product of these resultant forces with displacement derivatives are neglected. Now, the equilibrium equations can produced by summing the forces in the directions of the coordinate system variables using the sum of moment equations is given as

$$aN_{x,x} + N_{\theta x,x} - N_\theta v_{,x\theta} - N_\theta w_{,x} = 0 \tag{3.7.17a}$$

$$N_{\theta,\theta} + aN_{x\theta,x} + \frac{M_{\theta,\theta}}{a} + M_{x\theta,x} = 0 \tag{3.7.17b}$$

$$M_{\theta x,x\theta} + aM_{x,xx} + \frac{M_{\theta,\theta\theta}}{a} + M_{x\theta,x\theta} - N_\theta - N_\theta \frac{v_{,\theta}}{a} + N_{,\theta} \frac{w_{,\theta\theta}}{a} + pa = 0 \tag{3.7.17c}$$

Recalling the Brush -Almroth force summation equations (**3.7.2**), you will see that equations (**3.7.17a -3.7.17c**) show a slight variation. Brush and Almroth neglect the moment contributions in equation 3.7.17b due to the shallow cylinder assumption. Also, Timoshenko doesn't neglect the quadratic nonlinear interaction terms between transverse shear forces as do Brush and Almroth. Finally, Brush &Almroth assume that rotations are negligibly small. One thing to note is that for buckling analysis the applied load is taken to be compressive, and this accounts for the sign change on (**pa**).

Assuming that the cylinder remains circular and undergoes uniform circumferential compression under the externally applied pressure load, a particular solution can be obtained such that

$v=0 \qquad N_x = 0 \qquad N_\theta = pa$

$M_x = M_\theta = M_{x\theta} = 0 \qquad w = \frac{a^2 p}{Eh}$

In this this buckling derivation, only small deflections from the equilibrium position are considered. Taking this into consideration, we will set

$$N_\theta = pa + N'_\theta \tag{3.7.18}$$

where N'_θ represents a small variation in the resultant force **pa**. Next, substitute $N_\theta(1+\varepsilon_1)$ for N_θ and $p(1+\varepsilon_1)(1+\varepsilon_2)$ for **p** in the equilibrium equation. This action will take stretching of the midddle surface into account.

Finally, the resulting equilibrium equations can be solved by using the constitutive and kinematic relations given in **section 3.7.1** to get these equilibrium equations in terms of the displacement variables (u,v,w), but the boundary conditons must be satisfied. The boundary conditions for this problem requires that the ends be simply supported such that w and $w_{,xx}$ are zero at the ends. With this modified form of the equations, the buckling displacements given as

$$u = A \sin n\theta \sin \frac{\pi x}{L}$$

$$v = B \cos n\theta \cos \frac{\pi x}{L}$$

$$w = C \sin n\theta \cos \frac{\pi x}{L}$$

can be substituted into the equilibrium equations and solved by setting the determinant of the coefficients of (A,B,C) equal to zero. It must be noted that these equations are given with the assumption that x is measured from the middle cross-section of the cylinder. This methodology is very similar to the action perforrmed to find the critical load of the ring. After all the algebra has been done, with small terms neglected, the equation used to determine the critical load results in

$$-\frac{(1-\nu^2)p_{cr}a}{Eh} = \frac{1-\nu^2}{(n^2-1)\left(1+\frac{n^2L^2}{\pi^2a^2}\right)} + \frac{h^2}{12a^2}\left(n^2-1+\frac{2n^2-1-\nu}{1+\frac{n^2L^2}{\pi^2a^2}}\right) \tag{3.7.19}$$

with n= 2,3,4.....

Therefore, equation (3.7.19) can be used to calculate the critical load (p_{cr}) of a circular cylindrical shell. For more detailed information on this solution process can be found in reference 8 .

CHAPTER FOUR

Numerical Analysis and Results

4.1 Introduction

Since submarines are vessels that operate under hydrostatic loading conditions, these vessels can fail due to compressive yielding or shell instability. Submersibles that are used for shallow diving have hulls that are thin and strong. Consequently, they have a probability of buckling under hydrostatic loading. On the other hand, deep diving submersibles have thick shells, and the bending rigidity goes up as the cube of the shell thickness. Increasing the thickness tends to push the failure mode from shell instability to compressive yielding the structure. In the truss/cradle design concept, the truss is connected to the hull through point attachments. In this research investigation, the effects of these point attachments on cylindrical shell stability are studied. The research progressed from analysis of unreinforced to point-supported rings under external radial pressure, and then from unstiffened to point-stiffened cylinders.

With today's technology, high speed computers can be used to help improve the design of pressure hulls. Computer usage allows the designer more time for creative thinking by eliminating repetitive work. For structural problems, the finite element method provides an effective way to evaluate the structure's response to a change in its environment. The finite element method analyzes the structure as an assemblage of small elements. Furthermore, the ABAQUS finite element package provided the necessary routines to carry out the analysis of stability problem, and the eigenvalue buckling extraction routine was the primary program segment used in this research.

4.2 Buckling Load Determination-Eigenvalue Extraction

While studying eigenvalue problems, one should realize that there are no unique solutions to the problem. These problems involve solving for a series of solutions for

equations of the form.

$$Av=\lambda Bv \tag{4.2.1}$$

where
A &B are symmetric matrices
λ is the eigenvalue (frequency or critical load)
v is the eigenvector (mode shape)

Eigenvalue problems can be solved by taking the determinant of $(\lambda B-A)$ and setting it equal to zero, and this can be represented as

$$\det(\lambda B-A)=0 \tag{4.2.2}$$

The solution of the above equation yields a series of eigenvalues (λ) that satisfy the equation, and each eigenvalue has a corresponding eigenvector associated with it.

In structural stability problems, the eigenvalue problem finds the point at which the system collapses when the structure is slightly perturbed from it equilibrium position. This point is known as the critical buckling load of the structure. From this, we can see the sensitivity of the solution to the geometry and loading conditions. In reference to equation 4.2.1, the eigenvalue (λ) represents the critical buckling load, and **v** represents the mode shape associated with that load.

This type of analysis is termed linearized buckling analysis, and the finite element code solves the following equation

$$\det(K+\lambda K_G)=0 \tag{4.2.3}$$

where
K - linear strain stiffness matrix
K_G - nonlinear strain stiffness matrix

The critical load is then determined by multiplying the eigenvalue by the applied load.

$$P_{buckle}=\lambda P_{applied} \tag{4.2.4}$$

This linearized buckling analysis employs two key assumptions

1. The linear strain stiffness matrix does not change appreciably prior to buckling
2. The nonlinear strain stiffness matrix is simply a multiple of its initial value.

Therefore, the method assumes that prebuckling deformation effects have negligible effects on the stiffenesses. This basic analysis scheme was used to evaluate the structural advantages or disadvantages of point attachments in a Uniform Ring, a Resiliently Supported Ring, a Uniform Cylinder, and a Resiliently Supported Cylinder.

4.3 Circular Ring Stability

Many researchers investigated the stability of circular rings for many years in the early 20th Century, and their results provide good insight into the problem. Some of their results are given in Chapter 3. Two different approaches to solving the ring stability problem were illustrated. With this background, a finite element model was created to compare with the results from theory.

In the model creation, there are many parameters that must be selected, and they are the following:

1. Geometry
2. Element Type
3. Material
4. Loading Conditions
5. Boundary Conditions
6. Type of Analysis
7. Output Desired

The geometry necessary for this problem is a circular ring, and it is shown below.

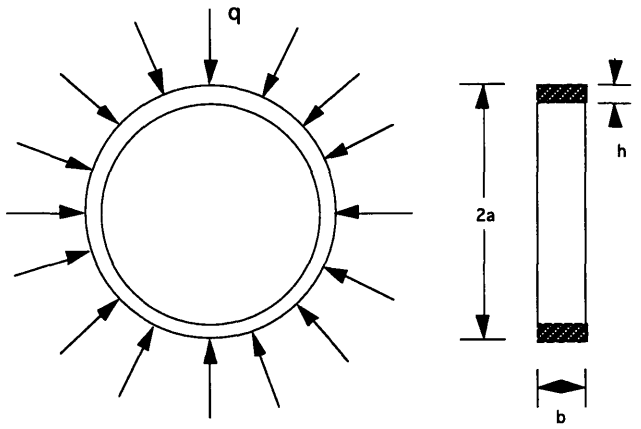

Figure 4.3.1: **Ring Under Uniform External Load**

Using quadrilateral shell elements(S8R), a titanium ring was made with a unit width and ratios

$$\frac{a}{b} = 22$$

$$\frac{h}{a} = 6.5568E-2.$$

S8R elements are 8 node elements that are primarily used for thick shell applications, and the ratios supports this choice of elements. Although 4 node elements would save computer time, it can't capture the higher order displacements resulting from buckling effectively. To capture a good convergent solution, a sufficient number of elements must be used around the perimeter of the ring. Through trial and error, the resulting number of elements around the perimeter was set equal to 144, with 2 elements along the width **b.**

Next, the ring has to be sufficiently constrained so that there are no rigid body motions. Rigid body motions results in zero pivots in the finite element stiffness matrix. These zero pivots are numerical errors that do not allow a convergent solution to be achieved. Since the ring was created in the x-y plane, the ring was constrained against movement in the z direction, and free to move radially. Finally, a uniform compressive radial load was applied to the ring, and an eigenvalue buckling extraction was performed. To see if the results were viable, they were compared to theory using the equation of the form

$$P_{crit} = \frac{(n^2 - 1)EI}{R^3 L} \tag{4.3.1}$$

where

n= circumferential mode number
I= cross sectional moment of inertia
E= Young's Modulus
R= radius (a)
L= width (b)

The comparative study involved comparing the critical buckling load of the two methods for a particular mode shape. Recall that the eigenvalue has a mode shape associated with it , and both methods should arrive at the same values for the same conditions. The result of this study is shown in **figure (4.3.2)**.

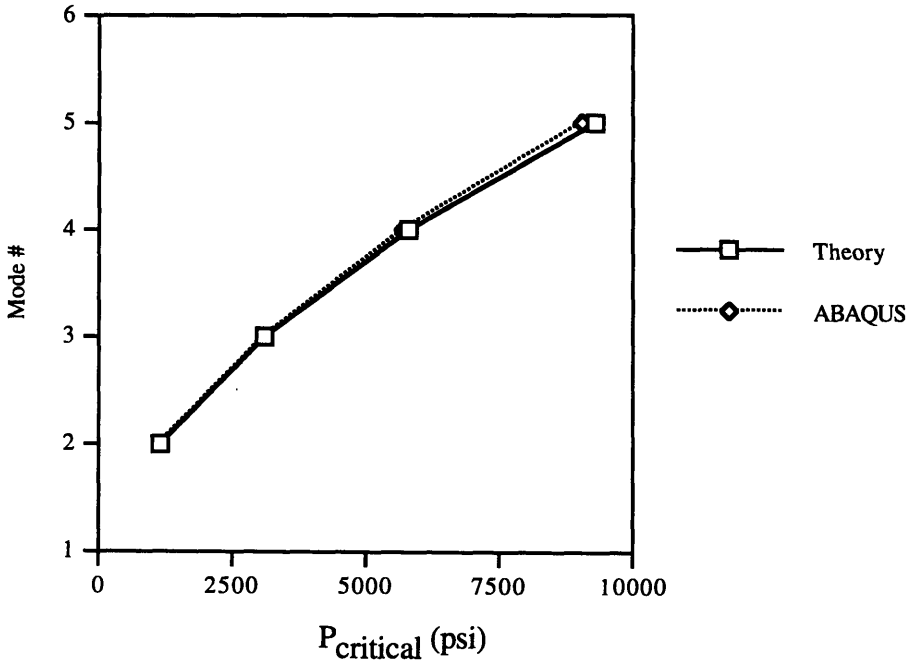

Figure 4.3.2: **Theory vs. ABAQUS for Unstiffened Circular Rings**

n	ABAQUS - P_{cr}	Theory - P_{cr}
2	1156.2 psi	1162 psi
3	3067.1 psi	3099 psi
4	5706.7 psi	5811 psi
5	9042 psi	9298 psi
6	13032 psi	13559 psi

Table 4.3.1: **Table of Graph Data**

With this favorable comparison, it has been shown that the model mesh was sufficiently fine to capture the necessary behavior. With this confidence, radial point

supports can be introduced to the model. These stiffeners were held fixed at the free end, and the end attached to the ring had zero moments (pinned). The stiffeners were in the form of spring elements (SPRINGA), and the number of stiffeners were varied along with their circumferential position. Although the length of these stiffeners could be another variable, it was decide that the length will be kept constant for these tests. In each case, the stiffeners were made with the ratio

$$\frac{L_k}{R} = .25 \qquad (4.3.2)$$

where

L_k - Length of the stiffener
R - Radius of the ring

This stiffener length is an analytical artifact and does not bear directly on the physical implementation . Obviously, the important parameter is radial support stiffness, which can be achieved in any number of configurations and geometric envelopes. This modified geometry is represented in **figure 4.3.3**

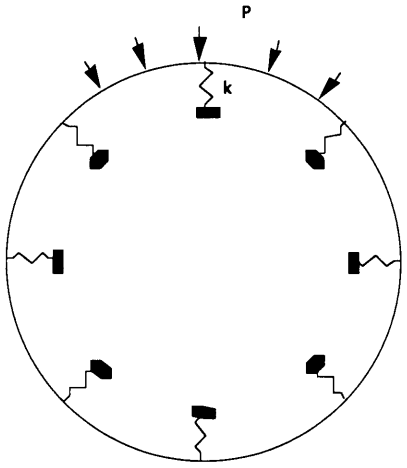

Figure 4.3.3: **Ring with Radial Stiffeners of Stiffeness (k) Under External Load (P)**

A large number of cases were run using ABAQUS, varying the number and spacing of radial supports as well as their relative stiffness. The stiffener comparison involved comparing the ratio of the computed critical load divided by the critical load for

unstiffened rings with the stiffness parameter KR^2/D. Where K is the stiffness of the springs, R is the radius and D is the bending stiffness variable .

$$D = \frac{Eh^3}{12(1-\nu^2)} \tag{4.3.3}$$

This comparison is shown in graphical form in **figure 4.3.5**, and the value of the bending stiffness variable (D) remains a constant 2951.15 lbs-in throughout the comparative study. In this graph we can see that as the number of stiffeners increases, the critical buckling load increases. That is something that should be expected seeing that structure becomes stiffer. Furthermore, we see that 4 stiffeners gives us no improvement. That is due to that fact 4 stiffeners still allow the lowest energy mode (mode 2) to take precedence (See Figure 4.3.4).

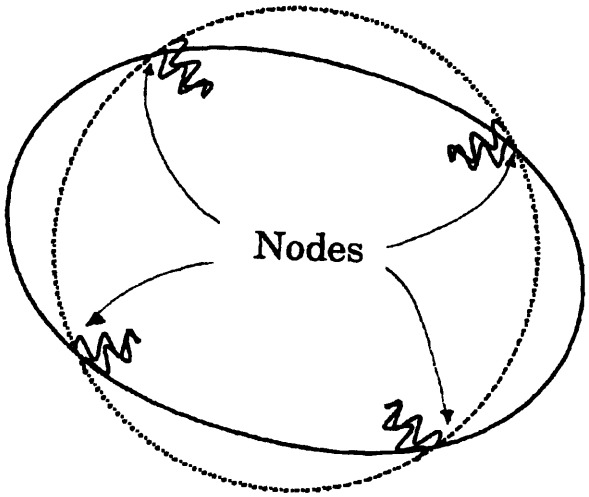

Figure 4.3.4: **Circular Ring with 4 Radial Supports in a Mode 4 Configuration with the Supports Becoming the Nodes of Deformation**

The point support locations simply become the nodes of the deformation mode. Also, we can see that in comparing even versus uneven spacing of stiffeners around the perimeter, the uneven spacing only gives us a small advantage for high stiffness values. Thus, it provides advantageous results if you are constrained to use a particular number of stiffeners with specific stiffnesses, but it must be remembered that for a particular

stiffness it could yield a lower result as evenly spaced stiffeners. (see Appendix for exact results)

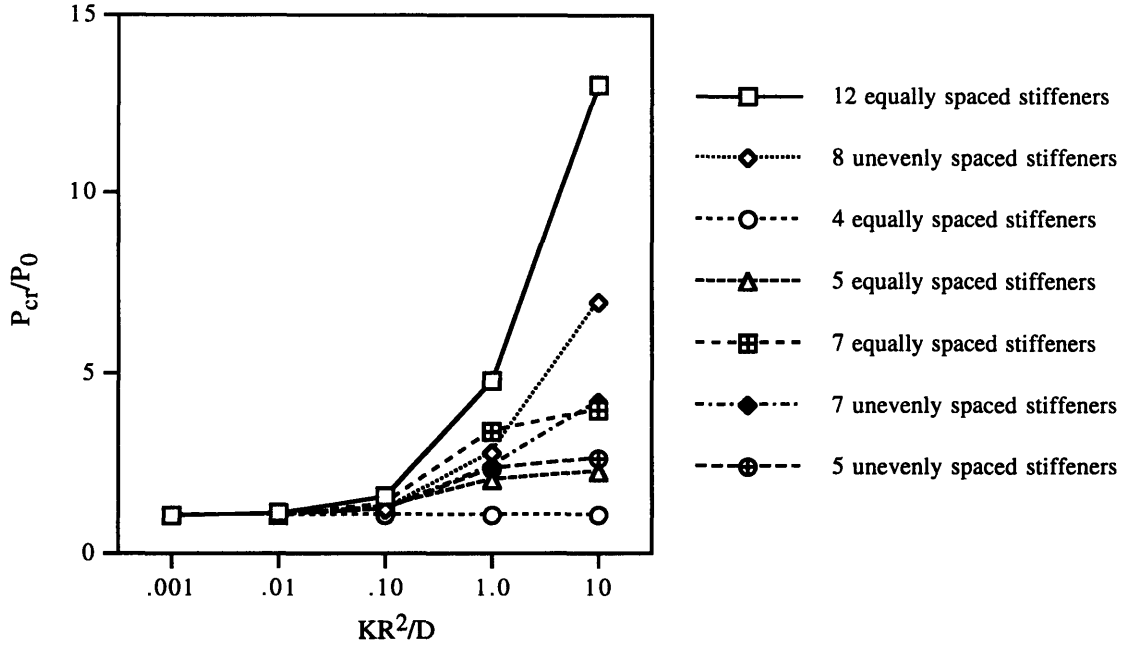

Figure 4.3.5: **Comparison of the Stiffness Parameter (KR^2/D) to Critical Pressure Ratio (P_{cr}/P_0) for Variuous Number of Stiffeners.**

4.3.1 Circular Ring Buckling Mode Shapes

When the ring buckles, it goes into the shape that represents its minimum energy state. As mentioned before, each eigenvalue has an eigenvector (mode shape) associated with it. In general, uniform rings subjected to external radial loads tend to go into symmetric modes, and these modes are generally characterized by the number of lobes the ring has after deformation. For example , mode two has a shape that resembles an oval looking at the ring down its axis, and mode three appears to have 3 finger-like projections from this perspective. To get a better idea of this concept , the following figures are provided.

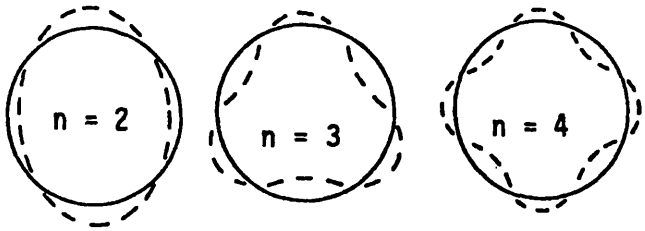

Figure 4.3.6: **Schematic of Symmetric Ring Deformation Modes**

Looking at the results from the stiffener comparison, the first mode in each case for any number of stiffeners and a stiffness range (10-1000 lbs/in) is characterized by mode 2. This implies that below a threshold K value, point supports have no effect. For the ring with 12 stiffeners at K=10,000 lbs/in, the first mode is mode 3, and this trend suggests a shift in dominance from ring properties to support stiffnesses. Furthermore, with an increased stiffness value (K=100,000 lbs/in), the lowest energy mode is mode 6. From these phenomena, it can be seen that with an increase in stiffness, the lowest energy mode increases. For this geometry, the structure requires more energy to deform the body into a mode 6 configuration than it does for a mode 3 or 2. **Some other configurations can be seen in figures 4.3.7 - 4.3.10**

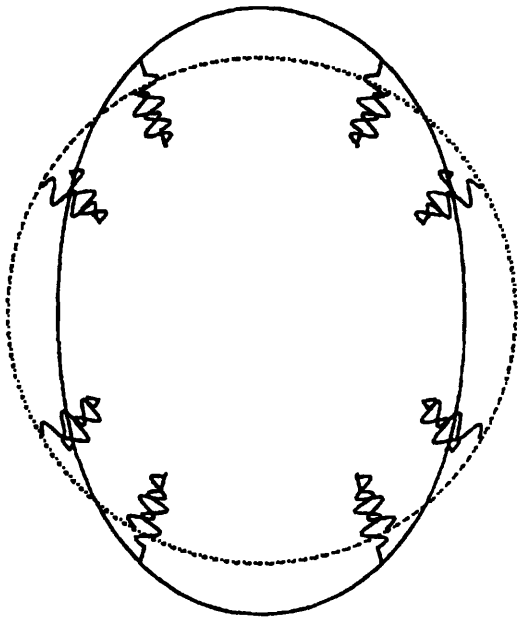

Figure 4.3.7: **Ring With 8 Supports of Stiffness K=10 lbs/in Buckled into a Mode 2 Configuration at a Critical Load P_{cr}=1158 psi**

Figure 4.3.7 represents a ring with 8 radial stiffeners in a buckled configuration corresponding to the mode shape n=2. For low stiffness values this mode is the critical buckling mode. For example, with K=10 lbs/in , the critical load associated with n=2 has a value of 1158.8 psi. Furthermore, other modes associated with the stiffness value K=10 lbs/in with an increasing load are shown in figures (4.3.8-4.3.9).

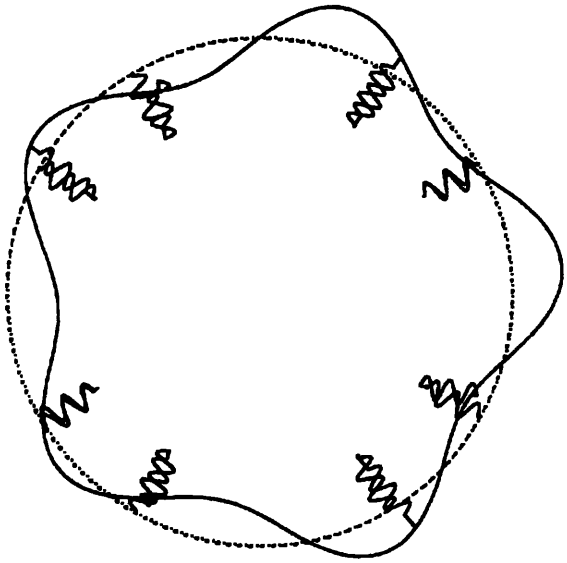

Figure 4.3.8: **Ring With 8 Supports of Stiffness K=10 lbs/in Buckled into a Mode 5 Configuration at a Load P=9043.1 psi**

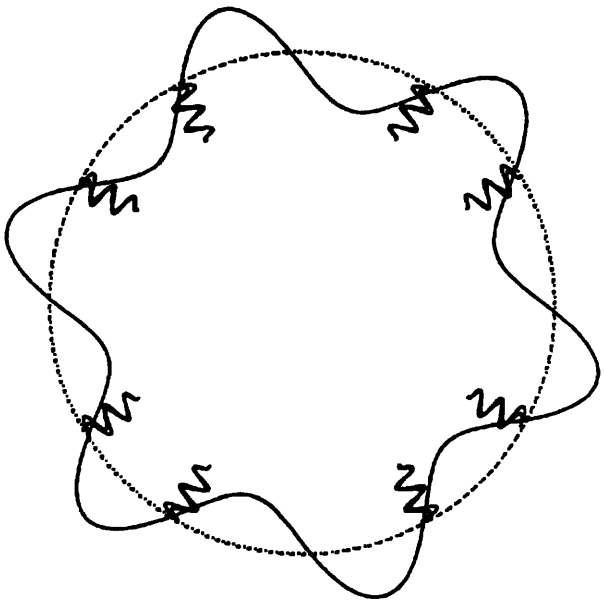

Figure 4.3.9: **Ring With 8 Supports of Stiffness K=10 lbs/in Buckled into a Mode 6 Configuration at a Load P=13031 psi**

With an increasing load, the mode shape is driven to a higher mode. We can see that if the ring can be pushed into a higher mode than the first mode, we would obtain the desired increase in the critical buckling load. Furthermore, with an increase in the stiffness value the ring structure may buckle in an unsymmetric shape or in a undeveloped critical mode shape. Figure 4.3.10 illustrates a undeveloped (circumferential lobes not clearly pronounced) critical mode 5 with K=100,000 lbs/in, and we have seen a fully developed mode 5 in figure 4.3.8.

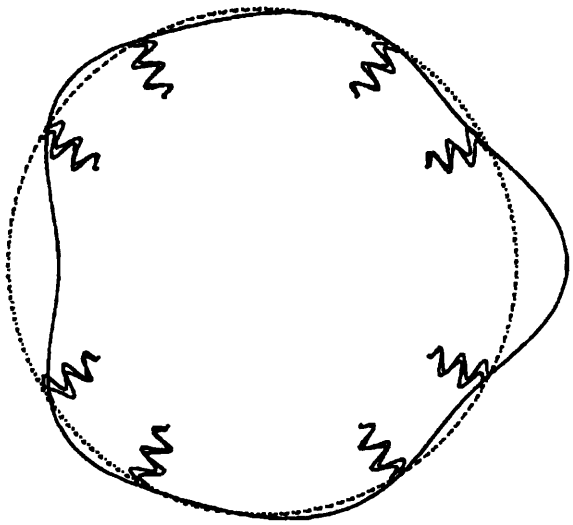

Figure 4.3.10: **Ring With 8 Supports of Stiffness K=100,000 lbs/in Buckled into a undeveloped Mode 5 Configuration at a Critical Load P_{cr}= 8059 psi**

Although this is close to an n=5 mode shape, it has a lower buckling load as a fully developed n=5. An increase in the load is required to make the circumferential lobes more pronounced. Since it is a critical mode for a ring with 8 supports, it is seen that it provides an increase in the critical load over that of figure (4.3.7) at K=10 lbs/in. Therefore, if there is a stiffener configuration that can force the ring into a higher mode shape, it should be able to increase the critical buckling load of the ring. For more mode shape information corresponding to **figure 4.3.5, see Appendix A.**

4.3.2 **Ring On An Elastic Foundation**

As a limiting case, a stability analysis was performed on a ring on an elastic foundation. This configuration is represented in **figure 3.6.1.** In the previous analyses, the number of stiffeners were varied, and these configurations utilized various stiffness magnitudes. The highest number of stiffeners tested was twelve stiffeners around the inner perimeter of the ring. The ring on an elastic foundation is essentially the case of an infinite number of stiffeners around this perimeter.

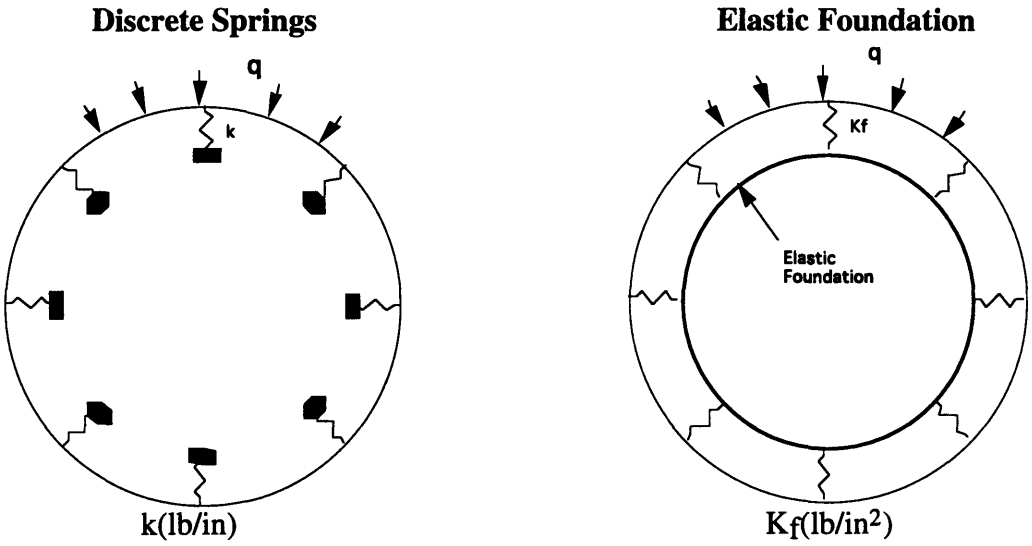

Figure 4.3.11: **Ring With Discrete Supports and a Ring on an Elastic Foundation Under a Uniform External Load (q)**

A comparative study was performed to see if an increase in the number of radial stiffeners would approach the elastic foundation case. To make a fair comparison, an equivalent stiffness (K_f) for the elastic foundation configuration needed to be determined. We can determine the equivalent stiffness(K_f) for each discrete radial stiffener case. For example, equation 4.3.4 can be used to calculate this equivalent stiffness from the stiffness of the discrete case and the number of stiffeners used in that case.

$$K_f = \frac{KN_{stiff}}{2\pi R} \tag{4.3.4}$$

where

K- stiffness of the stiffeners in the discrete spring case(K= 100,000 lb/in)

R- radius of the ring
N_{stiff} - number of stiffeners used in the discrete case

Using the data retrieved from the finite element analysis and equation 4.3.4, a graph was made to compare the discrete stiffener case to the elastic foundation configuration .

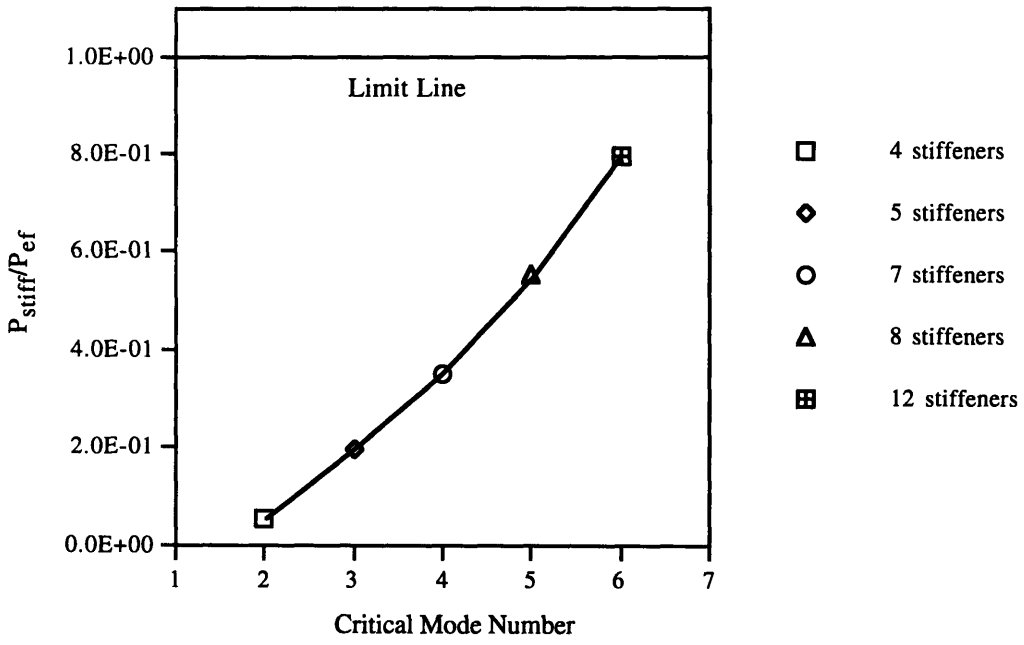

Figure 4.3.12: **Critical Pressure Achieved by Using Point-Supports Compared to the Critical Pressure Achieved by Using an Elastic Foundation for Several Stiffeners**

The ABAQUS data gives us the critical buckling load (P_{stiff}) for the discrete case with a corresponding mode shape, and equation 3.6.5 uses equation 4.3.4 to calculate the critical load(P_{ef}) for the elastic foundation case for a specified mode shape. As seen in figure 4.3.12, an increasing number of discrete radial stiffeners seems to approach the elastic foundation limit line. Therefore, if additional stiffeners are attached to the ring, we would be able to approximate the critical buckling load using the equations for an elastic foundation seen in chapter 3.

Furthermore, to see the advantages of using an elastic foundation configuration let's compare it to the unstiffened case. The unstiffened critical pressure can be calculated using equation 3.5.6, and the critical pressure for the elastic foundation case is represented as P_{cr}, where $P_{cr}=P_{ef}$. This information was used along with various

equivalent stiffness values (K_f) at a constant value K=100,000 lbs/in to perform an elastic foundation comparison.

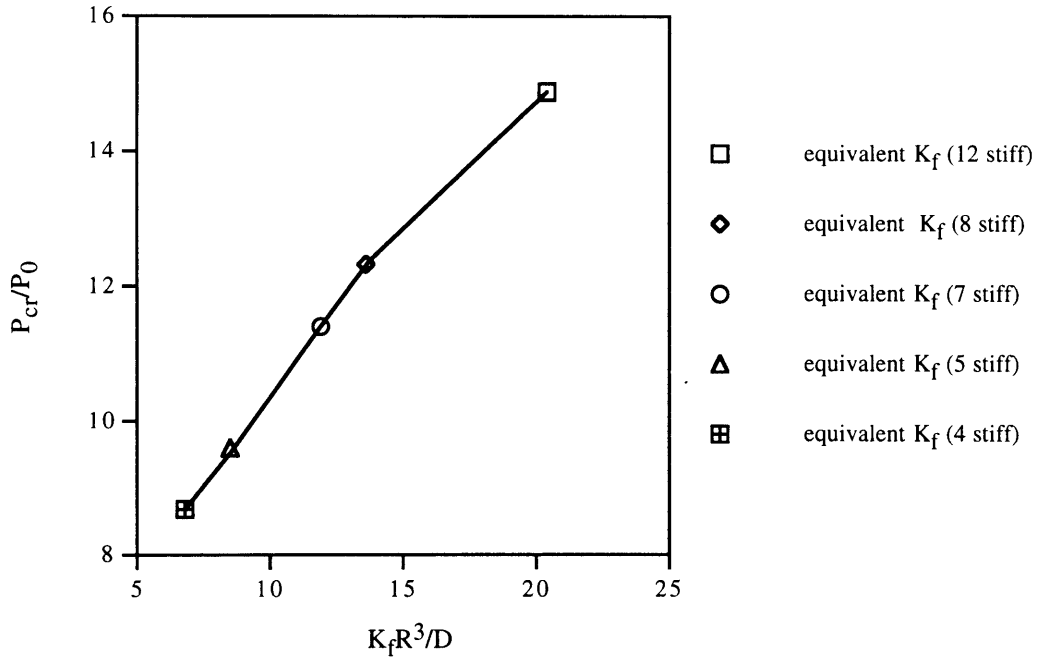

Figure 4.3.13: **With K=100,000 lbs/in and Equivalent K_f Values, the Effects of the Elastic Foundation on the Critical Pressure Load of the Ring is Compared to the Unstiffened Ring.**

From the graph, it can be seen that at an increasing equivalent stiffness yields incredibly large improvements in the critical buckling load. Therefore, the designer can pick the number of stiffeners to use and their stiffness to achieve the desired improvements. For example, from figure 4.3.13, one obtains the buckling strength ratio (compared to unstiffened ring) as a foundation of elastic foundation stiffness. Figure 4.3.12 shows the efficiency of varying numbers of discrete stiffeners in achieving the elastic foundation improvement. Combining the results of these graphs provides the designer with an estimate of the improvements to be expected as a function of both the total support stiffness and number of stiffeners.

These comparative studies provided some insight into the effects on radial stiffeners on circular shells. Since submarines are primarily fabricated using cylindrical shells, this information can used to provide some initial configurations for cylindrical shells.

4.4 Cylindrical Shell Stability

Cylindrical shells are simple structures that are subject to instabilities in axial compression, under uniform lateral pressure, and under combined loading. Research has been done in these areas of stability for many years, and much of this work was utilized in the stability analysis of submarine structures. Chapter 3 provides some of the results used as today's standard for determining the critical buckling load. Using these past results as the reference solution, a finite element model was created with buckling theory conditions in mind.

As we have seen in section 4.3, there are seven parameters that must be dealt with in the creation of a finite element model. The geometry takes the form of a circular cylinder shown in **figure 4.4.1**.

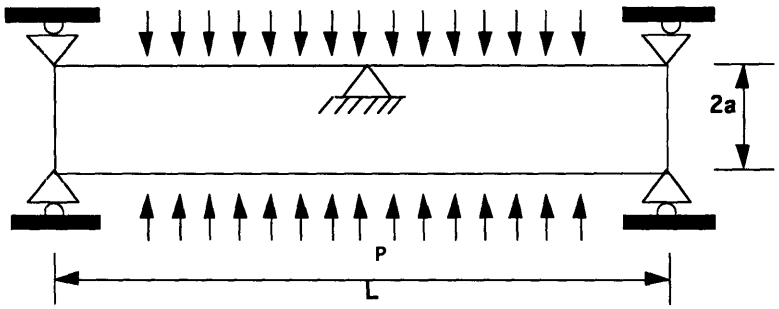

Figure 4.4.1: **Cylinder Held Circular at the Ends and the Middle Held Fixed in the Axial Direction**

Quadrilateral shell elements (S8R5) were used to create the required circular cylindrical shell in the ABAQUS finite element code, and S8R5 elements are used for thin shell applications. These element were arranged in a fashion such that the cylinder had 24 elements around the perimeter and 36 element along the length of the cylinder. Numerical studies were done to ensure that the mesh density used provided converged solutions. Since the theory derived in chapter 3 assumes that the shell is thin, thin shell elements were used to achieve good correlation with theory. To be considered a thin shell, the thickness of the shell must be small compared to the radius of curvature of the

cylinder. In complying with this rule, a structure was made of titanium with particular design ratios, and these ratios can be represented as the following:

$$\frac{a}{L}=.1$$

$$\frac{h}{a}=5.6818E\text{-}3$$

Also, shell designers use a dimensionless z-parameter that provides a scaling reference for the structure, and this parameter is given as

$$z=\frac{L^2}{rh}(1-\nu^2) \tag{4.4.1}$$

The finite element model that was created for this analysis has a value of

$$z= 16016$$

From the geometry, we can see that the length of the cylinder was relatively large with respect to the radius and thickness. Although the length was large with respect to radius, it is not long enough to assume an infinitely long cylinder.

Also, like the ring, the cylinder must be constrained to get rid of rigid body motions. The nodes in the middle (L/2) of the cylinder were constrained to move in the axial direction to negate the rigid body motion effects. Keeping with the boundary conditions given in the cylinder stability theory, the ends were held circular and they were allowed to move in the axial direction. This is represented by rollers in figure 4.4.1. Finally, an eigenvalue buckling extraction was performed on the cylindrical shell with an externally applied load.

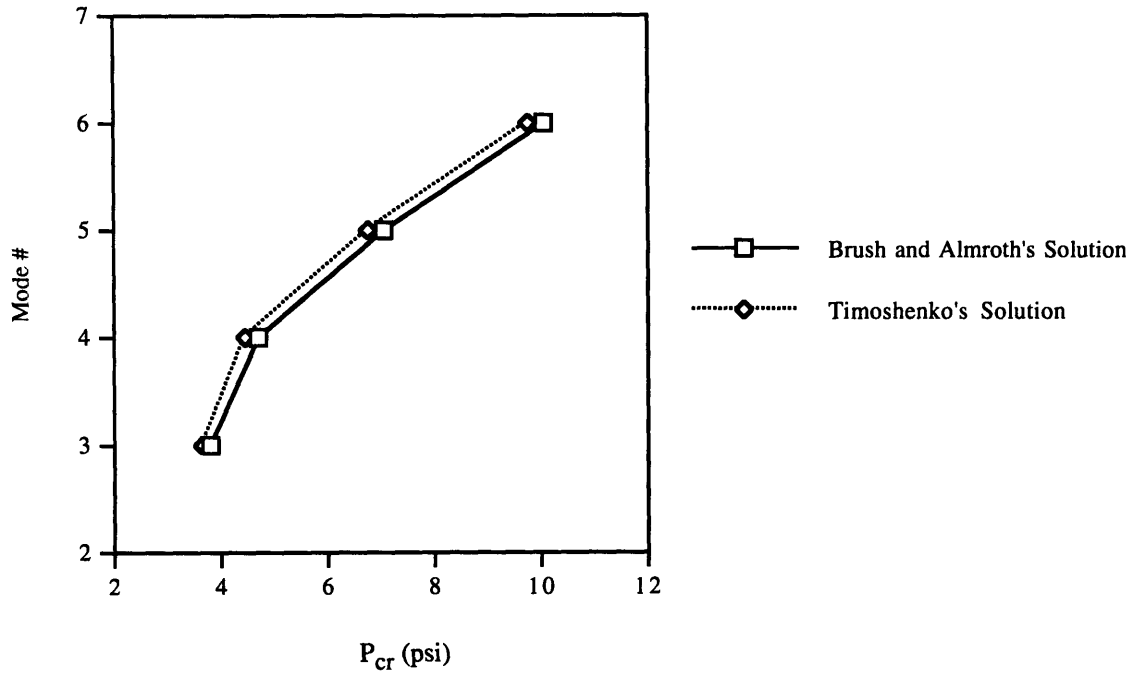

Figure 4.4.2: **Comparison of the Critical Load Solutions of an Unstiffened Circular Cylindrical Shell as Calculated by Timoshenko and Brush & Almroth**

	P_{cr} (psi)	
n	Timoshenko	Brush & Almroth
3	3.6463	3.7750
4	4.4400	4.7096
5	6.7655	7.0417
6	9.7740	10.0518

Table 4.4.1: **Theory Comparison Data Table**

For model verification, the finite element model was compared to theory, and it was decided to use the Timoshenko solution for cylinder buckling. We can see from figure 4.4.2, that the solutions for both methods were within less than 6% of each other using the Timoshenko solution as the reference. Timoshenko's model includes the higher order terms that were neglected by Brush and Almroth. We can see from the results, that the omission of these terms in essence makes the structure appear rather stiff compared to Timoshenko's model. Since Timoshenko's model includes these higher order terms in its derivation, his model was used for verification of the Finite Element Model. Timoshenko's equation of the form

$$\frac{(1-\nu^2)q_{cr}a}{Eh} = \frac{1-\nu^2}{(n^2-1)\left(1+\frac{n^2L^2}{\pi^2a^2}\right)^2} + \frac{h^2}{12a^2}\left(n^2-1+\frac{2n^2-1-\nu}{1+\frac{n^2L^2}{\pi^2a^2}}\right) \qquad (4.4.2)$$

where

n= mode number
L= length
a= radius
q_{cr}= critical load
h= thickness
E= Young's Modulus

was used to calculate the theoretical solution.

	P_{cr} (psi)	
n	ABAQUS	Theory
3	3.6570	3.6463
4	4.4668	4.4400
5	6.8329	6.7655
6	9.9541	9.7740

Table 4.4.2: **ABAQUS vs Theory Data Table**

For this model verification, the critical buckling load calculated by ABAQUS was compared to the solution generated by Timoshenko's equation for given mode shapes. This comparative study is illustrated best in graphical form, and this can be seen in figure 4.4.3. Since both methods should arrive at the same solution, the lines on the graph should be identical. The ABAQUS solution was very close to the solution calculated by theory, but the slight variation is due to several factors. These factors include the number of degrees of freedom per element (8 node elements vs. 9 node elements), the coarseness or fineness of the mesh, and the iterative approximation methods used that are inherent to the finite element method. All these factors contribute to the error between the analytical and finite element results. For the critical mode (mode #3) the analytical and finite element results agreed within a **.29%** error.

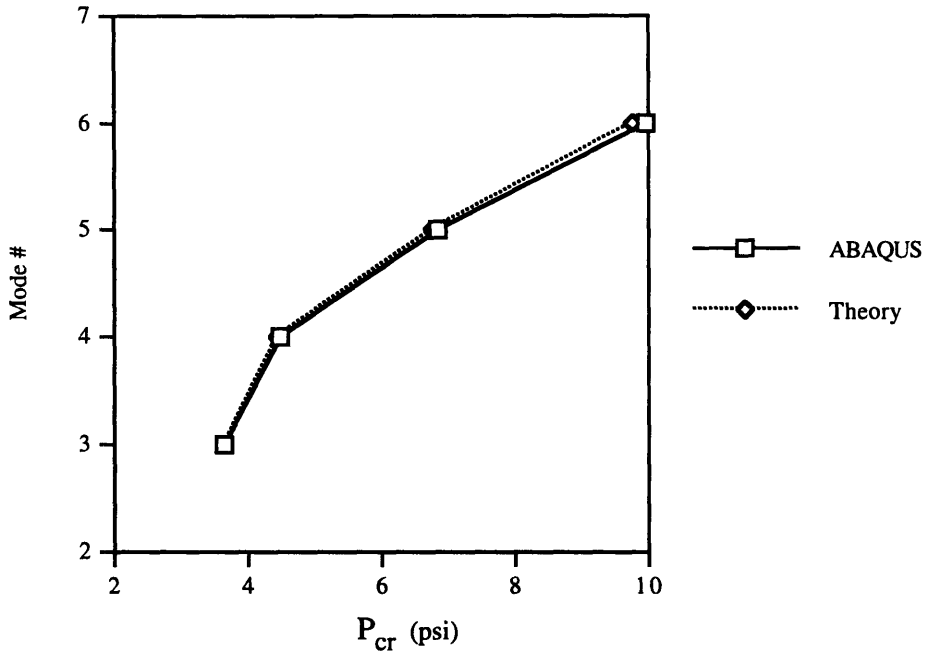

Figure 4.4.3: **Theory vs. ABAQUS for Unstiffened Cylindrical Shells**

This comparison shows that the model contained a sufficiently dense mesh to capture the required solutions . With a good working model, stiffeners can be added to the structure. In the truss/cradle design concept, the truss is octagonal; thus, it has 8 corners where attachments can be made between it and the submarine hull. The truss is assumed to be very stiff and rigid. With this in mind, the end of the stiffener that would be attached to the truss is fixed, and the end that is attached to the hull was pinned. As before, the stiffeners were simulated by using spring elements (SPRINGA). The ring cases were simplified versions of the cylinder problem. Although the ring allowed a few parameterizations, the cylinder has many more. For example, there are vast variations that can be achieved, and some of them are the following:

1. Varying the number of stiffeners
2. Varying the circumferential spacing of the stiffeners
3. Varying the number of stiffener sets along the length of the cylinder
4. Varying the stiffness of the stiffeners
5. Varying the orientation of the stiffeners

Due to the number of parametric possibilities and resource limitations, only a few of these cases are studied. The main cases observed involved the variations(1-4) mentioned

previously. The length of the stiffeners is another variation, but it is kept constant for all the cylinder stability analyses. Therefore, the stiffener ratio

$$\frac{L_k}{R} = .25$$

will remain the same.

First, an eigenvalue buckling extraction was performed on a cylindrical shell with 8 stiffeners placed in the middle of the cylinder (L/2) with equal spacing, and picture showing this configuration can be see in the **figure 4.4.4 below (reference configuration).**

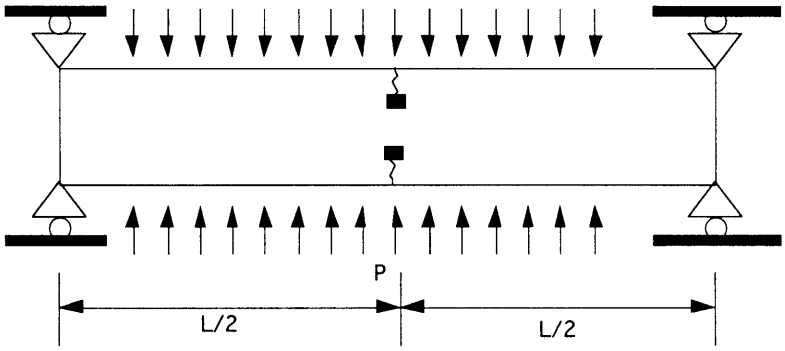

Figure 4.4.4: **Cylinder with Stiffeners at Midpoint Under Hydrostatic Load (P)**

As a result of running this test, it was found that the critical buckling load increased with an increase in stiffness up to a particular point (**See figure 4.4.5**). After this stiffness level is reached, an increase in radial support stiffness provides no further advantages. The critical stiffness at which improvement is plateaued appears to be that at which the stiffeners created effective modes. As the stiffness values were increased, the cylindrical shell moves from a mode 3 to a mode 4 under uniform external radial loads. On a positive note, we can see that there is approximately a 22% increase in the critical buckling load for this configuration. This limit point is found to begin at a value of

$$\frac{KR^2}{D} \approx 164.$$

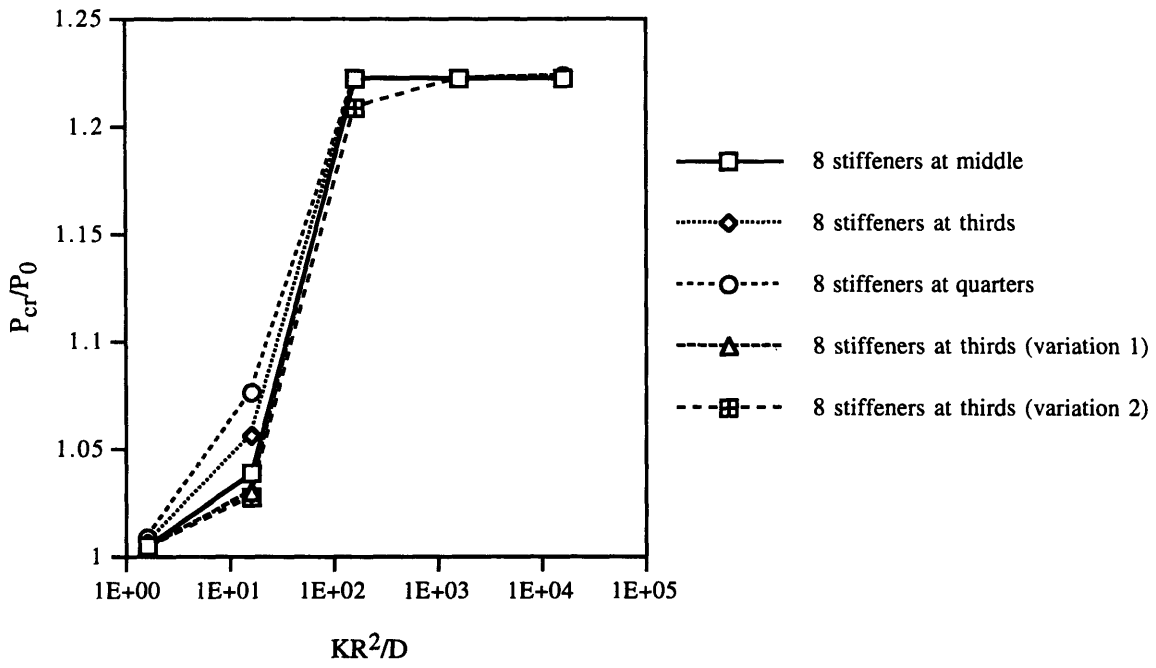

Figure 4.4.5: **Effects of the Radial Support Configuration on the Critical Load Ratio (P_{cr}/P_0) with Varying Stiffness Values**

In a effort to achieve a greater increase in the critical buckling load, a second model was created with stiffeners at the L/3 and 2L/3 (**See Figure 4.4.6**). This modification was thought to provide a tougher path for the structure to travel in achieving its minimum energy configuration. This configuration resulted in a very small increase in the critical buckling load (about a 5% increase) at low stiffness levels, but it leveled off and remained constant for increasing stiffness values (**See Figure 4.4.5**).

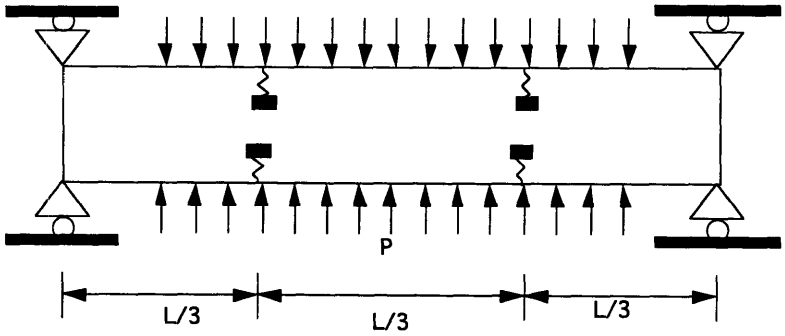

Figure 4.4.6 : **Cylinder with Stiffeners at 1/3 Points Under Hydrostatic Load (P)**

Although the stiffeners at the thirds points achieved some increase in the critical load, higher critical load are still desired. Another model with stiffeners at L/4, L/2, 3L/4 was created to help bring us closer to our goal (**See Figure 4.4.7**). To achieves its minimum energy configuration , the structure required a higher applied load for this stiffened case over the unstiffened case. Again this critical load showed an improvement over the previous 2 configuration at low stiffness levels (a 8% total increase in the critical load), but it to remained constant for increasing stiffness level beyond this limit point (**See Figure 4.4.5**).

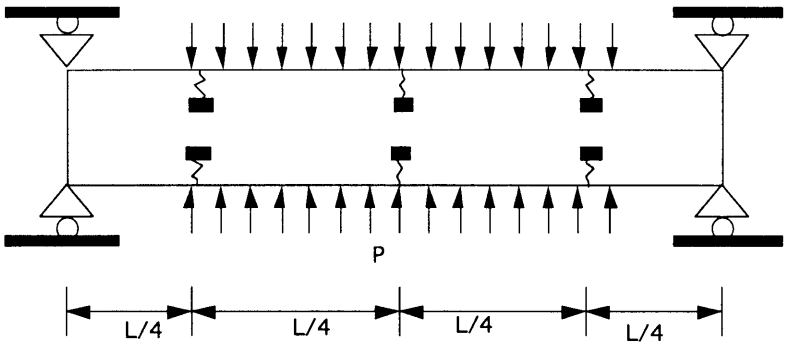

Figure 4.4.7: **Cylinder with Stiffeners at 1/4 Points Under Hydrostatic Load (P)**

As a result of observing these different configurations, it appears that largest increase in the critical load that can be achieved is about 22%. Furthermore, it appears that an increase in the number of stiffener stations along the length of the cylinder doesn't increase the critical buckling load over 1 station at L/2. This result means that further stations of stiffeners have little effect since they don't effect the m=1 (one longitudinal lobe) half wave (See section 3.7.4 and Figure 4.4.11). Looking at the Brush and Almroth solutions for an increasing m value, we can see that the critical buckling load increases (**See Table 4.4.3**). Since it was shown that m=1 exhibits the critical modes for various values of n, a higher value of m will increase the critical load. For example, let's compare m=1 to m=2 for various values of n using equation (3.7.15).

n	m	P_{cr} (psi)
3	1	3.7750
4		4.7096
5		7.0417
6		10.0518
3	2	21.1100
4		8.0535
5		8.0560
6		10.5000

Table 4.4.3: **Effects of Increasing the Longitudinal Mode (m) on Critical Load**

From the table above, it is clearly shown that we can achieve a sizable improvement in the critical buckling behavior by pushing m=1 to m=2 for modes 3 and 4. Therefore if the stiffeners can be arranged in such a fashion to force m=1 behavior to m=2, then it would advisable to do so. Furthermore, at modes 5 and 6 there isn't much improvement gain by pushing the longitudinal half wave from m=1 to m=2, and it would be beneficial to just increase the number of circumferential stiffeners in this case. Note that all the springs stiffeners have had the same stiffness value for each of the 3 analyses configurations shown, and a change in this area could provide the desired improvements.

Taking a closer look into varying the stiffness of the stiffeners, a new configuration was developed. In this effort, the model with the stiffeners at the third points was modified, and two different modifications to the same model was analyzed. First, the stations at L/3 and 2L/3 had a stiffener configuration that looked like the following:

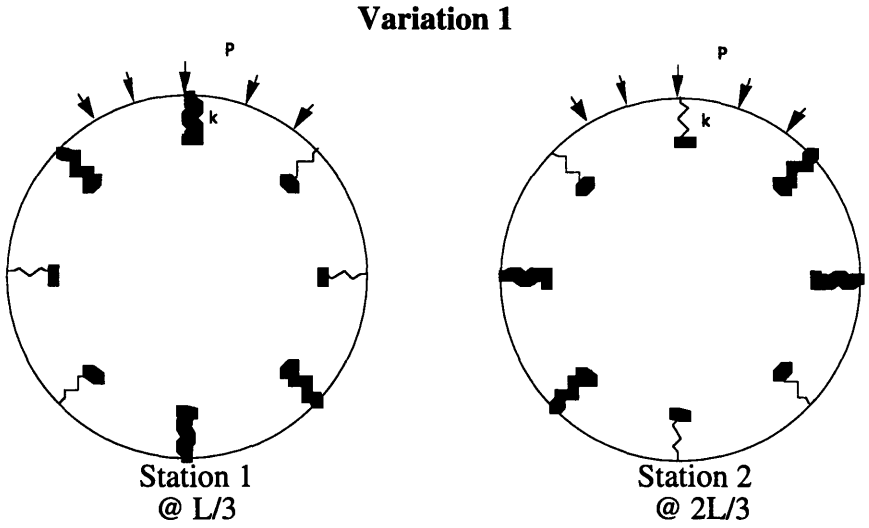

Figure 4.4.8: **Rotated Stiffener Configuration - Variation 1**

In this setup, the bold spring represents the springs that were varied during the analysis, and the remaining springs represents the springs that held a constant stiffness value (K=10 lb/in). In this attempt to achieve a higher critical mode shape, this non-symmetric stiffness configuration was implemented. As a result of this attempt, lower buckling loads than the previous configurations were achieved at low stiffness values, but the same limit point (@ $KR^2/D \approx 100$) was achieved at higher stiffness values.

Also, a second attempt at using a non-symmetric stiffness configuration was made, and this can be seen in variation 2 (Figure 4.4.9). Variation 2 had the same behavior as variation 1 at low stiffness level, but it had a lower buckling load at the same limit value as the other configurations. After this point was passed, it leveled off at the $P_{cr}/P_0 (\approx 1.22)$ value of the other configurations for increasing stiffness.

Therefore, performing this analysis for many different configurations provided useful information for the design of submarine shell stability. For all the configurations tested, the maximum increase in the critical buckling load is about 22%. With that information in mind, it was concluded that 8 stiffeners in the middle was sufficient for an improved design. When looking at cost, manufacturability, time, and weight, the small 5%

improvement at lower stiffness levels is not enough to warrant a design change over the configuration with 8 stiffeners in the middle.

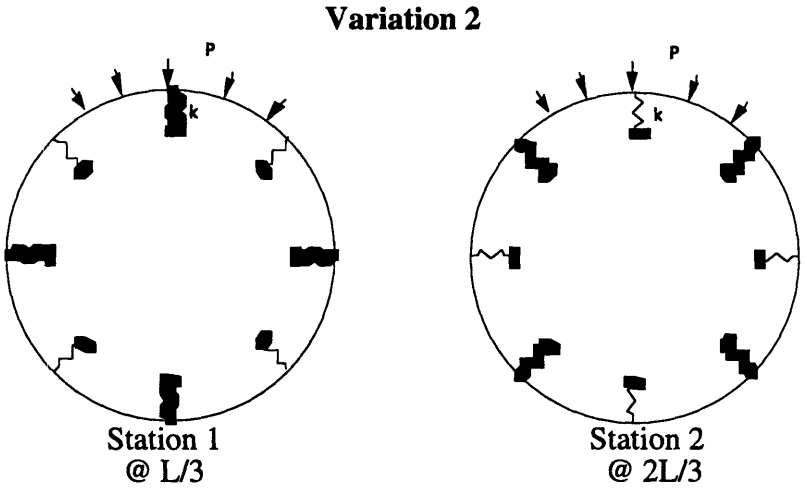

Figure 4.4.9: **Rotated Stiffener Configuration - Variation 2**

If we look at mode shapes, we see that the small improvements in performance are due to the fact that we plateau the performance once we enforce the m=1, n=4 mode shape from the m=1, n=3 mode shape. Significant improvements in performance must change this behavior. Since it has been determined that stiffeners in the middle is sufficient for achieving desirable improvements in its structural performance at high stiffness levels, the number of stiffeners at this position was varied at a constant stiffness value (K=100,000 lbs/in) to obtain to evaluate the effectiveness of that configuration. The result of this test gives a nice comparison chart shown in figure 4.4.10. From this chart, we can see that increasing the number of stiffeners at the "plateau" value of **K** provides great improvements in its stability behavior. For instance, using 12 stiffeners at this position results in approximately 130% increase in the shell's critical buckling load. On the other hand, there isn't much improvement going from 11 stiffeners to 12 stiffeners. Comparing these other configurations to the configuration with 8 stiffeners in the middle, shows that largest jumps in improvements occurs in configurations using an even number of stiffeners. For the truss/cradle design , it would be easier to use an even

number of stiffeners, and that gives us only 3 choices (8,10, &12 stiffeners @ L/2). From this test, it is clear that 12 springs at L/2 provides the best results. Some generalized m=1 mode shapes for general instability of cylindrical shells can be seen in figure 4.4.11, and other mode shape information corresponding to these modified structures can be seen in the **Appendix B**.

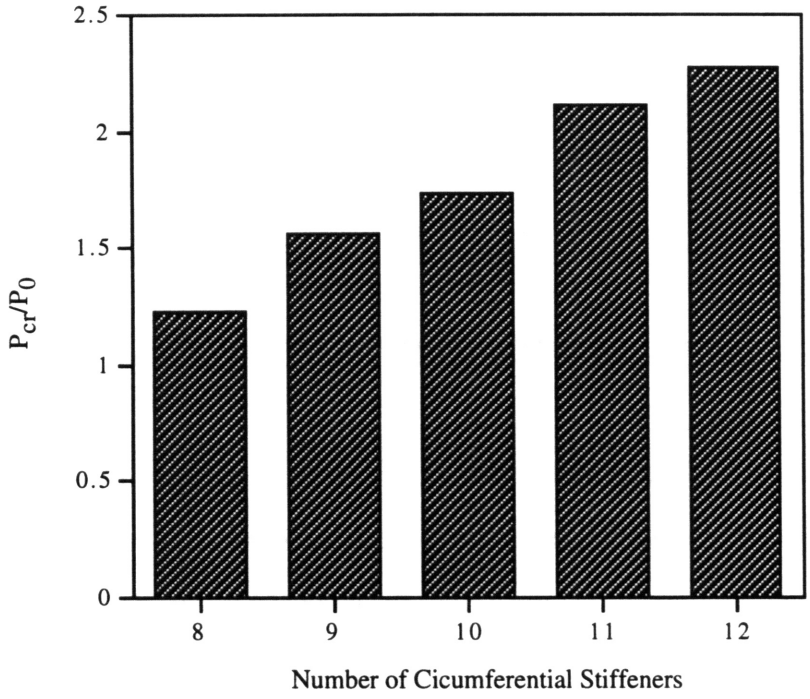

Figure 4.4.10: **Comparison of the Critical Load Achieved by using a Number of Circumferential Stiffeners at L/2 to the Critical Load of the Unstiffened Cylindrical Shell.**

Results Summary

- Given the above, it seems that one plane of stiffeners in the middle of the cylinder gives the bulk of the strength improvements.
- We were not able to increase the longitudinal wave number above m=1 with the values of stiffness attempted (this could be investigated further)
- Odd numbers of stiffeners appear more effective than even.

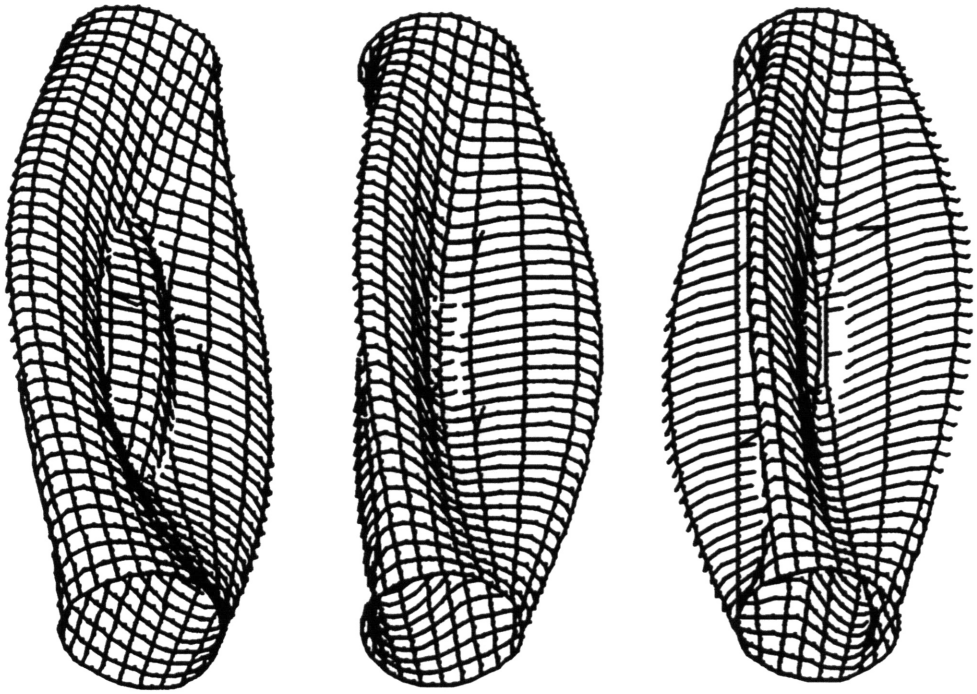

Mode 2 Mode 3 Mode 4

Figure 4.4.11: **Key Cylinder Buckling Mode Shapes @ m=1**

4.4.1 **Other Possible Variations and Comparisons**

Up to this point, we have looked at the phenomena of circular shell stability with radial point supports through several examples using a common cylinder geometry. To see the advantages of using radial stiffeners, we must look at some of the other parameters considered in the design of submarines. Although there are many such parameters, we will look at two of the more vital design parameters such as shell thickness and the weight of the shell.

Shell thickness plays a large role in determining the circumferential bending stiffness of these structures which is a key parameter in shell stability. The stiffness of the shell structure can be estimated using the parameter **D** (see equation 4.3.3). Using equation 4.3.3 it is easily seen that an increase in the thickness of the shell rapidly increases the

stiffness of the shell. Depending upon the application, the shell may have ring stiffeners to increase its bending stiffness, but an optimal configuration will have a particular number of ring stiffeners for a specified thickness. Using this same concept, we will compare the effects of 8 radial stiffeners at L/2 for various stiffness magnitudes at the **reference thickness (t=.125 in.)** to the same stiffness configured shell at various thickness. The result of this comparative study is shown in figure 4.4.12.

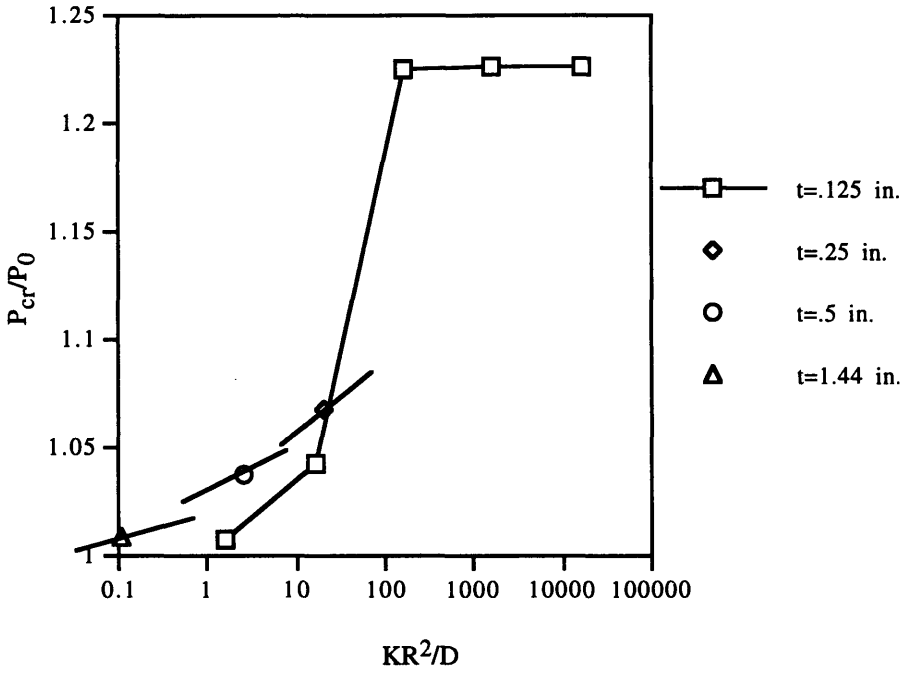

Figure 4.4.12: **Comparison of the Effects of 8 Radial Stiffeners at L/2 for Various Stiffness Values at t=.125 in to Other Shell Thickness Values**

The points at t= 0.25 in., 0.50 in., 1.44 in. represent actual data points at a constant thickness and stiffness (K=1000 lb/in), and the lines were drawn to show that the behavior will look something like that of the line representing t=0.125 in. when the stiffness is also varied. The critical pressure P_{cr} represents the ABAQUS results for these configurations, and P_0 represents the theoretical solution obtained from equation 4.4.2 for the unstiffened shell with these various thicknesses. The result is a graph with lines of constant thickness as the stiffness of the stiffeners are varied. Therefore, we can see that

as the thickness is increased, the lower the effect the stiffeners have on the shells instability pressure, and the sloped lines in figure 4.4.12 indicate this behavior. See **Appendix D** for the exact numerical results.

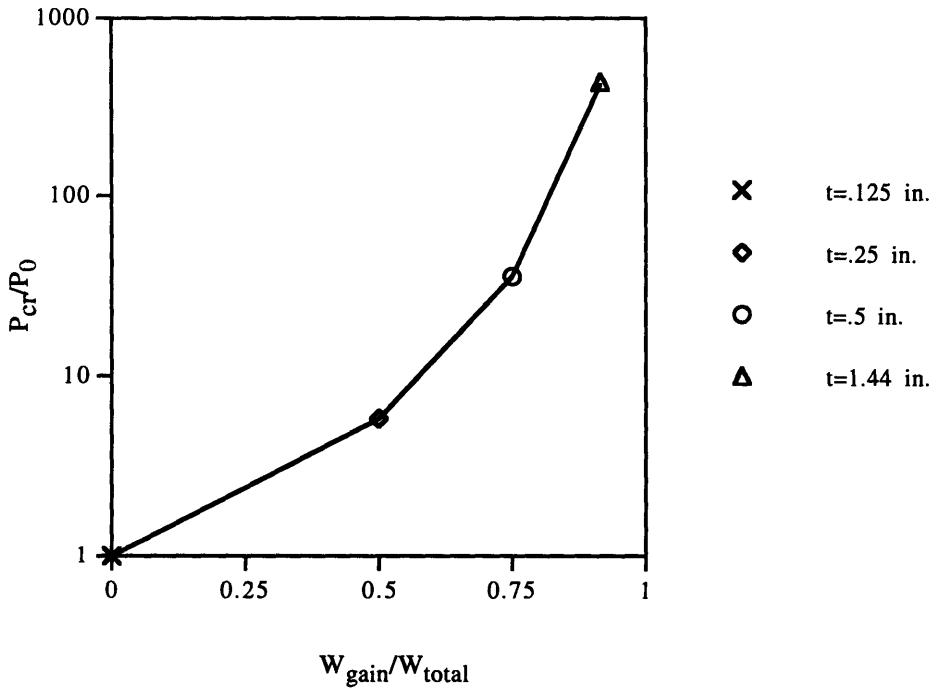

Figure 4.4.13: **Comparing the Effects of Increasing the Shell Thickness and Shell Weight to a Shell Thickness and Weight associated with t=.125 in..**

Next, let's look at weight considerations. From the previously shown results, we know that an increase in shell thickness will increase the value of the critical load, and that more radial stiffeners will yield higher buckling loads. Although these are good attributes, we must keep in mind that hull weight is an important parameter in submarine design.

To see the advantages of using radial stiffeners over increasing the shell thickness, we will first compare the performance of the shell with various thicknesses to the **reference configuration (see graph 4.4.13).**

Reference Configuration

1. 8 Stiffeners @L/2
2. Thickness t=.125 in.

In this comparison, we must calculate the amount of weight increase (W_{gain}) with the different shell thickness values, and calculate the critical load at these thicknesses (P_{cr}). Theses values are compared against the reference critical pressure (P_0) and Weight (W_0). Where the $W_{gain} = W_{total} - W_0$, and the total weight can be calculated using the expression

$$W_{total} = (2\pi Rt)L\rho \tag{4.4.3}$$

where

R- shell radius L- shell length

t- shell thickness ρ- shell density

A result of the hull weight shows that an improved stability performance can be achieved at the expense of sizable weight gains.

However, radial stiffeners are rather small compared to the massive hull structure, and they weigh very little in comparison to the hull. To see this, the weight of the stiffeners must be calculated corresponding to various stiffness values. These values can be calculated using **equation 4.4.4** .

$$W_{stiff} = N_{stiff} \frac{KL^2}{E} \rho \tag{4.4.4}$$

where

N_{stiff}- number of stiffeners E- Young's Modulus

K- spring stiffness ρ- material density

L- length of the spring

This comparison uses steel stiffeners with a high spring stiffness value (K=100,000 lbs/in), and the critical load was calculated with the FEM (Finite element method). The reference configuration was compared to these stiffened configurations, and figure 4.4.14 shows the results of this comparative study.

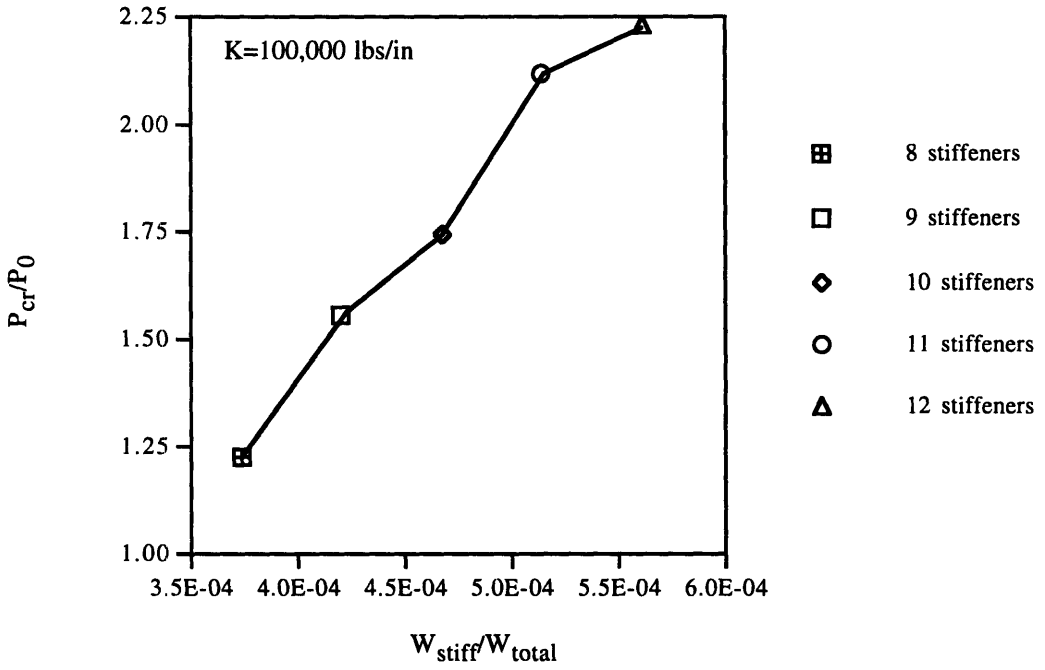

Figure 4.4.14: **Comparison of the Critical Load Achieved at Various Stiffener Weight Ratios to the Critical Load of the Unstiffened Circular Cylindrical Shell.**

This graph shows us that as the number of stiffeners are increased we get an improved performance, but looking at the W_{stiff}/W_{total} ratio shows that this improvement comes with minimal increases in weight. Therefore, in comparing the data in figure 4.4.13 to the data in figure 4.4.14 , we can see that using radial stiffeners is far more efficient than increasing the hull weight for improved performance.

4.5 Finite Element Model Reliability

The finite element method is a good method to use for obtaining structural performance. The main routine used in stability analysis is the eigenvalue buckling routine which is based on linear stability theories. For many problems, this linear theory is sufficient for obtaining the desired information, but it doesn't always predict the complete behavior of the structure. Nonlinear theories may be used to capture this complete behavior. Furthermore, on the manufacturing aspect of things, real structures are not perfect. When modeling structures, we tend to have models that are more precise

than what can be actually be manufactured, and imperfections in the model must be introduced to predict the behavior of a manufactured structure. Therefore, an analysis was performed using nonlinear theories, and a separate test was run taking shape imperfections in account.

4.5.1 **Shape Imperfection Effects**

Thin elastic shells' equilibrium can be affected by the applied loading conditions and any deviations of the structure, geometry, or material properties from the nominal configuration. Under these conditions, the structure can undergo 3 types of deformation

1. Prebuckling deformation
2. Buckling deformation
3. Postbuckling deformation

The response of these thin shells can be extremely sensitive to loading and geometrical imperfections. Geometrical imperfections are characterized by any divergence in the shape of the structure from the geometrically ideal structure. M. Farshad defines the geometrical imperfections of shell structures as

Any deviation of middle surface geometry from a conceived ideal shape.[18]

Loading imperfection come in the form of deviations in the magnitude and/or direction of the applied load from the ideal magnitude and/or direction (e.g. nonuniformities in circumferential pressure distribution). Past research has shown that shell structures made for laboratory experiments often have critical buckling pressures lower than the ones predicted for ideal structures. Since manufactured shell structures are never geometrically perfect, the critical load predicted for the ideal structure can never be

achieved. Here we can see how prebuckling deformation plays a role in determining the buckling load of the structure.

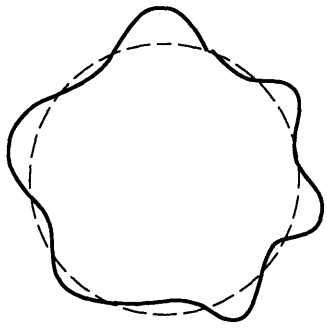

Figure 4.5.1: **Exaggerated Out of Circularity Imperfection**

The imperfection that concerns us most is geometrical imperfections. To induce an imperfection into the model, the ABAQUS mesh configuration with 10 stiffeners in the middle was modified by placing an out of circularity imperfection on the order of ±0.0001 in. at L/2. For example, the out of circularity induced imperfection would resemble the configuration shown in Figure 4.5.1. A static lateral load was applied to the structure in small increments, using linear load increments. With a step size equal to .01 of the total load applied to the structure, where the total load applied was 32 psi. The load increased linearly until the buckling load was reached.

In the analysis, the critical buckling load was found by recording displacement vs. time and load vs. displacement plots. To create these plots, a node in the middle of the cylinder (L/2) was monitored, and the displacement values at each time increment were recorded. Figure 4.5.2 illustrates the x and y displacement value for a prescribed time history. The critical point is easily seen as the point where the lines reach a discontinuity in the lines original path. The load vs. displacement plots (4.5.3 &4.5.4) for x and y displacements of the monitor node shows the exact load at which the discontinuity appears, and this load is the critical buckling load of the structure. From this we can see that the critical buckling load for this configuration was approximately 6.3 psi. By

comparison, the linear eigenvalue extraction predicted 6.4 psi **(see figure 4.4.10 and Appendix B).** These figures helped visualize the rapid change in stability of the cylindrical shell. This phenomenon can be explained best with bifurcation of equilibrium theory.

During loading of structure in increments, the equilibrium state of the structure will reach a point of bifurcation. At this point, two possible equilibrium paths exist for the structure. After this point is passed, the structure can remain in its original equilibrium state or it could deviate from this path and go into a new equilibrium state. The path the structure chooses depend upon total energy state of each respective choice. Given this choice, we know that the structure will choose the path corresponding to minimum total energy of the system. Therefore, the bifurcation point of the system corresponds to the critical buckling load of structure.

Imperfection Results With K=100,000 lbs/in

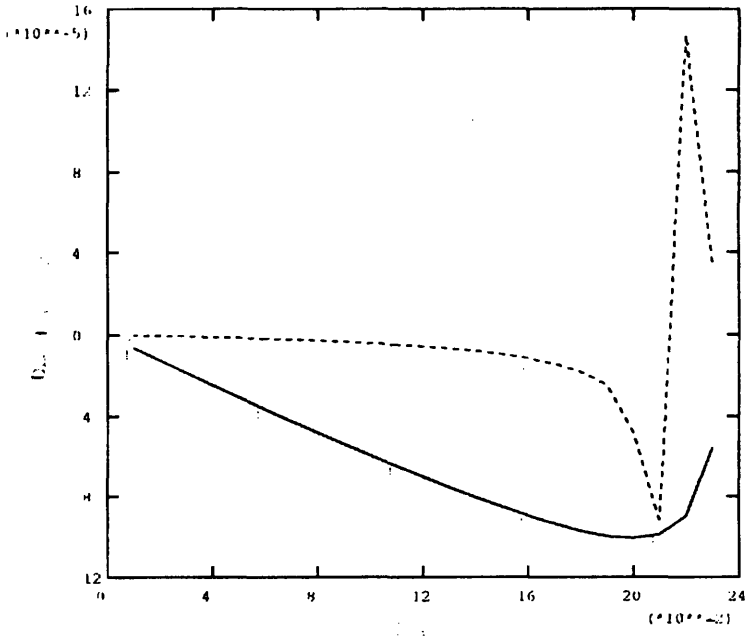

- - y displacement
- x displacement

Figure 4.5.2: **Displacement vs Time for Cylinder with 10 Stiffeners at L/2**

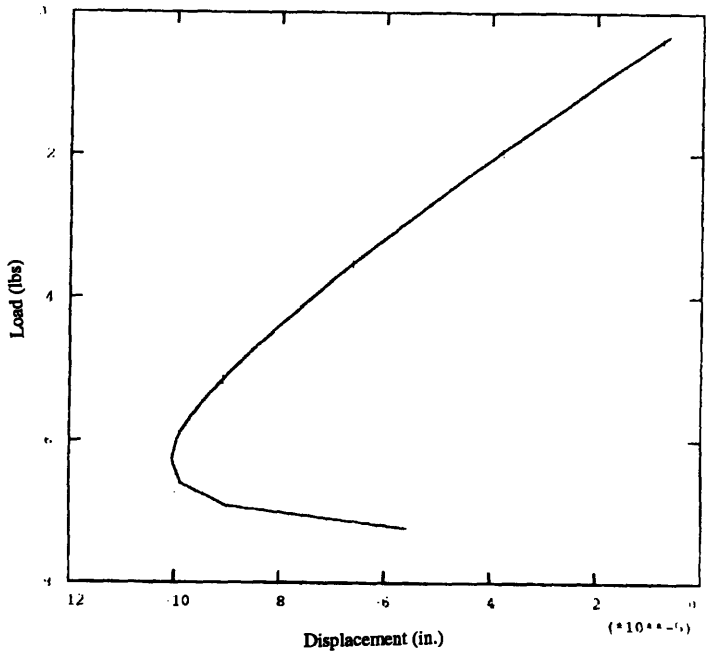

Figure 4.5.3: **Load vs X-Displacement for Cylinder with 10 Stiffeners at L/2**

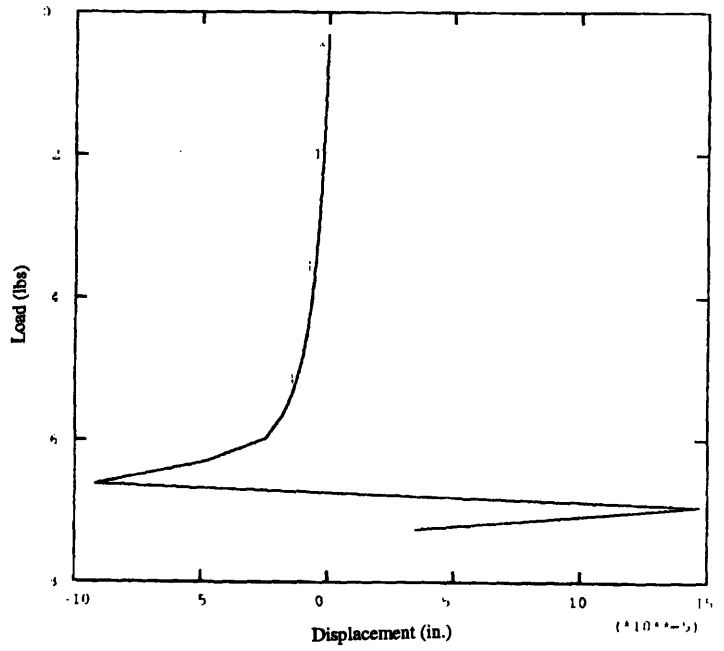

Figure 4.5.4: **Load vs Y-Displacement for Cylinder with 10 Stiffeners at L/2**

4.5.2 **Nonlinear Theories**

Linear theories of shell buckling that are based on perfect systems predict behavior that is not often realized. This linear stability theory has the ability to predict the bifurcation point or critical buckling load of the structure. Shell structures with small imperfections can go from the unbuckled equilibrium state to the buckled equilibrium state at a lower critical load than that predicted by linear theories. From this fact, we question whether linear theory is sufficient to determine the entire behavior of the combined shell- stiffener structure. Therefore, we will evaluate system stability using mathematically more complex nonlinear theories.

In the finite element analysis, the ABAQUS program uses the modified RIKS method for these nonlinear studies. This algorithm assumes that all the load magnitudes vary with a single parameter (proportional loading). The method attempts to find an equilibrium path in a solution space defined by the nodal variables and the loading parameter. With a reasonable step size, the solution traverses this equilibrium path as far as it can go. When the structure begins to buckle, the load doesn't increase with an increasing displacement. This behavior can be observed with a plot of Load vs. Displacement. With this method, you can limit the amount of time history data you need for your analysis. Furthermore, the step size is very critical in obtaining an accurate buckling load. If the step size is to large, the algorithm can't capture the desired solution. In essence, it would over-shoot the solution point. With a small step size, the method can capture the solution effectively, but may absorb large run times to find it.

The model used in this analysis used 10 springs at L/2 , and the RIKS method was used to analyze the model for various stiffeners. A static lateral load was applied to the structure, and the program uses the step size to apply the load gradually. After each step , the algorithm outputs a load proportionality factor (λ). This proportionality factor is used to calculate the applied load on the structure at that point. The main equation used for this tasks is given as

$$P_{total} = P_0 + \lambda(P_{ref} - P_0) \tag{4.5.1}$$

where

P_{total}- current magnitude of the load
P_0- load magnitude at the beginning of the step
λ- load proportionality factor
P_{ref}- load defined by engineer

Since there were no pre-loads in this analysis, P_0=0. Therefore, we can obtain the current load magnitude at the end of each increment by multiplying the proportionality factor times P_{ref}. Finally, the results were obtain in graphical form, and the plots giving the most information being

1. Load vs. Displacement
2. Load vs. Time
3. Displacement vs. Time

These plots are selected at a node in the mid-length of the shell and show two components of displacement (x and y displacements)

RIKS Results With K=100,000 lbs/in

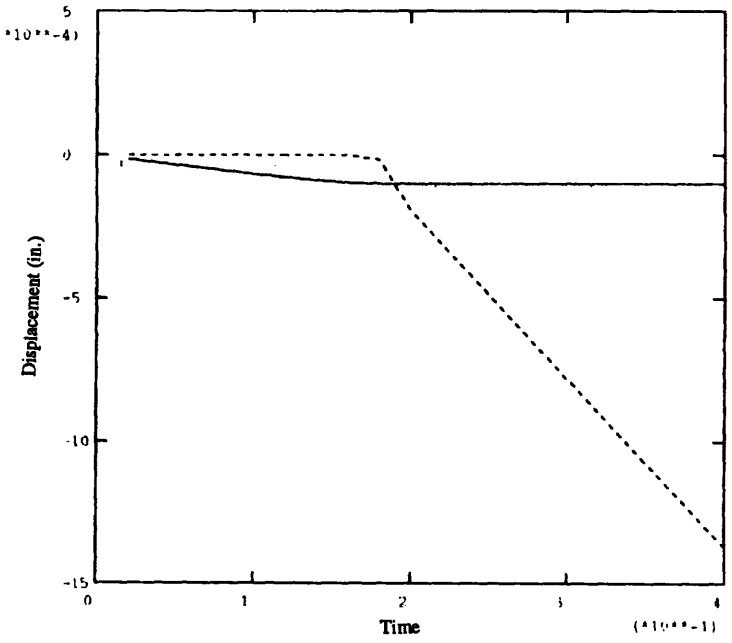

— x- displacement
- - - y- displacement

Figure 4.5.5: **Displacement vs Time for Cylinder with 10 Stiffeners at L/2**

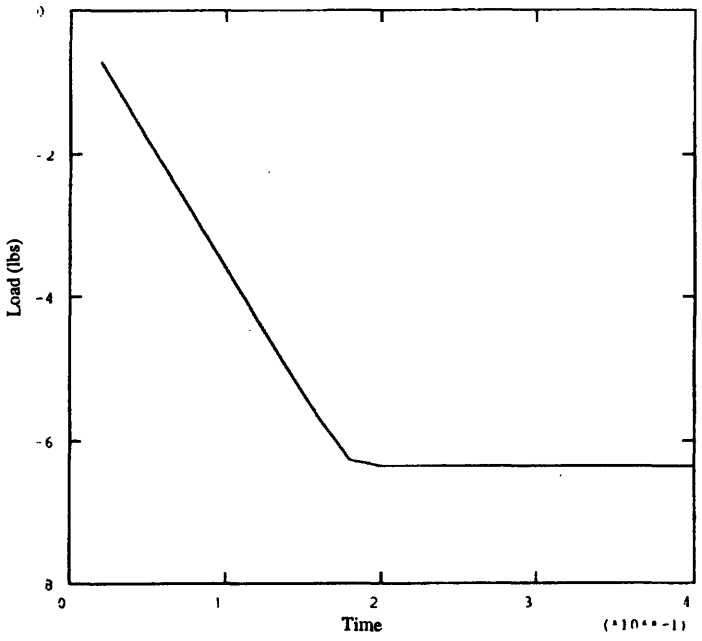

Figure 4.5.6: **Load vs. Time for Cylinder with 10 Stiffeners at L/2**

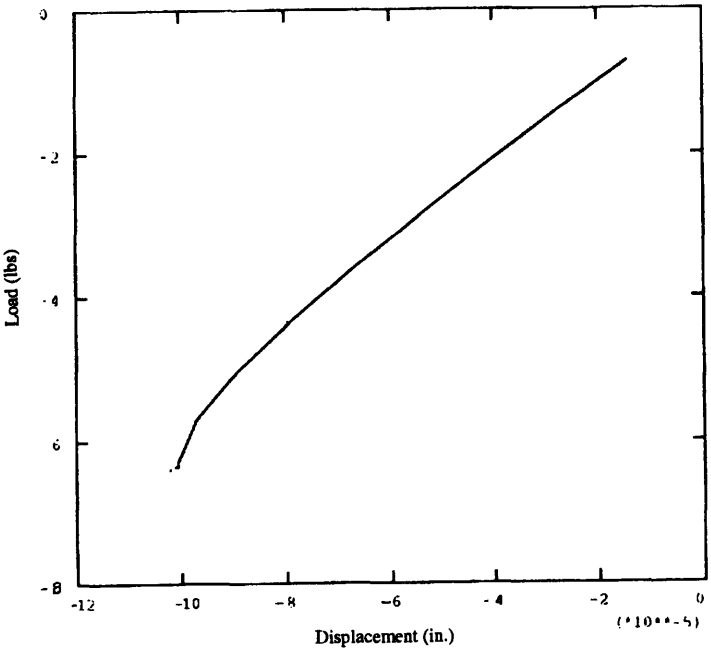

Figure 4.5.7: **Load vs X-Displacement for Cylinder with 10 Stiffeners at L/2**

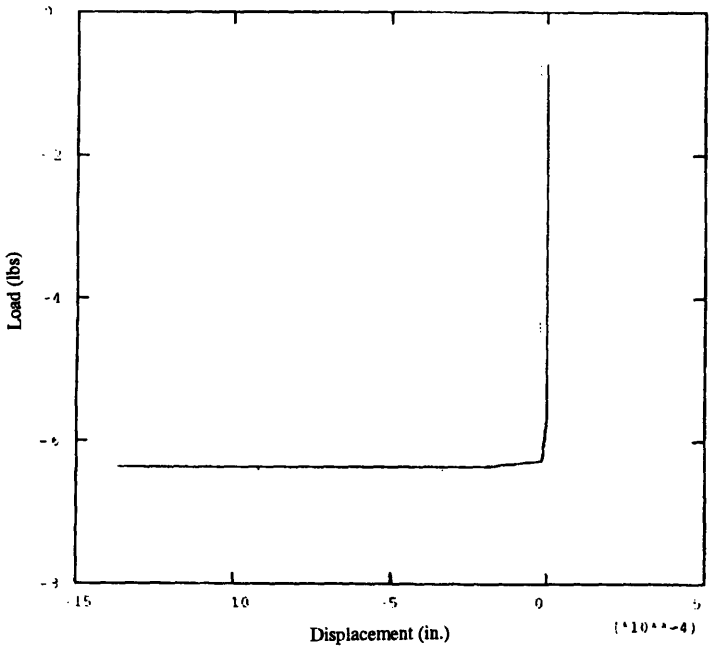

Figure 4.5.8: **Load vs Displacement for Cylinder with 10 Stiffeners at L/2**

Again, we see the discontinuities in the paths of the lines. The lines seemed to follow a particular equilibrium path in the beginning, but as time went on and loads increased, a point (bifurcation point) was reached at which the lines found another equilibrium path. In figures 4.5.6 - 4.5.7, we see that at this point the displacements increased a great deal for a constant load which indicates that bifurcation buckling has occurred. For this case, the bifurcation point occurred at a load of 6.354 psi., and eigenvalue predictions yielded a load of 6.3559 psi. Therefore, we can see that the eigenvalue predictions were sufficient in predicting the critical buckling load of these modified cylindrical structures, and more RIKS results an be seen in the Appendix.

The practical result is that inexpensive eigenvalue calculations can be confidently used for parametric evaluation of these configurations (see Table 4.5.1).

Analytical Method	Critical Pressure (P_{cr}) psi
Eigenvalue Buckling Extraction	6.3559
Static Load Step	6.3000
RIKS Method	6.3540

Table 4.5.1: **Analytical Method Comparison**

From table 4.5.1, we can see that all three methods are relatively close in there prediction of the critical load. The imperfection load step case has a lower predicted critical load than the other methods, but that is expected. Also, the RIKS Method's solution compared to the Eigenvalue solution tells us that the nonlinear effects are negligible in the stability analyses shown. Further solutions using these methods can be found in the **Appendix C**. Using the eigenvalue method as the reference, the largest percent difference is less than 1%. With such a small percent difference, any of the three methods are sufficient for predicting the critical load. Since the static load step and RIKS Method cost more computer time than the eigenvalue extraction, then it is more economical to use eigenvalue extraction methods.

4.6 Stresses at Stiffener-Hull Intersection

During the deformation process, the stiffeners are applying a load to the hull structure as point reaction forces. Since these forces act on the structure at a finite point, there is a stress concentration at this point. In design, one of the most important things to consider is the yield point of the material. Yielding of the material can cause the structure to failure, and we want to design against failure.

The material used in these stability analyses was titanium. Titanium was chosen for its high strength to weight properties; therefore, it has low mass with a high yield stress. This stress analysis was performed to make sure that the hull structure doesn't yield under the applied load for various stiffness values. A finite element model was made to represent the area in the vicinity of the point support, and this area was subjected to a load that is significantly higher than the critical load for a thin cylindrical shell with 12

stiffeners in the center. Since this is small piece, the **dxdy** slice was approximated as a flat plate, and this plate was model using S8R5 shell elements arranged in a 6 x 6 mesh.

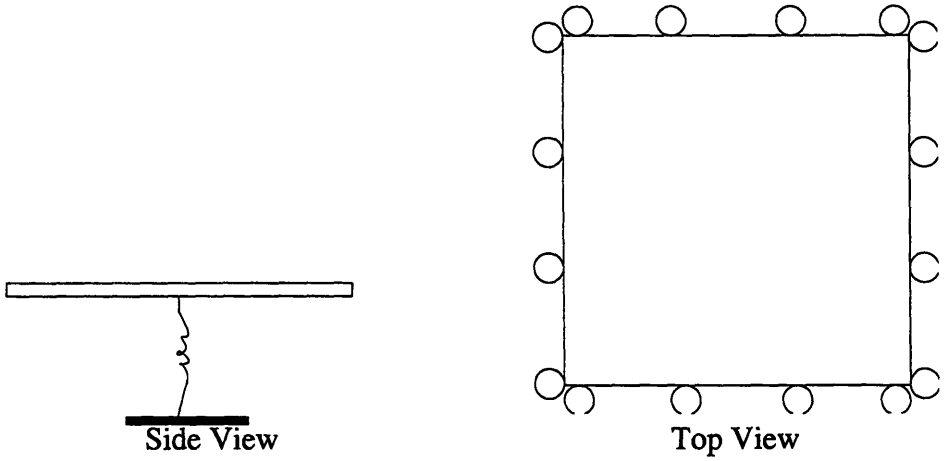

Figure 4.6.1: **Finite Element Model Configuration**

Figure 4.6.1 shows configuration of the model. From pressure vessel theory , we know that cylinders under uniform lateral loads have a hoop stress and an axial stress. These stresses can be estimated from the following:

$$\sigma_{\theta\theta} = \frac{pr}{t} \qquad \sigma_{xx} = \frac{pr}{2t} \tag{4.6.1}$$

The top view in the figure shows how the dxdy slice is constrained to induce the required reaction forces at the edges. Next , the spring was placed in the center of the plate, and it was model using a SPRINGA element with a length corresponding to a quarter of the radius. Using a high stiffness value for the spring, an uniform pressure load was applied to the plate. The applied load produces the stress distribution shown in figure 4.6.2. From this figure , we can see that the highest stress is at the intersection of the spring and the hull, and σ_{xx} and σ_{yy} have a maximum value at this point equal to 3.02 $x10^3$psi. The yield strength of titanium is 150 x 10^3 psi, which is significantly higher than the stresses shown. Furthermore, to look at this nondimensionally, consider the ratio of σ_{max}-$\sigma_{\theta\theta}$.

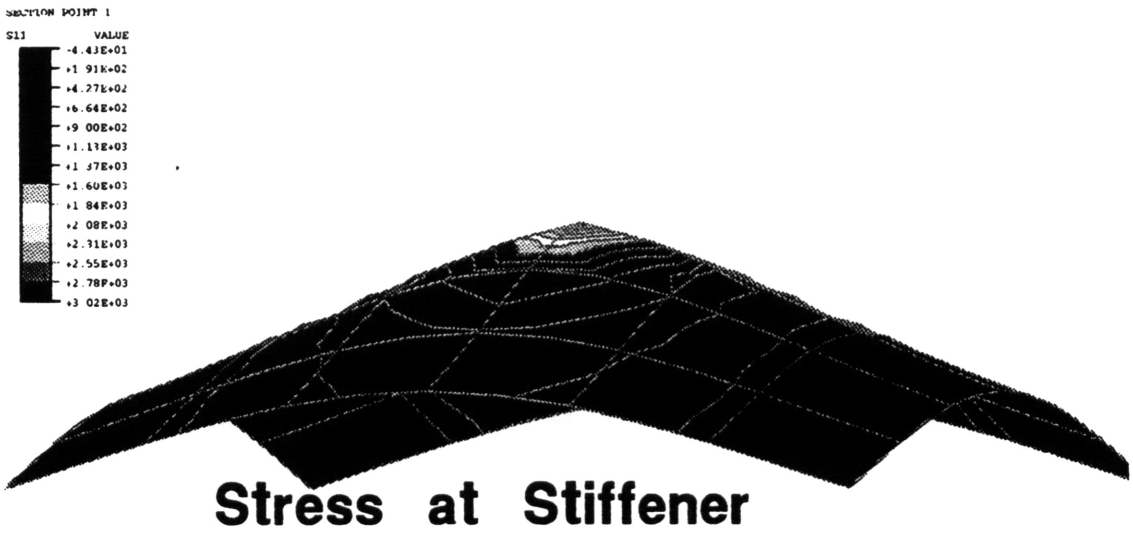

Figure 4.6.2: **Stress Contour Plot of a Cylinder Path in the Vicinity of a Radial Point Support**

$$\frac{\sigma_{max}}{\frac{pr}{t}} \approx 4.3$$

where

p= 4 psi t=.125 in.

r= 22 in. σ_{max}= 3.02 x 10^3 psi

From this ratio, we can see that the maximum stress with radial stiffeners is 4.3 times the maximum shell stress without stiffeners. Therefore, the critical stress is dominated by the regions of stress near the point supports. Since most submarines are designed up to approximately 60%-70% of the yield strength, the load at the point of hull-stiffener attachment should be distributed over a specified area. This design change gets rid of the point load and replaces it with a distributed load. Also, a distributed load decreases the chances of the structure yielding at the point of attachment. Although this model is not an accurate account of the effects a set of stiffeners will have on the stress level, it does give some insight into how the stresses are distributed in this region, and with the interaction of stresses with other stiffeners, this maximum value will change. These stress interactions only become important with closely spaced stiffeners. Therefore, the structures used in the stability analyses will not yield before it buckles because the stiffeners are spaced far enough apart and the yield stress wasn't reached.

4.7 Stability Analysis of a Cylinder with an Internal Truss Structure

Up until this point, we have been examining the buckling characteristics of rings and cylinders with radial stiffeners held fixed at one end. Holding the end fixed at free end of the stiffener assumes that the truss structure is very stiff. In general, the truss structure may not be as stiff as we assumed. To investigate this assumption, a finite element model of a cylinder with an internal truss was created. In this particular model, the truss was made of steel bars while the cylindrical shell was made from titanium. To illustrate the

truss arrangement, a section view is shown in **figure 4.7.1**. The same shell element configuration was used for the hull as before (reference configuration), but the 3-D truss used 2 node truss elements(C1D2). Also, 8 stiffeners were used to attach the truss to the hull, and they were created using spring elements (SPRINGA). To examine the buckling phenomena of a this structure, a uniform lateral pressure load was exerted onto the cylindrical shell structure with an internal truss.

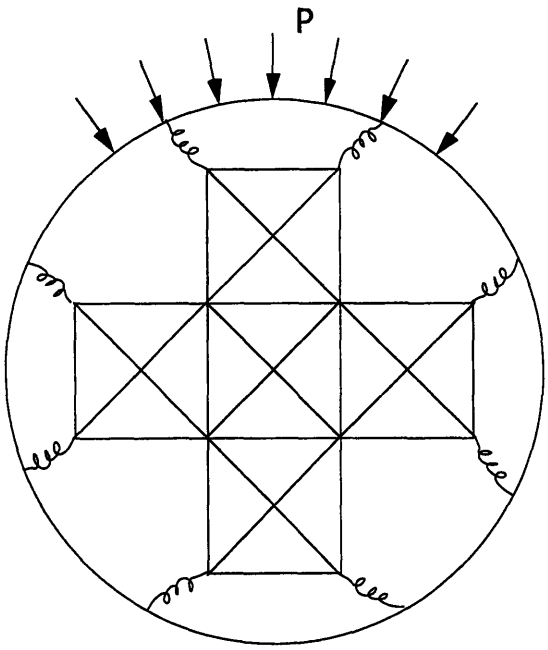

Figure 4.7.1: **Axial View of the Truss Connected to the Cylindrical Shell through Radial Point Supports Under Hydrostatic Load (P)**

Using the eigenvalue bucking extraction routine, the critical buckling load was calculated with various stiffener stiffness values for a unit cross-sectional area of the truss members. As a result of this test, it was found that for this particular truss member cross-sectional area, the calculated critical loads were very close to the case with 8 stiffeners that were fixed at the free end. A comparison of the two different case is shown in **figure 4.7.2**.

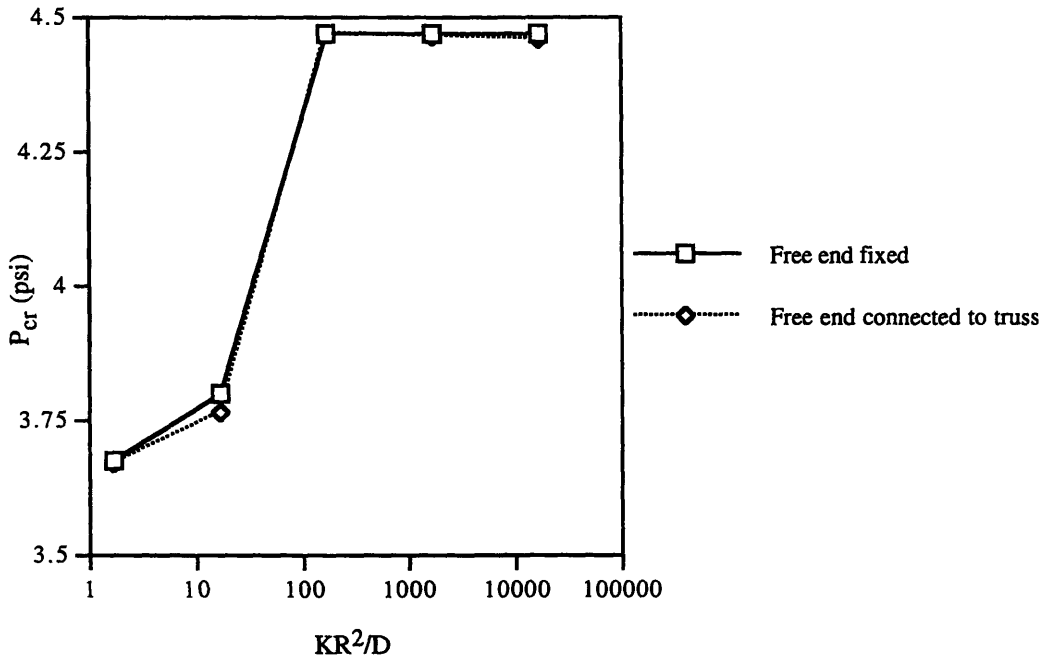

Figure 4.7.2: **Effects Two Different Boundary Conditions (Free End Fixed & Free End Connected to a Truss) on the Critical Load of a Circular Cylindrical Shell with 8 Radial Supports.**

From this we can conclude that for this cross-sectional area, the truss behaves as a very stiff structure.

Since we know that the stiffness of the truss structure is related to the cross-sectional area, the cross-sectional area can be varied to give us a better idea of the effects truss stiffness on hull stability. First , the truss stiffness has to be determined. To ascertain truss stiffness, a static analysis was performed on the truss. In this analysis, the truss was pinned at all the corners at the top and bottom, but in the middle all were pinned except one. On that one particular node, a 10,000 lb load in the radial direction was exerted onto the truss, and the amount of displacement of this node in the radial direction was measured. This allowed us to calculate the stiffness of the truss using the expression

$$K_{Truss} = \frac{F}{\delta}. \qquad (4.7.1)$$

where δ is the resulting radial deflection.

With this setup, the stiffness of the truss was evaluated using the ABAQUS finite element model for different cross-sectional areas of the truss members. **Figure 4.7.3** shows the

results of this study, and we can see that there is a linear relationship between truss stiffness and the cross-sectional area of its members.

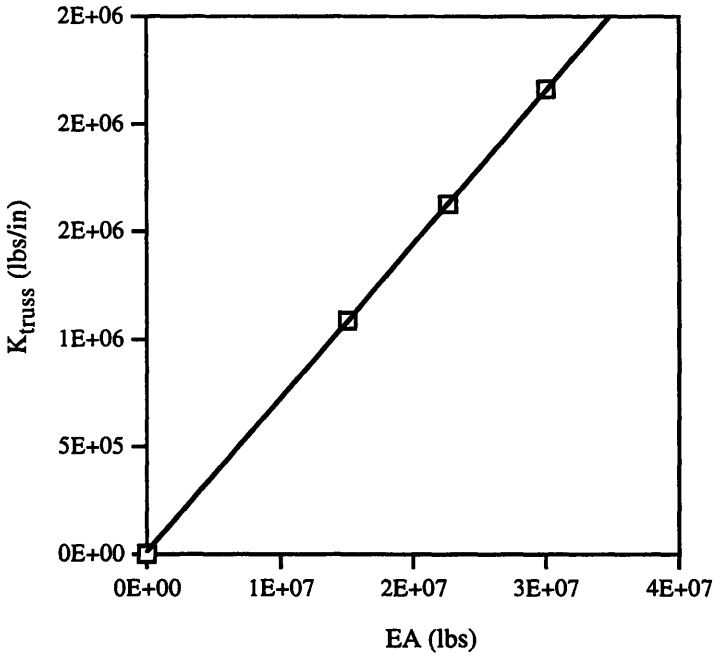

Figure 4.7.3: **Effects of Varying the Truss Member Cross-Sectional Area on the Truss Radial Stiffness**

With an increase in cross-sectional area or an increase in Young's Modulus of the truss members, the stiffness of the truss increases accordingly. Keeping in mind that the total weight of the submarine structure is important for performance attributes, we don't want to increase the area of the truss members to much, and as expected, we can see that a linear relationship exist between truss weight (W_{truss}) in pounds and EA **(see figure 4.7.4).**

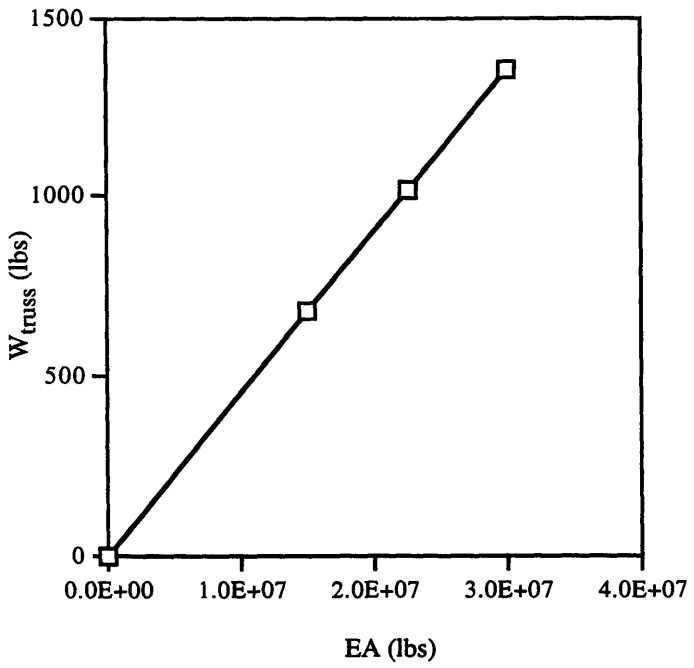

Figure 4.7.4: **Effects of Varying the Parameter (EA)on the Total Weight of the Truss**

Figure 4.7.4 illustrates the variation in truss weight with bar stiffness, assuming that the material is steel and the variable is cross-sectional area. The previous two studies showed the linear relationship between EA and truss weight and truss stiffness. To place these effects into the overall context, the interaction of the truss stiffness and the radial stiffener stiffnesses was studied. To accomplish this task, a total effective stiffness was calculated using the following expression:

$$\frac{1}{K_{tot}} = \frac{1}{K_{Truss}} + \frac{1}{K_{Stiff}} \tag{4.7.2}$$

where

K_{stiff} varied between 10 and 100,000 lbs/in

The calculated value for K_{tot} was used to compare the ratio of truss weight to hull weight to the nondimensional parameter ($K_{tot}R^2/D$) used in the critical load analyses of **section 4.4.** In the other analyses, the free ends were fixed; therefore, K_{truss} was infinitely large, and the inverse of this large value is approximately zero. The results of the comparative study can be seen in **figure 4.7.5.**

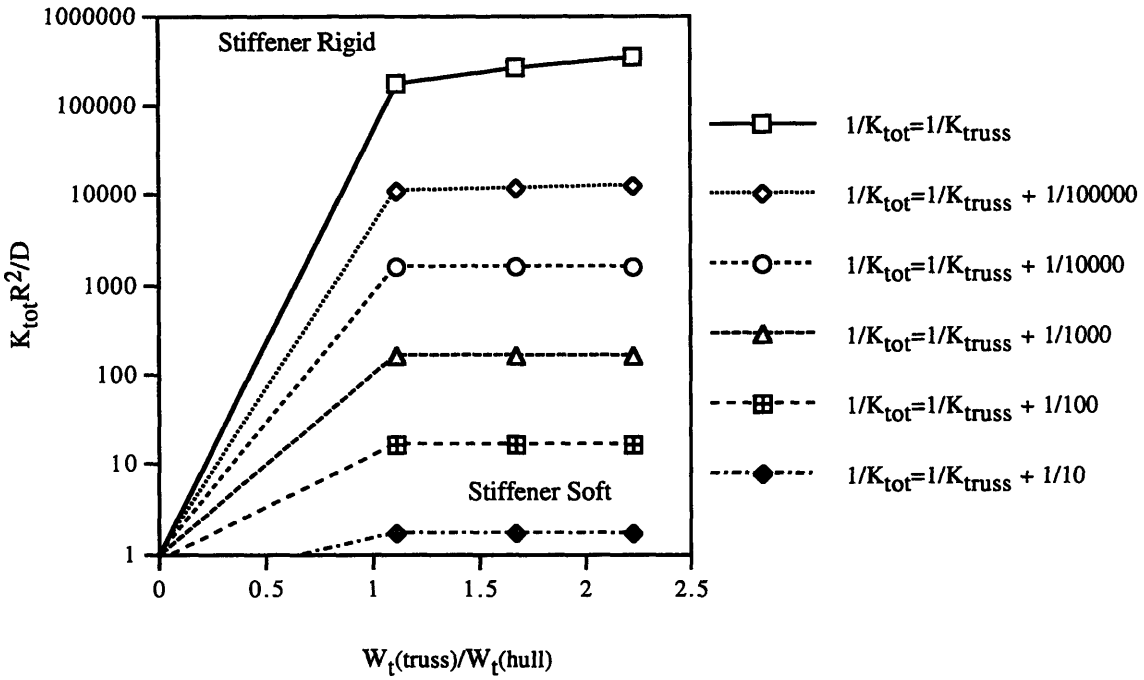

Figure 4.7.5: **Effects of Varying the Truss Weight on the Stiffener Parameter (K_{tot} R^2/D)**

From this figure , we can see that increasing the truss weight doesn't really provide any increase in the nondimensional stiffness parameter beyond a truss weight approximately equal to the skin weight. To really understand how light we can make the truss, more cases must be run @ W_t(truss) / W_t(hull) less than 1.0. Certainly above W_t(truss) / W_t(hull)=1 there is no further benefit to be had by increasing truss weight (stiffness). It was shown in previous sections that an increase in this parameter results in an increase in the critical buckling. Since the truss is very stiff ($O(10^6)$), the stiffener stiffness dominates the total stiffness variable K_{tot}. The truss stiffness provided slight improvements when the stiffener stiffness values were of order $O(10^5)$. This told us that as the stiffeners' stiffness values were increased, we approached the stiffness of the truss structure. Finally, the most valuable information is that the radial stiffeners have a greater effect on the stability of the cylindrical shell than the truss. Therefore, it would be advantageous to make the lightest truss allowable to fulfill stiffness requirements , and this would improve

the W/D ratio of the total submarine structure. By improving the W/D ratio, we improve the efficiency of the submarine structure, which will allow a greater payload.

CHAPTER FIVE

Conclusions and Recommendations

5.1 Summary

Since the recent focus of U.S. submarine designers has been on the French truss/cradle design concept, the advantages of this concept were addressed along with integrated design tools to help improve the overall design process. In this design, the cradle is attached to the hull envelope through several point attachments as compared to the welded plating attachments of current machinery. The main objective of this thesis was to evaluate the effects of these point attachments on the stability behavior (buckling) of the hull envelope. To get a general idea of the stability behavior of circular shells with point supports under hydrostatic loading, circular rings with various numbers of radial stiffener supports were modeled numerically using the ABAQUS finite element code. This finite element model without point supports was checked with Timoshenko's analytical model before the supported case could be evaluated effectively. The spacing and stiffness of these supports were varied throughout the analysis. As a result of the model, it was shown that increasing the number of radial stiffener supports around the circumference of the shell increased the critical load of the structure. Finally, as a limiting case, the analytical solution of a ring on an elastic foundation was compared to the numerical solution of a resiliently supported ring with many stiffener supports.

The buckling phenomena of circular rings provided some insight into the stability behavior of circular shells under radial loading, and this knowledge was used to investigate the stability of point supported cylindrical shells. As in the rings, a finite element model was created to comply with Timoshenko's model, which used the Donnell stability relationships for cylindrical shells. Once a good working model had been established, the number of stiffeners was varied around the circumference and along the

length of the cylinder, and the stiffness values of these supports were varied. As a result of the analysis, it was shown that there was a maximum level of improvement that can be obtained for a given number of stiffeners around the circumference of the shell. Furthermore, for the geometries evaluated, there was no improvement in the critical load for an increasing number of stiffeners along the length. Finally, it was shown that increasing the number of stiffeners around the circumference of the shell in the middle of the shell length increases the critical buckling load greatly.

Next, to put the design concept to the actual test, a truss structure was modeled inside the hull envelope to evaluate the effects of truss stiffness on the critical buckling load of the truss-hull structure. It was found that for low stiffness values of the discrete spring stiffeners, the stability behavior was dominated by the bending stiffness of the hull. At higher discrete spring stiffness levels, the stiffness of the truss began to affect the critical load of the truss-hull structure.

Although cylindrical shells tend to be dominated by general instability failure, stresses can be just as harmful to the life of the structure. Taking this part of the analysis into account, a stress analysis was performed on a small patch in the vicinity of the point support. The stress levels found were much lower than the yield stress of the material. Since the applied load was greater than the buckling load, the structure would buckle before it locally yielded.

5.2 **Discussion of Results**

The radial supports provided a significant increase in the critical instability pressure of thin rings and cylinders, but the stiffness value of these supports must be of order $O(10^3)$ lbs/in or higher to achieve these improvements. First, the ring stability analysis provided basic insight into the effects of radial stiffeners on circular shells. In this analysis, we found out that as the number of stiffeners used increased, the critical pressure of the resulting structure also increased. The physical explanation seems to be

that above a threshold stiffness, the point supports enforced circumferential nodes, and more nodes imply a higher mode and pressure. Also, a ring on an elastic foundation was used as limiting case for a circular ring with many radial stiffeners. The simple elastic foundation model provided a useful guide to the level of stiffness needed to improve cylinder buckling performance. Furthermore, the stiffener's circumferential spacing had very little effect on the shell's instability pressure. Therefore, from the parameter variations tested, we saw that main variables were the number of stiffeners used around the shell circumference and the stiffness values of these stiffeners.

Although radial supports provided improvements in the stability behavior of cylindrical shells, we discovered some limitations. For a given number of supports around the perimeter of the cylinder, there was a limit reached at which there was no improvement in the critical load for increasing support stiffness. As in the rings, an increased number of supports around the perimeter increased the critical stability pressure. Considering the thickness of the cylindrical shell, the results showed that the radial supports' effects were reduced as shell thickness increased. Also, the radial supports give appreciable improvement with very little effect on the total weight of the structure. Therefore, radial supports are effective buckling inhibitors for thin shells, and there is a large improvement in stability performance with little additional weight.

The truss structure placed in the cylindrical shell was attached through the radial supports, and large truss stiffnesses had very little of effect on the stability of the shell. If the truss stiffness is large, the shell support is dominated by the discrete springs. The support stiffness values seem to have a greater effect on the critical instability pressure for large truss stiffness values. It was shown that the lower the truss stiffness is, the greater effect it will have on the critical buckling load. Also, an increase in cross-sectional area (increase in weight) of the truss members provided trivial increases in instability performance for low support stiffness values. Therefore, it would be

advantageous to use a truss with the lowest weight allowable, and use the radial supports to tailor the structure to the desired stability behavior.

Finally, in all designs it is important consider the stresses seen in the structure before it yields. Taking this into consideration, it has been shown that the titanium structure doesn't not yield before it buckles. Multiplication or safety factors were developed which relate the peak shell stress to PR/t . For the case studied, this factor is about "4.3". This suggest that (unless local reinforcement is used) the nominal skin stress should be held to 20% or less of the material yield strength. This will ensure that the primary failure mode is general instability of the cylindrical shell structure.

5.2 **Recommendations for Future Work**

Although this work provided useful design information into the use of radial supports for submarine design, there are other areas that can be looked into to improve the stability performance of cylindrical shells with this cradle design concept.

- Other stiffener arrangements can be tested to see which arrangement is more effective at inhibiting buckling of the cylindrical shell structure. These might include asymmetric combinations of supports at different axial stations.

- A dynamic analysis can be performed to find out what is the maximum support stiffness that can be used to meet submarine acoustic requirements. This would include calculating transfer functions from truss to hull surface.

- A cylindrical shell could be fabricated implementing the truss/cradle design concept to examine the behavior of an actual structure to hydrostatic pressures with various support stiffnesses.

- A design sensitivity algorithm can be written to find the optimal design of a submarine hull structure with an internal truss.

REFERENCES

1. Friedman, N.,"Submarine Design & Developement", Naval Institute Press-Maryland, 1984.

2. Polmar, N., "The American Submarine", The Nautical & Aviation Publishing Co. of America-Maryland, 1981.

3. Gorman, James. CSDL senior engineer. Personal Communication in Sept. 1993.

4. Ross, C. T.F., "Pressure Vessels Under External Pressure - Statics and Dynamics" Elsevier Applied Science-London, 1990.

5. Krenzke, M., Jones, R., and Kiernan, T., "Design of Pressure Hulls for Small Submersibles", ASME Paper 67-WA, UNT-7, November 1967.

6. Comstock, J. (ed.), Principles of Naval Architecture, Section 8, "Submarine Pressure Hull Design", SNAME, 1967.

7. Brush, D., Almroth, Bo., "Buckling of Bars, Plates, and Shells", McGraw-Hill-New York, 1975.

8. Timoshenko, S., " Theory of Elastic Stability", McGraw-Hill-New York, 1959.

9. Timoshenko, S. and Woinowsky-Krieger, S., "Theory of Plates and Shells", McGraw-Hill-New York, 1936.

10. Bathe, Klaus-Jurgen, "Finite Element Procedures in Engineering Analysis", Prentice-Hall, Inc., New Jersey, 1982.

11. Farshad, M., "Design and Analysis of Shell Structures", Kluwer Academic Publishers-Boston, 1992.

12. Gorman, J. and Louie, L., "Submersible Pressure Hull Design Parametrics", SNAME Transactions, Vol. 99, pp 119-146, also Annual Meeting Paper No. 3, November 1991.

13. Perry, T., Douglas, C. and Gorman, J., "Analytical Design Procedures for Buckling Dominated Graphite/Epoxy Pressure Hulls", SNAME Transactions, Vol. 100, pp. 93-115, also Annual Meeting Paper No. 3, October 1992

14. Daniel, R., "Considerations Influencing Submarine Design", Proc. of the Royal Institute of Naval Architects International Symposium on Naval Submarines, Vol. I, 1983.

15. ABAQUS User's Manual, Version 4.8, Hibbitt, Karlsson, & Sorenson, Inc. 1990.

16. Farshad, M., "Design and Analysis of Shell Structures", Kluwer Academic Publishers-Boston, 1992, p. 344.

17. Brush, D., Almroth, Bo., "Buckling of Bars, Plates, and Shells", McGraw-Hill-New York, 1975, p. 15.

18. Farshad, M., "Design and Analysis of Shell Structures",
Kluwer Academic Publishers-Boston, 1992, p. 350.

Appendix A: Ring Buckling Results

During the eigenvalue extraction for a circular ring with various stiffeners and stiffener orientations, the first 15 modes were calculated for a given spring stiffness value and number of stiffeners, but only the first 5 modes were recorded. Although the critical mode is the first mode encountered, it was desired to push the critical mode to a higher mode. With the data shown in tables A-1 & A-2, we can see the advantages of pushing the critical mode higher.

		P_{cr} (psi)		
K (lbs/in)	n	12 Stiffeners	8 Stiffeners	4 Stiffeners
10	2	1163	1158.8	1156.6
	3	3069.7	3068.5	3066.9
	4	5708.5	5707.6	5707.1
	5	9043.6	9043.1	9041.4
	6	13034	13031	13031
100	2	1220.2	1178.1	1156.6
	3	3091.6	3079.5	3066.9
	4	5720.7	5711.9	5707.1
	5	9052.1	9046.9	9041.4
	6	13035	13033	13031
1000	2	1792	1369.6	1156.6
	3	3310.5	3188.6	3066.9
	4	5843.1	5755	5707.1
	5	91370	9092.3	9041.4
	6	13055	13046	13031
10000	2	7490.9	3150.9	1156.6
	3	5502.4	4182.9	3066.9
	4	7059.7	6176.8	5707.1
	5	9961.2	9609.8	9041.4
	6	13253	13168	13031
100000	2	-	-	1156.6
	3	-	-	3066.9
	4	-	-	5707.1
	5	-	8059	9041.4
	6	15105	14610	13031

Table A-1: **Data Table 1 for Stiffness Comparison**

From table A-1, we can see that as the stiffness values increases, the critical load increases. Furthermore, some of the modes present at low stiffness values are not present

at high stiffness values for the first 15 modes calculated. This tells us that the load required to produce those mode shapes are much higher than the loads required to produce some of the higher mode shapes. Therefore, mode 2 doesn't always correspond to the lowest mode. For example, the critical mode can be mode 3, and mode 2 could require a higher load such as the case with K= 10,000 lbs/in and 12 stiffeners used.

		P_{cr} (psi)			
K (lbs/in)	n	7 Stiffeners	7 Stiffeners[1]	5 Stiffeners	5 Stiffeners[1]
10	2	1160.3	1158.4	1159.2	1158.5
	3	3068.6	3068	3068.3	3067.6
	4	5707.8	5707	5707	5707.4
	5	9042.7	9042.8	9042.3	9042.4
	6	13032	13031	13031	13031
100	2	1193.2	1174.4	1182.2	1175.3
	3	3079.7	3075.3	3077.1	3070.5
	4	5713.9	5709.9	5707.5	5711.1
	5	9047.2	9045.3	9042.9	9046.5
	6	13030	13032	13031.2	13030
1000	2	1520.4	1332.5	1398.8	1341.2
	3	3187.5	3146.9	3178.9	3099.4
	4	5778.3	5736.3	5708.7	5746.8
	5	9093.7	9076.5	9048.6	9044.3
	6	13038	13043	13038	13039
10000	2	4450.7	2736.9	2274.2	2627.4
	3	3914.5	3745.1	5482.1	3626
	4	6814.2	5957.4	5729.9	6066.3
	5	9842.1	9440.3	9101.7	9056.9
	6	13097	13125	13108	13069
100000	2	-	-	-	-
	3	-	-	2545.5	3386.4
	4	4611.2	4833.4	5804.2	4879.6
	5	8027.5	6741.3	9364.8	9073.2
	6	13186	13418	13451	13110

1. Unevenly Spaced Stiffeners

Table A-2: **Data Table 2 for Stiffness Comparison**

Table A-2 shows the effects of using an odd number of stiffeners and uneven stiffener spacing. The general trend seems to be that the even spacing provides slightly better results than uneven spacing, but there is some variance at high stiffener stiffness values. Therefore, from the two figures , we can conclude that increasing the number of stiffeners

around the perimeter of the circular ring provides the needed advantages in the stability behavior.

Appendix B: Cylinder Buckling Results

For the first part of the cylinder buckling analysis, a set of stiffeners were placed at various stations along the length of the cylinder. At these various station, the stiffness value of the stiffeners were varied. The data given in table B-1 gives the results for the first 5 m=1 modes with stiffeners at the mid-section, third points, and quarter points.

		P_{cr} (psi)		
K(lbs/in)	n	8 stiffeners @L/2	8 stiffeners @L/3 & 2L/3	8 stiffeners @L/4, L/2 & 3L/4
10	3	3.6715	3.6780	3.6859
	4	4.4668	4.4668	4.4668
	5	6.8378	6.8400	6.8427
	6	9.9575	9.9590	9.9608
100	3	3.7973	3.8601	3.9351
	4	4.4668	4.4669	4.4669
	5	6.8828	6.9077	6.9388
	6	9.9857	9.9998	10.016
1000	3	-	-	-
	4	4.4672	4.4674	4.4676
	5	7.4041	7.9501	7.2867
	6	10.146	10.231	10.293
10000	3	-	-	-
	4	4.4687	4.4698	4.4707
	5	-	-	-
	6	10.334	10.427	10.560
100000	3	-	-	-
	4	4.4698	4.4716	4.4729
	5	-	-	-
	6	10.373	10.565	10.613

Table B-1: **Stiffener Configuration Comparison**

As a result of this analysis, we can see that increasing the number of stiffeners along the length of the cylinder doesn't give a significant improvement over the case with one station of stiffeners at the mid-section of the cylinder. In an attempt to force the structure into a higher mode shape, the stiffness values were varied with in each station instead of a global stiffness variation. Table B-2 shows the results of this analysis.

K (lbs/in)	n	P_{cr} (psi)	
		8 stiffeners @L/3 & 2L/3 (Var. #1)	8 stiffeners @L/3 & 2L/3 (Var. #2)
10	3	3.6692	3.6679
	4	4.4668	4.4668
	5	6.8370	6.8366
	6	9.9570	9.9567
100	3	3.7670	3.7537
	4	4.4668	4.4668
	5	6.8715	6.8669
	6	9.9787	9.9761
1000	3	-	-
	4	4.4671	4.4174
	5	7.2493	7.2090
	6	10.101	10.097
10000	3	-	-
	4	4.4682	4.4681
	5	-	-
	6	10.243	10.256
100000	3	-	-
	4	4.4689	4.4687
	5	-	-
	6	10.273	10.286

Table B-2: **Stiffness Variation Comparison**

We can see that these variations provided lower critical buckling loads than the ones provided in table B-1. Therefore, varying the stiffness values within a particular station doesn't provided any added advantages over uniform stiffness values for the entire hull-stiffener structure. Since increasing the stiffener along the length of the cylinder for the cases tested doesn't provided any advantages over one set of stiffeners at the mid-section, the number of stiffeners at L/2 were varied at a constant stiffness value (see table B-3). A constant stiffness value of K=100,000 was used because the maximum improvement gained seemed to plateau between K=1000 lbs/in and K=100,000 lbs/in. (see figure 4.4.5).

		P_{cr} (psi)				
K (lbs/in)	n	8 stiffeners	9 stiffeners	10 stiffeners	11 stiffeners	12 stiffeners
100000	3	-	7.5498	-	-	-
	4	4.4698	5.6910	6.3559	7.7337	8.5655
	5	-	9.4678	-	7.9235	8.3147
	6	10.373	11.123	10.857	10.535	9.9713

Table B-3: **Stiffener Comparison @L/2**

From table B-3, we can see that as we increase the number of stiffeners circumferentially, the critical load increases dramatically. The critical load almost goes up approximately 1 psi for each additional spring added. If the stiffness value of the circumferential stiffeners at L/2 are sufficiently large, the structure will be pushed to an m=2 logitudinal half wave (See Figure B-4). This mode has a higher critical load than the critical load achieved in an m=1 mode. Therefore, increasing the number of stiffeners circumferentially and increasing their stiffness values will approach the desired improvement in the critical load.

Figure B-1: **Circular Cylindrical Shell in an (n=2, m=2) Buckled Configuration**

Appendix C: RIKS Method Results

The RIKS Method is a nonlinear analysis routine that was used to predict the critical buckling load of the cylindrical shell. By picking a step size, the ABAQUS program calculates a proportionality factor at the end of each increment. By looking at the output, one is able to determine the load at which the structure buckled. The following is a series of plot of Load vs Time, Displacement vs. Time, Load vs X-Displacement, and Load vs. Y-Displacement. Table C-1 summarizes the results gathered from the plots (Figures C-1 to C-8).

	P_{cr} (psi)	
K (lbs/in)	Riks Method	Eigenvalue Extraction
10	3.685	3.6860
100	3.816	3.8203
100000	6.354	6.3559

Table C-1: **Solutions from RIKS Method for a Cylinder with 10 Stiffeners @L/2**

The point at which the bifurcation point is reach, the solution path reaches a point of discontinuity (a sharp bend). This point is the spot at which the structure buckles. As a result of these tests , one can tell that the solution from the RIKS Method was very close to the Eigenvalue solution with a .11 % difference. To see if it was case sensitive, another case was tried with stiffeners at the third points. Again the results are represented in graphical form in figures C-9 to C-16. Also, a table summary of the results depicted in these graphs are shown in table C-2

	P_{cr} (psi)	
K (lbs/in)	Riks Method	Eigenvalue Extraction
100	3.756	3.7537
100000	4.452	4.4687

Table C-2: **Solutions from RIKS Method for a Cylinder with 8 Stiffeners @L/3 & @2L/3**

Finally, the results show that the RIKS Method agreed with the eigenvalue solution within a .37% difference. Therefore, there were no significant nonlinear effects that would affect the solution outcome, and the eigenvalue extraction is a sufficient method for predicting the critical load.

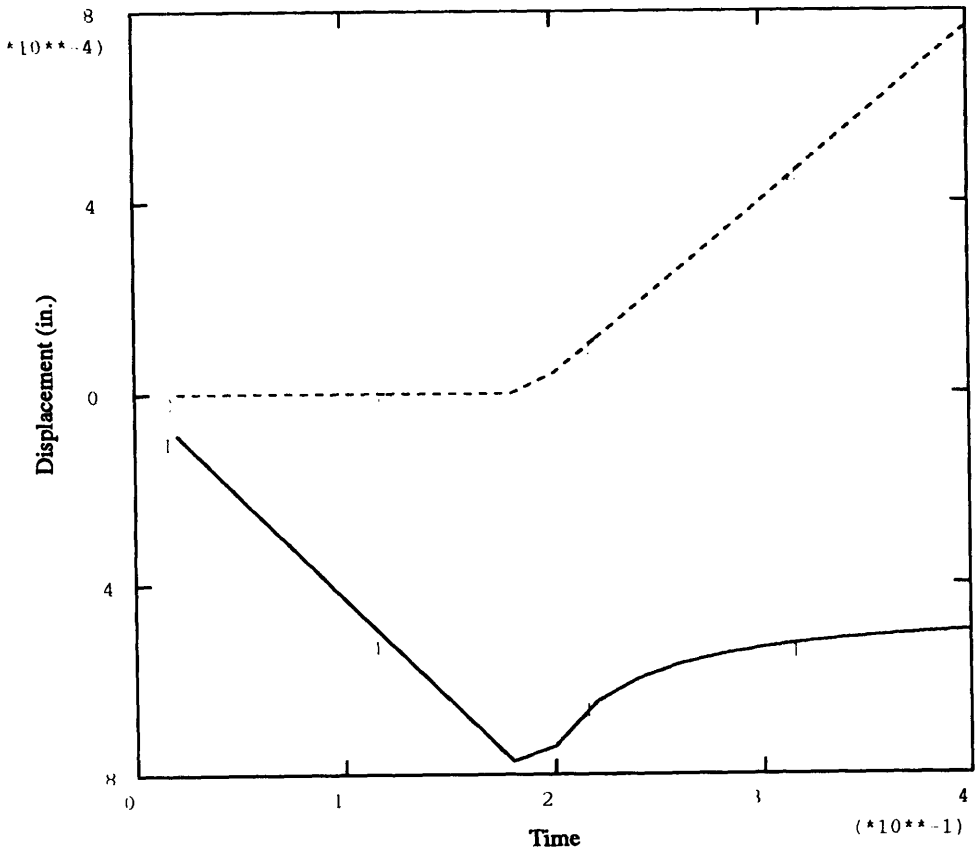

Figure C-1: **Displacement vs. Time for Cylinder with 10 Stiffeners at L/2 with K=10 lbs/in**

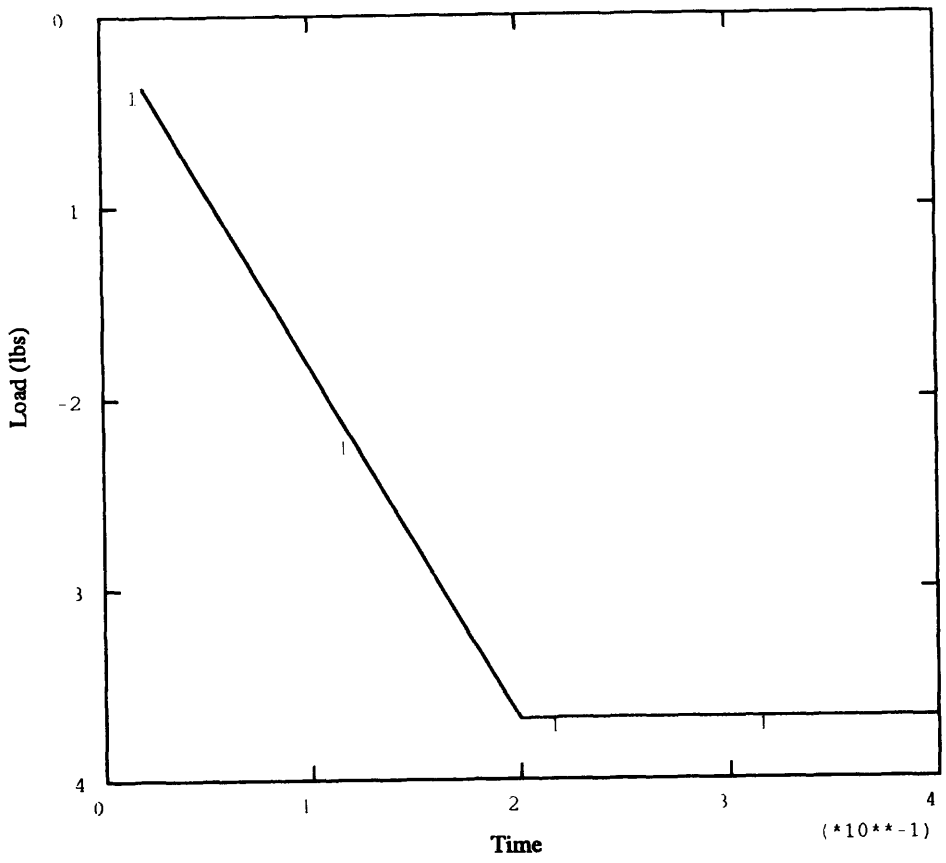

Figure C-2: **Load vs. Time for Cylinder with 10 Stiffeners at L/2 with K=10 lbs/in**

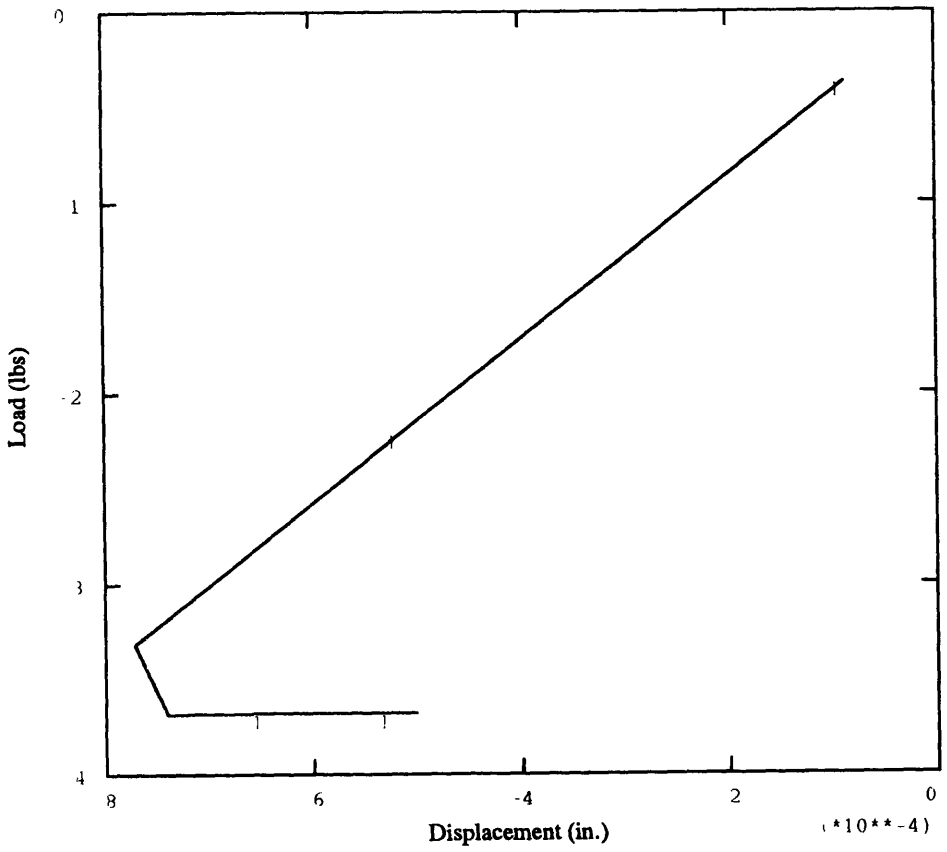

Figure C-3: **Load vs X-Displacement for Cylinder with 10 Stiffeners at L/2 with K=10 lbs/in**

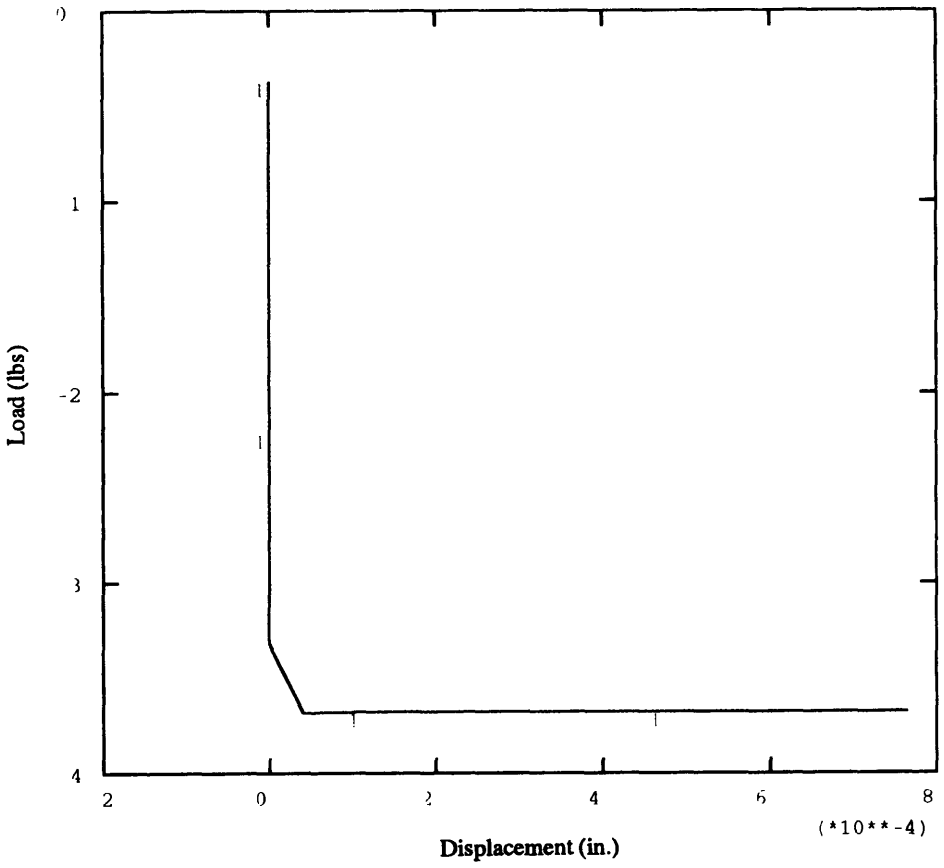

Figure C-4: **Load vs Y-Displacement for Cylinder with 10 Stiffeners at L/2 with K=10 lbs/in**

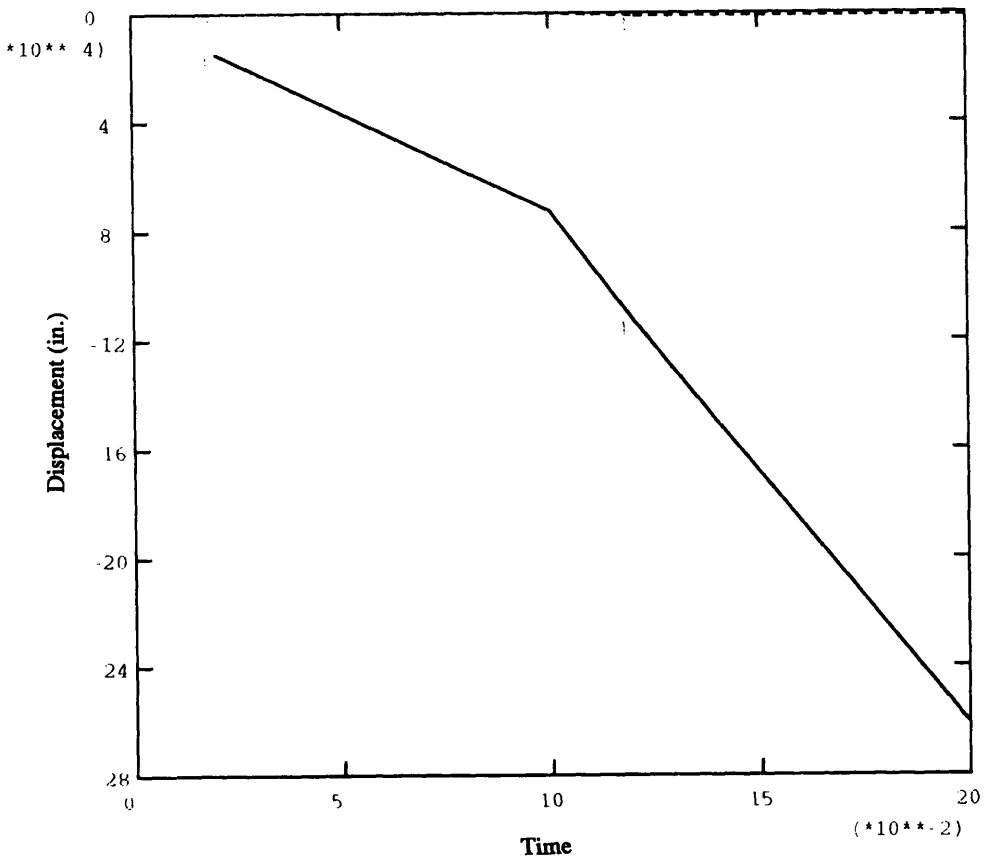

Figure C-5: **Displacement vs. Time for Cylinder with 10 Stiffeners at L/2 with K=100 lbs/in**

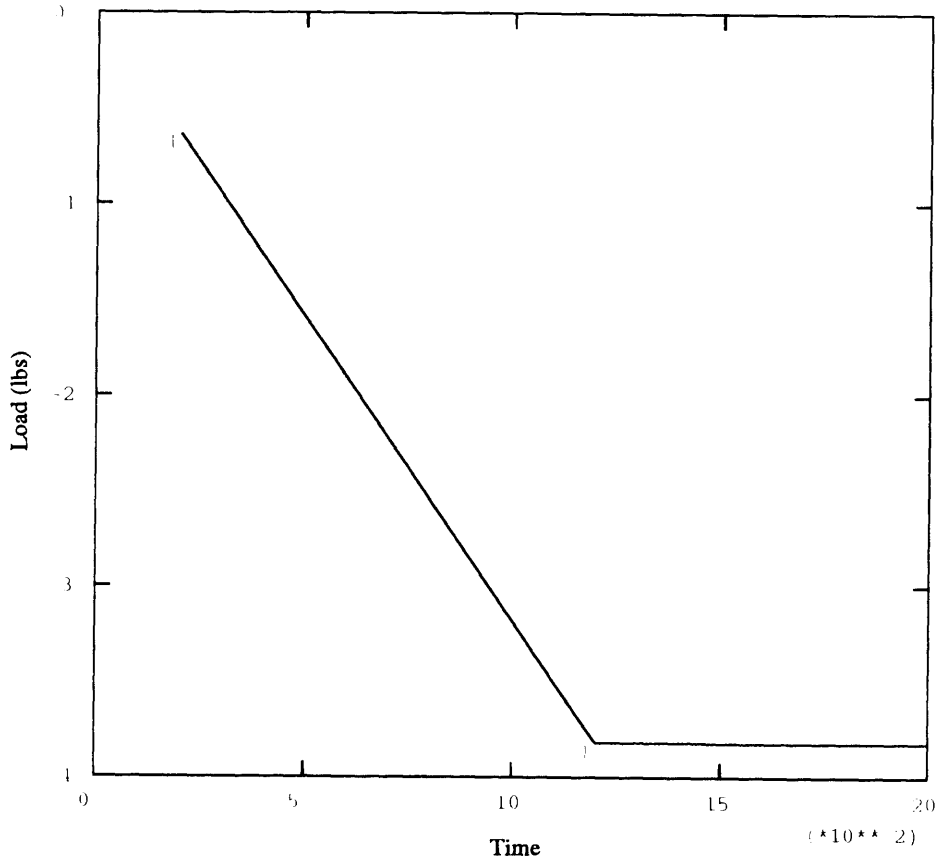

Figure C-6: **Load vs. Time for Cylinder with 10 Stiffeners at L/2 with K=100 lbs/in**

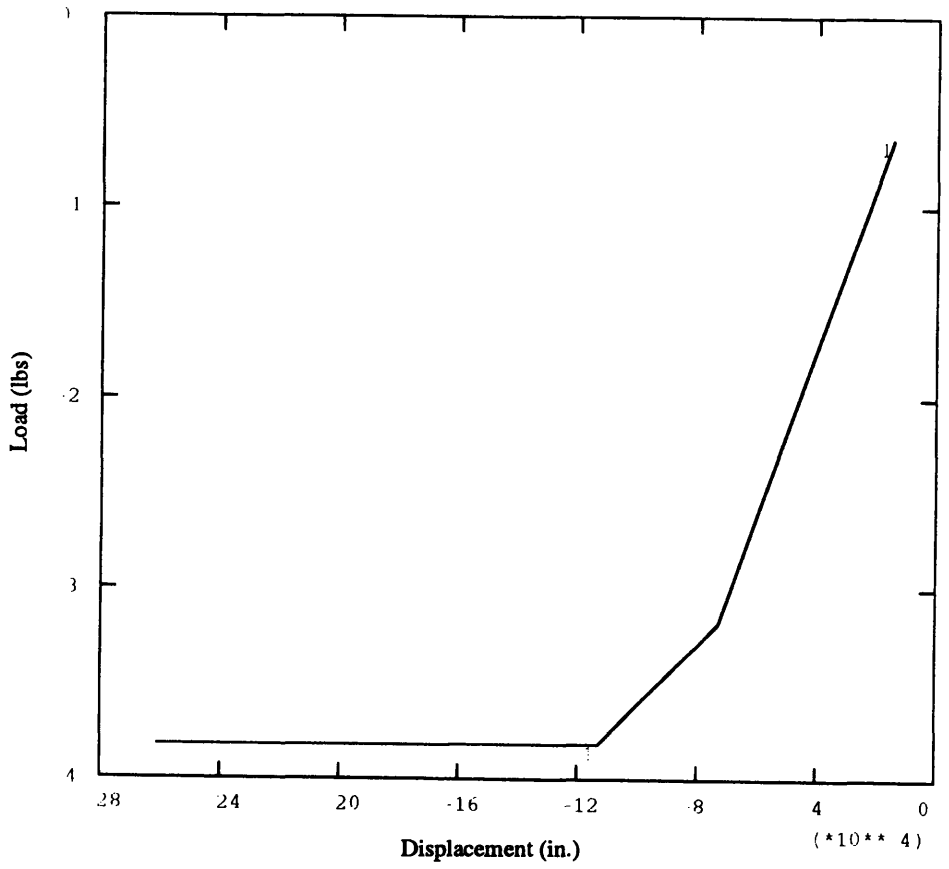

Figure C-7: **Load vs X-Displacement for Cylinder with 10 Stiffeners at L/2 with K=100 lbs/in**

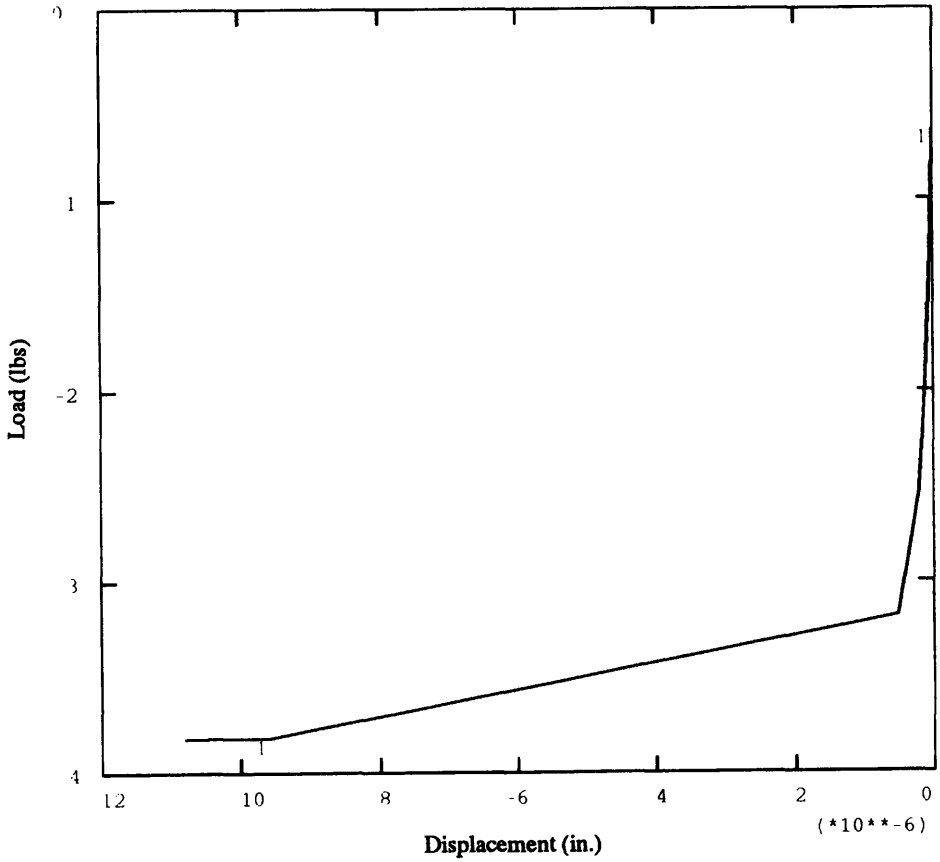

Figure C-8: **Load vs Y-Displacement for Cylinder with 10 Stiffeners at L/2 with K=100 lbs/in**

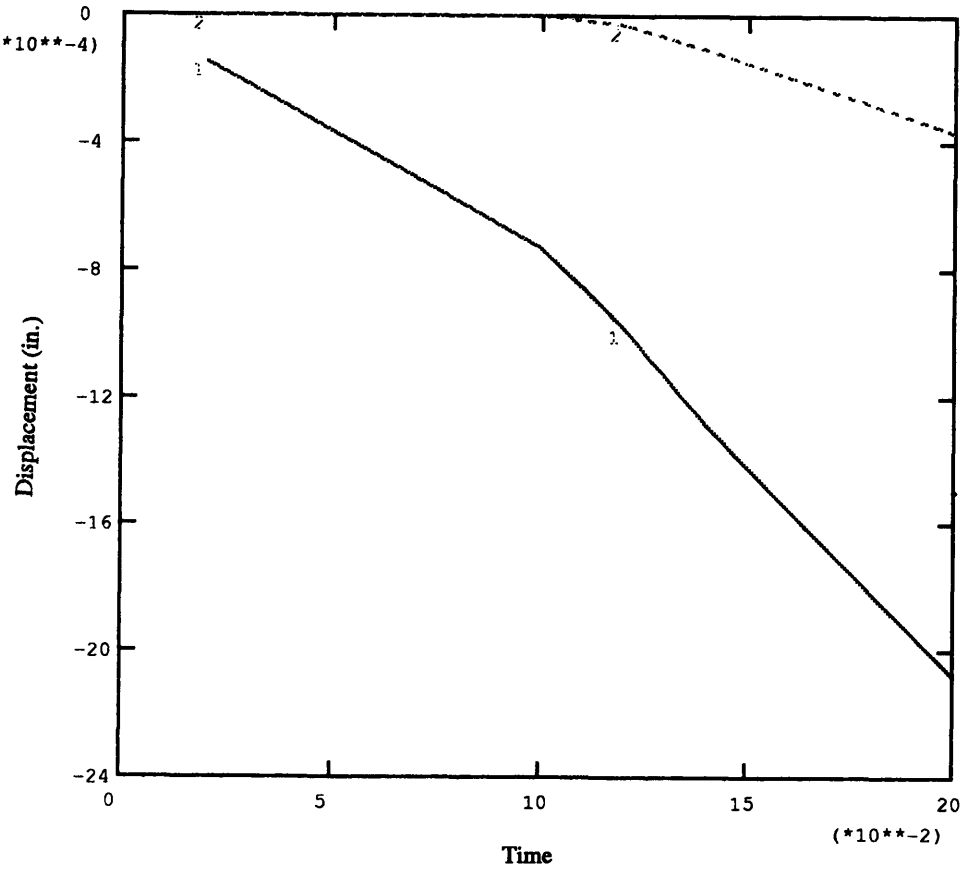

Figure C-9: **Displacement vs. Time for Cylinder with 8 Stiffeners at L/3 and 2L/3 using Alternating Stiffness Values (Variation 2) with Every Other Stiffness K=100 lbs/in**

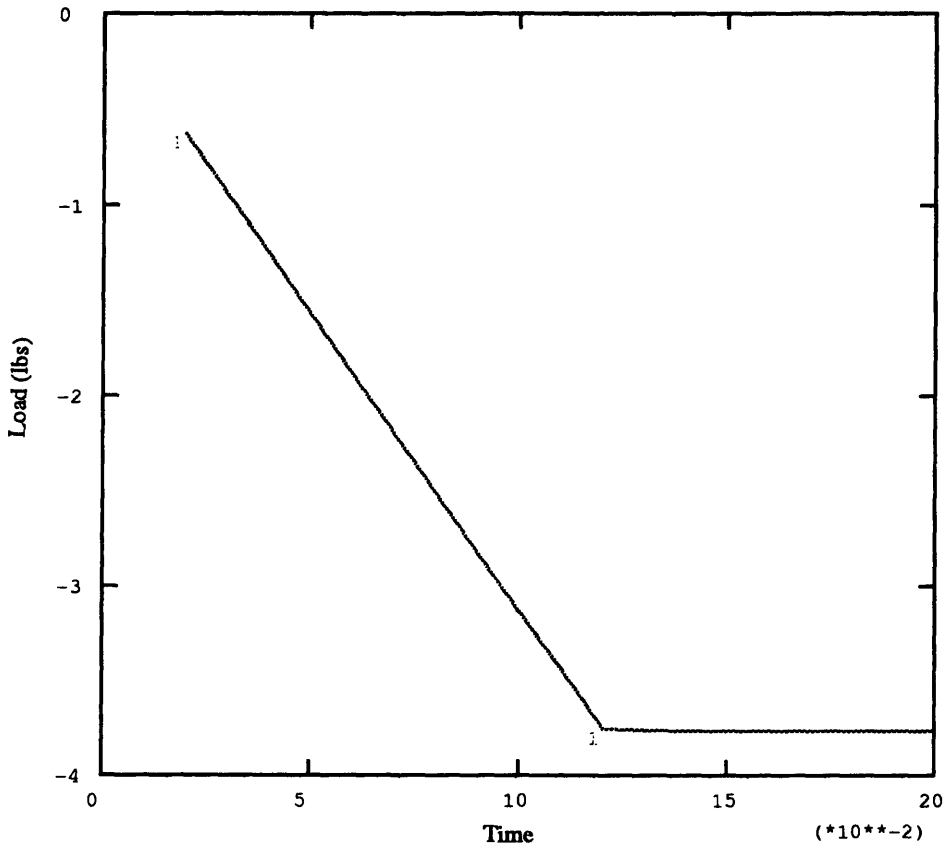

Figure C-10: **Load vs. Time for Cylinder with 8 Stiffeners at L/3 and 2L/3 using Alternating Stiffness Values (Variation 2) with Every Other Stiffness K=100 lbs/in**

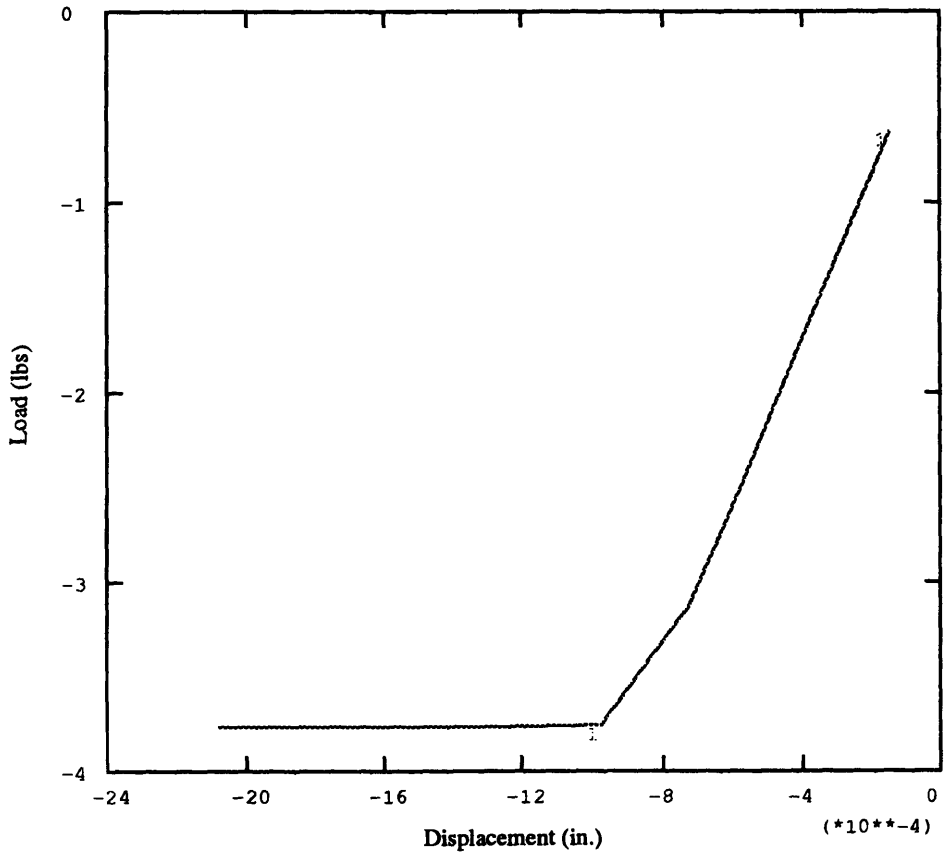

Figure C-11: **Load vs X-Displacement for Cylinder with 8 Stiffeners at L/3 and 2L/3 using Alternating Stiffness Values (Variation 2) with Every Other Stiffness K=100 lbs/in**

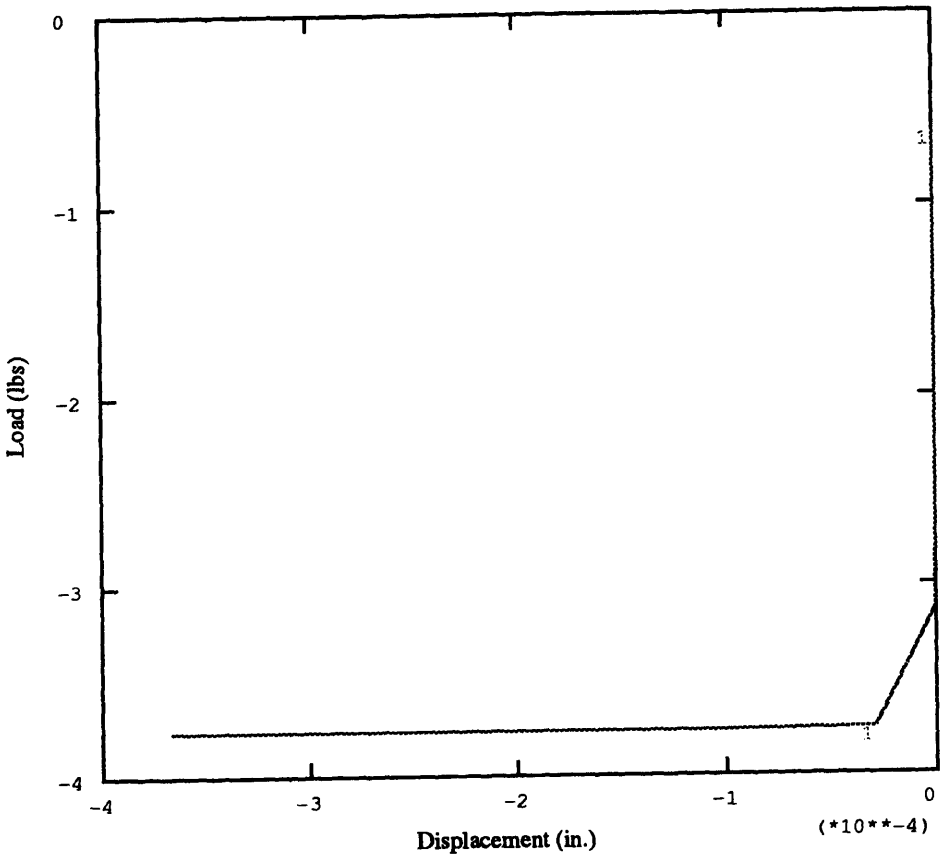

Figure C-12: **Load vs Y-Displacement for Cylinder with 8 Stiffeners at L/3 and 2L/3 using Alternating Stiffness Values (Variation 2) with Every Other Stiffness K=100 lbs/in**

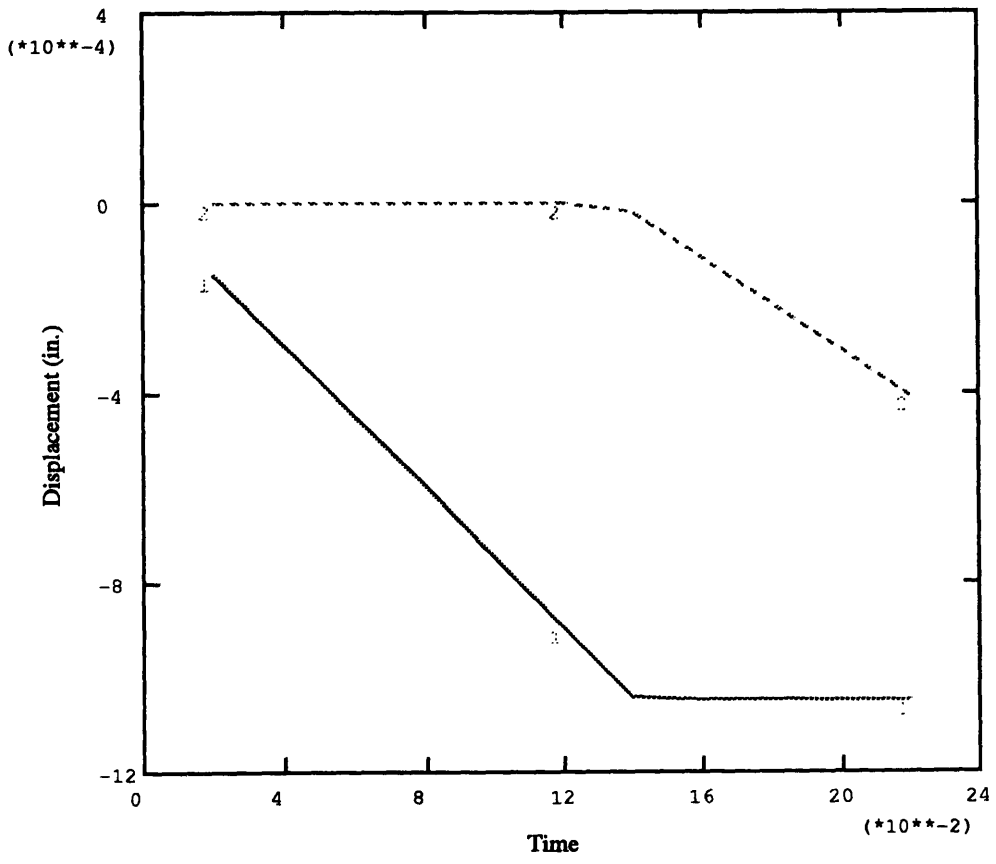

Figure C-13: **Displacement vs. Time for Cylinder with 8 Stiffeners at L/3 and 2L/3 using Alternating Stiffness Values (Variation 2) with Every Other Stiffness K=100,000 lbs/in**

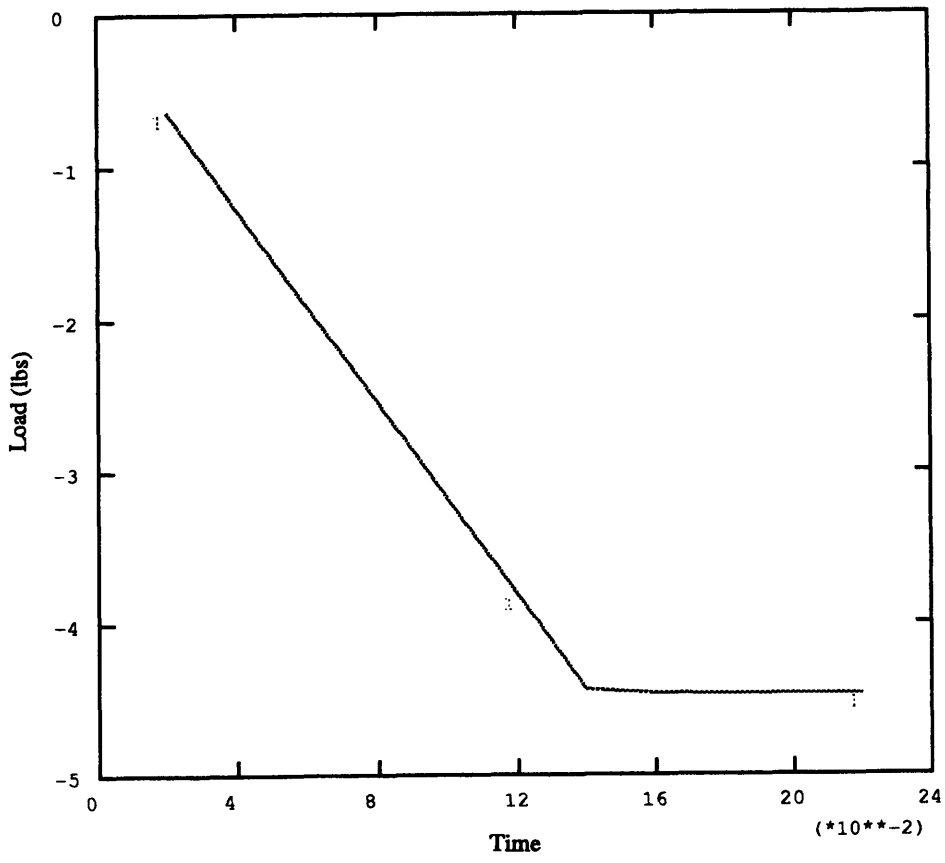

Figure C-14: **Load vs. Time for Cylinder with 8 Stiffeners at L/3 and 2L/3 using Alternating Stiffness Values (Variation 2) with Every Other Stiffness K=100,000 lbs/in**

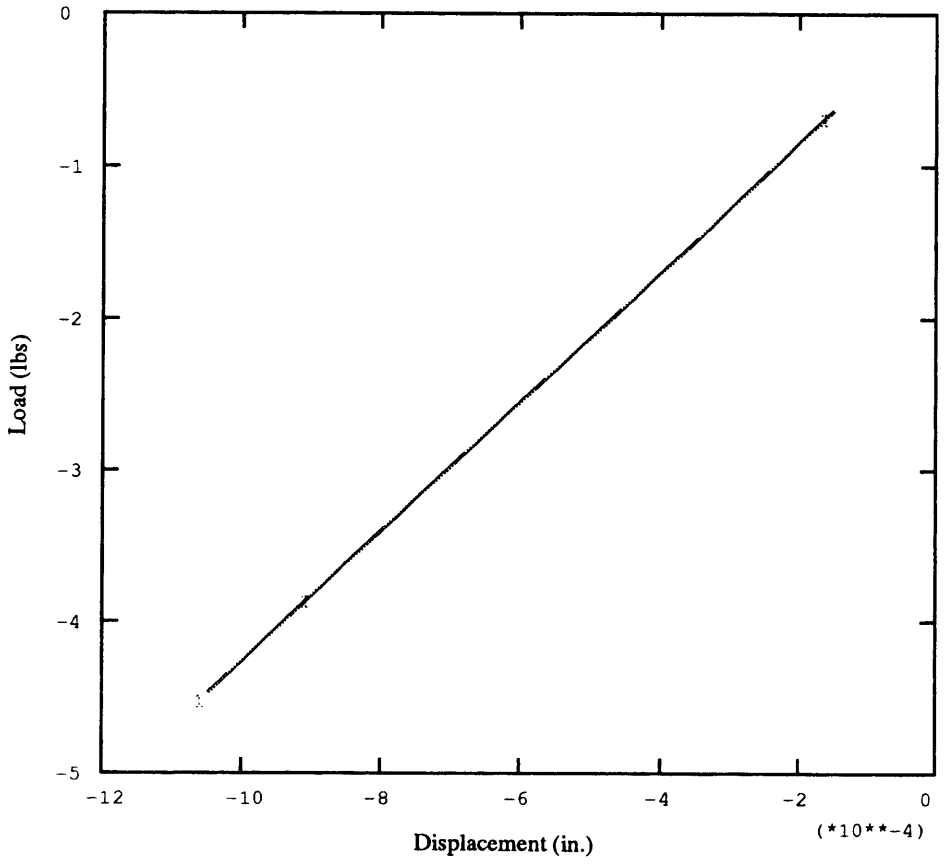

Figure C-15: **Load vs X-Displacement for Cylinder with 8 Stiffeners at L/3 and 2L/3 using Alternating Stiffness Values (Variation 2) with Every Other Stiffness K=100,000 lbs/in**

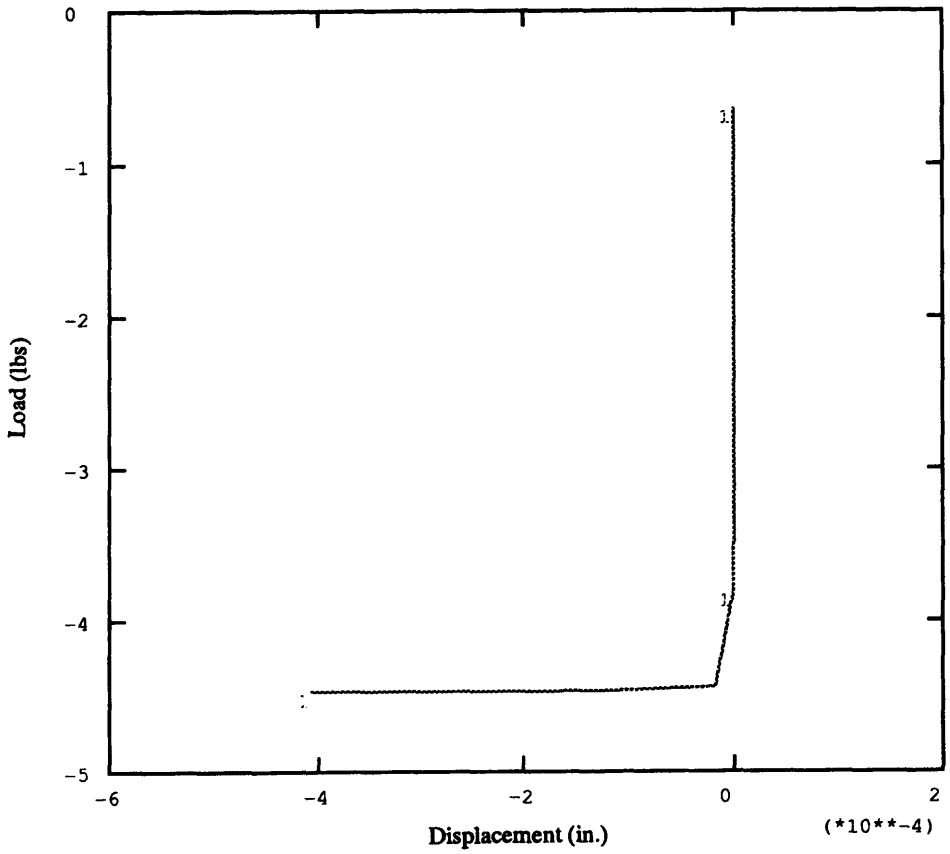

Figure C-16: **Load vs Y-Displacement for Cylinder with 8 Stiffeners at L/3 and 2L/3 using Alternating Stiffness Values (Variation 2) with Every Other Stiffness K=100,000 lbs/in**

Appendix D: The Effects of Shell Thickness on the Critical Load

The bending stiffness of the shell plays a large role in determining the buckling load of the cylindrical shell. This bending stiffness is a function of the shell thickness. The thicker the shell, the stiffer the structure. Previous solutions given in this thesis have shown that increasing the number of stiffeners around the perimeter of the shell provides stability advantages. Although these radial stiffeners increased the critical load for rather thin cylindrical shell, the stiffener effectiveness decreased as the shell thickness increased. For example, take a cylinder with radial stiffener of a stiffness value K=1000 lbs/in and vary the shell thickness. The result of performing a stability analysis on these structures, results in stiffener effectiveness dropping off as shell thickness increases (see table D-1).

Thickness t (in)	n	Pcr (psi) @K=1000 lbs/in 8 stiffeners @L/2
.125	2	-
	3	-
	4	4.4672
	5	7.4041
	6	10.146
.25	2	47.319
	3	22.303
	4	34.234
	5	54.565
	6	-
.5	2	133.35
	3	152.13
	4	270.53
	5	431.25
	6	-
1.44	2	1561.2
	3	3465.7
	4	6358.9
	5	-
	6	-

Table D-1: **Shell Thickness Comparison**

Therefore, for the constant stiffness value of the stiffeners given , a rather thick shell's stability behavior will be dominated by the shell stiffness. For the thicker structures, the stiffness value of the stiffeners will have to increase dramatically to be effective for thick cylindrical shells.